2-1-2019

Characterization and effects of halloysite nanotubes and date palm fibers on thermoplastic starch based nanocomposites

Ahmed Mostafa Aboelsoud

THE AMERICAN UNIVERSITY IN CAIRO
School of Sciences and Engineering

Nanotechnology Master Program

Thesis title

Characterization and effects of halloysite nanotubes and date palm fibers on thermoplastic starch based nanocomposites

Supervised by

Associate Professor: Mohamed Fawzy Aly

Department of Mechanical Engineering
School of Science and Engineering
American University in Cairo

Submitted by

Ahmed Mostafa Abdelkhalek
800112122

Table of Contents

List of figures:

List of tables

Acknowledgment

I would like to thank Allah for helping me to accomplish this work. I would like to show my gratitude to my advisor Associate Prof. Dr. Mohammed Fawzy for his guidance and support because this thesis would not have been possible unless him. I also wish to express my appreciation to the foresight and guidance of Prof. Dr. Mahmoud Farag.

I have to express my appreciation to Prof. Dr. Amal Esawi the Nanotechnology program director in American University in Cairo.

In addition, I would like to thank Eng. Dina Foud for his advices and laboratory assistance. I am also grateful to Eng. Jilan Elhennawy the manager of Mechanical department laboratories in American University in Cairo (AUC) and showed an enthusiasm for cooperation.

Lastly, I offer my regards and blessings to my family, friends and colleagues for their support.

Ahmed Mostafa

ABSTRACT

Great attention was paid to develop new eco-friendly “green” materials with growing environmental awareness in recent years. Composites of environmental friendly reinforcements and resins that provide high performance at affordable costs are in continuous progress. In this work, completely biodegradable thermoplastic starch (TPS) based matrix was reinforced with Halloysite nanotubes (HNTs) and date palm fibers (DPFs) individually with different HNTs weight fractions (2.5 to 10 wt. %) in order to investigate their effect on composite mechanical properties. HNTs and DPFs were then combined to reinforce TPS-based matrix at the optimum fiber weight content.

Thermoplastic starch (TPS) was obtained by blending native corn starch with glycerin and water. The plasticized starch was emulsified before being added to the previously bleached and NaOH-treated date palm fibers. The composites were preheated and then hot pressed at 5 MPa and 160oC for 30 minutes. FTIR spectra showed the increase in hydrogen bonds formation to all HNTs and DPFs composites. FE-SEM investigation showed strong adhesion at HNTs and fiber-matrix interface and good fibers wettability. Static tensile and flexural mechanical properties (stiffness and strength) of the composites appeared to markedly increased with the HNTs fraction increase until 7.5 and 5 wt. % for HNTs/TPS nanocomposites and HNTs/DPFs/TPS nanocomposites respectively. Also the composite stability was improved in thermal degradation, water uptake tests by the addition of HNTs and increasing its content. The results showed that composites mechanical properties improved by adding HNTs until certain wt. % content because above it the HNTs aggregate and adversely affect the mechanical properties. Such nanocomposites have competitive properties, qualifying these materials to be inexpensive and appropriate alternatives for various applications.

Keywords: Biodegradable composites, Halloysite nanotubes, Date palm fibers, reinforcing corn starch.

Chapter (1) - Introduction

1.1 Historical Overview

The use of natural fibers in life is not the neonate of this age; however, our ancestors had mastered them in many fields of their routine life, such as: manufacturing textiles, cordage, and papers and buildings. The use of natural fibers has increased in importance and innovation during the last few years as it is appeared in significant growth in research in this field. Not only natural fibers are used solely, but also as an excellent and sustainable reinforcements in composites fabrications. The great focus on natural fibers in the last few years compared to the synthetic fibers because of their sustainability, durability, low coast, low environmental impact and their potential to be used in wide range of applications.

The ancient Egyptians were pioneered in utilizing natural fibers such as using linen for mummification. Also they were the first in the production of composites by mixing mud and straw to create strong and durable buildings (1500s B.C.). Straw remained the most common reinforcement to ancient composite products like pottery and boats.

Another example of biodegradable composite application was the Great Wall of China in 121 B.C. it was constructed from earth works made strong by clay bricks, the clay bricks were made of Red Willow reeds and twigs with gravel during the Han dynasty [1].

Later, in 1200 AD, extremely powerful composite bow was invented by Mongols. Bows were made of a combination of wood, bone and animal glue, then pressed and wrapped with birch bark. These composite bows were the most powerful weapon on earth until the invention of gunpowder and were the main reason behind the Mongols' military dominance.

Natural fibers and resins derived from plants and animals were the only source for composite products until the modern era of composites began with the development of synthetic plastics in the early 1900s such as polyester and vinyl polystyrene and with the invention of fiberglass by Owens Corning in 1935. Adding fiberglass to plastic polymer created a very strong and lightweight structure that was the start of Fiber Reinforced Polymer (FRP) industry.

World War II had a great impact in the development of FRP industry, where alternative materials were needed for military applications like aircrafts. Fiberglass composites satisfied the strength and lightweight desired for such applications, besides, being transparent to radio frequencies. In the 1970s better resins and improved reinforcements were developed leading to a great expansion in the composite industry. Most important reinforcements developed in

1970s were Kevlar and Carbon fibers. Kevlar was developed by DuPont and quickly became the standard in armor due to its high tenacity.

In the 1990s another generation of composite materials was developed based on hybridization and Nanotechnology especially in the academic and industrial research areas.

The futuristic trends of research in composites are on the path towards being more environmentally friendly, by replacing synthetic resins by bio-based polymers and synthetic fibers by natural fibers [2].

1.2 Environmental and Economic Impact

During the last two decades, the awakening of the world's conscience towards the environment led to many attempts to develop new composites that can be eco-friendly and sustainable. And therefore, the attention has been paid to the use of natural polymers and lignocellulosic fibers as good alternatives. The Problem in the conventional petroleum based polymers is that they are not sustainable. They also have a harmful impact on the environment during manufacturing and after their final use, where their generated solid waste has a toxic effect on soil. These reasons increase the importance of biodegradable polymers and composites.

On the other hand, the importance of biodegradable polymers/composites are not limited on the environmental effect, where they can provide opportunities to improve the standard of life of people around the world especially in the developing countries and rural areas. The biodegradable composite industry can provide another use of agriculture products and waste besides being food, which can lead to economic improvement in these areas based on these agricultural materials. For example, lignocellulosic fibers such as jute, sisal, pineapple, Palm-date, bagasse, etc have been used as reinforcement in many polymers. The extraction and preparation process of these fibers can generate rural jobs [3]. Another example for the generation of jobs by using agro-based materials is the utilization of rice husk as reinforcement in polymers, knowing that rice husk constitutes more than 10% of world rice production [4].

Several developing countries such as India, Malaysia, Indonesia, Philippines, Brazil and some of the African countries have national projects for the utilization of several of their agro wastes [3]. Egypt possesses the capabilities that qualify her to be a leading country in using many types of agricultural products such as Flax, sugarcane (bagasse), palm date fibers and

Corn starch that can be used in biodegradable composite products. In Egypt straws of rice and bagasse often represent a problem and sometimes burned in the fields as means of disposal, these agro-wastes can be utilized as fillers/reinforcements in polymer or cement to develop new materials (composites), thus providing jobs and improving the living conditions of the rural population.

In conclusion; the reasons push us to think in biodegradable composites can be:

- The great concern about sustainability about the use of renewable and biodegradable sources of raw materials with lower cost.
- Reducing the harmful environmental impact of petroleum-based polymers and composites due to the increased awareness to environment.
- Developing the rural areas and creating new job opportunities.

But there are challenges face the use of biodegradable composites and limit their use in large scale like:

- Problem of stocking raw material for extended time.
- Possibility of degradation, due to biological attack.
- Matrix and fibers are hydrophilic (sensitive to humidity).
- Need more work and research to enhance their properties to be feasible and competitive to conventional polymers.
- Issues of compatibility with Matrix such as fiber-matrix interface and fibers distribution.
- Ultra violet (UV) light (sunlight) resistance – not better than conventional plastics.

So, many efforts are exerted in the research area to overcome these challenges and reach the best utilization of biodegradable composites [5].

1.3 Biodegradable Materials in Industry

As mentioned before, synthetic polymers are considered environmental abusive materials beside their high cost. The large use of these polymers in different sectors leads to disposal problems. Agro-based materials such as plant fibers and natural polymers become competitive alternative, especially after approving laws for the reduction of using environmentally harmful materials in some countries that have an environmental

consciousness. It is therefore forces many leading plastics companies in the U.S. and other European countries to be in the forefront in developing biodegradable materials from natural materials [3]. For example, the use of natural fibers in the German automotive production has increased from 9,600 ton in 1999 to 19,000 ton in 2005 without wood and cotton see Figure (1.1) [6].

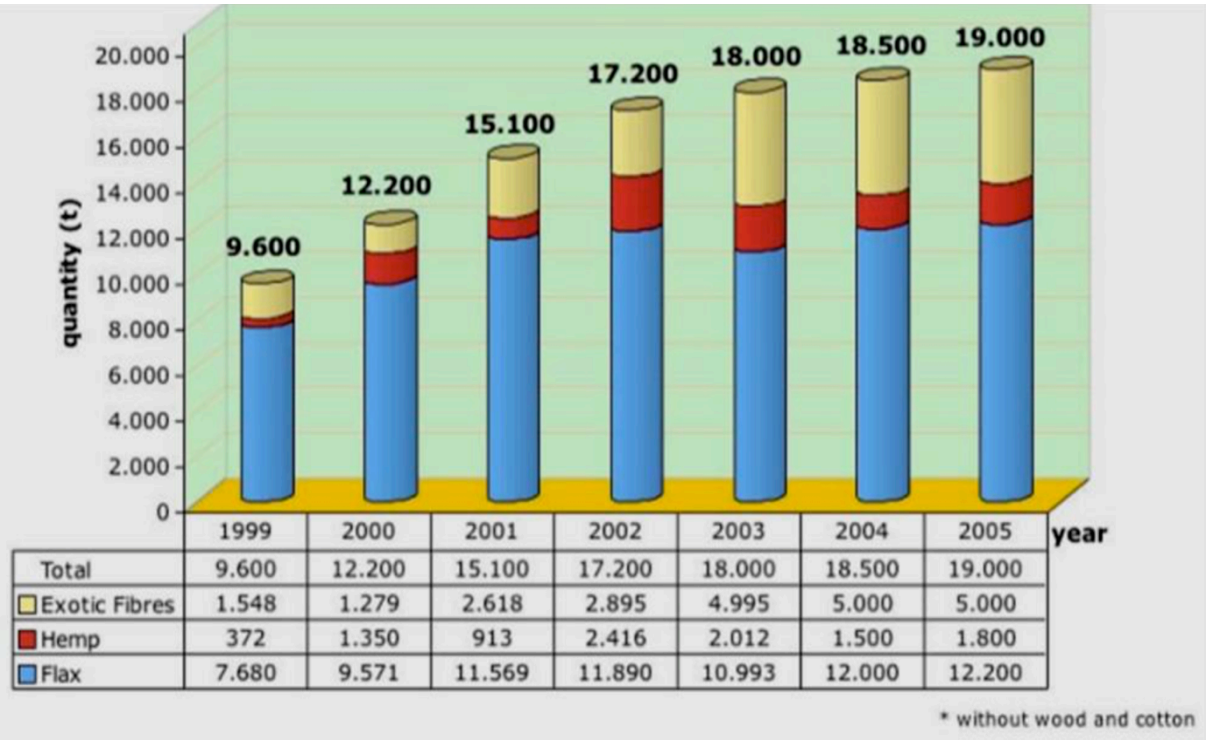

	1999	2000	2001	2002	2003	2004	2005
Total	9.600	12.200	15.100	17.200	18.000	18.500	19.000
Exotic Fibres	1.548	1.279	2.618	2.895	4.995	5.000	5.000
Hemp	372	1.350	913	2.416	2.012	1.500	1.800
Flax	7.680	9.571	11.569	11.890	10.993	12.000	12.200

Figure 1. 1: the usage of natural fibers in the German automotive industry from 1999 to 2005 adopted from [6].

Natural fibers have become more popular to be used in many industrial sectors, e.g. as a reinforcement for plastics because of their sustainability and their hidden innovation properties. Natural Fibers have been used in wide range of composite Products with conventional synthetic polymers. Some of products made by using natural fibers such as flax and jute are shown in Figure (1.2). These products include panels (a) made of Jute-Coir Hybrid Composite; lightweight bike (b) made of Flax- carbon hybrid composite; Suitcase (c) made of Jute-Polypropylene composite and car inner door panels (d) made of mixed natural Fibers-Polypropylene composite [7].

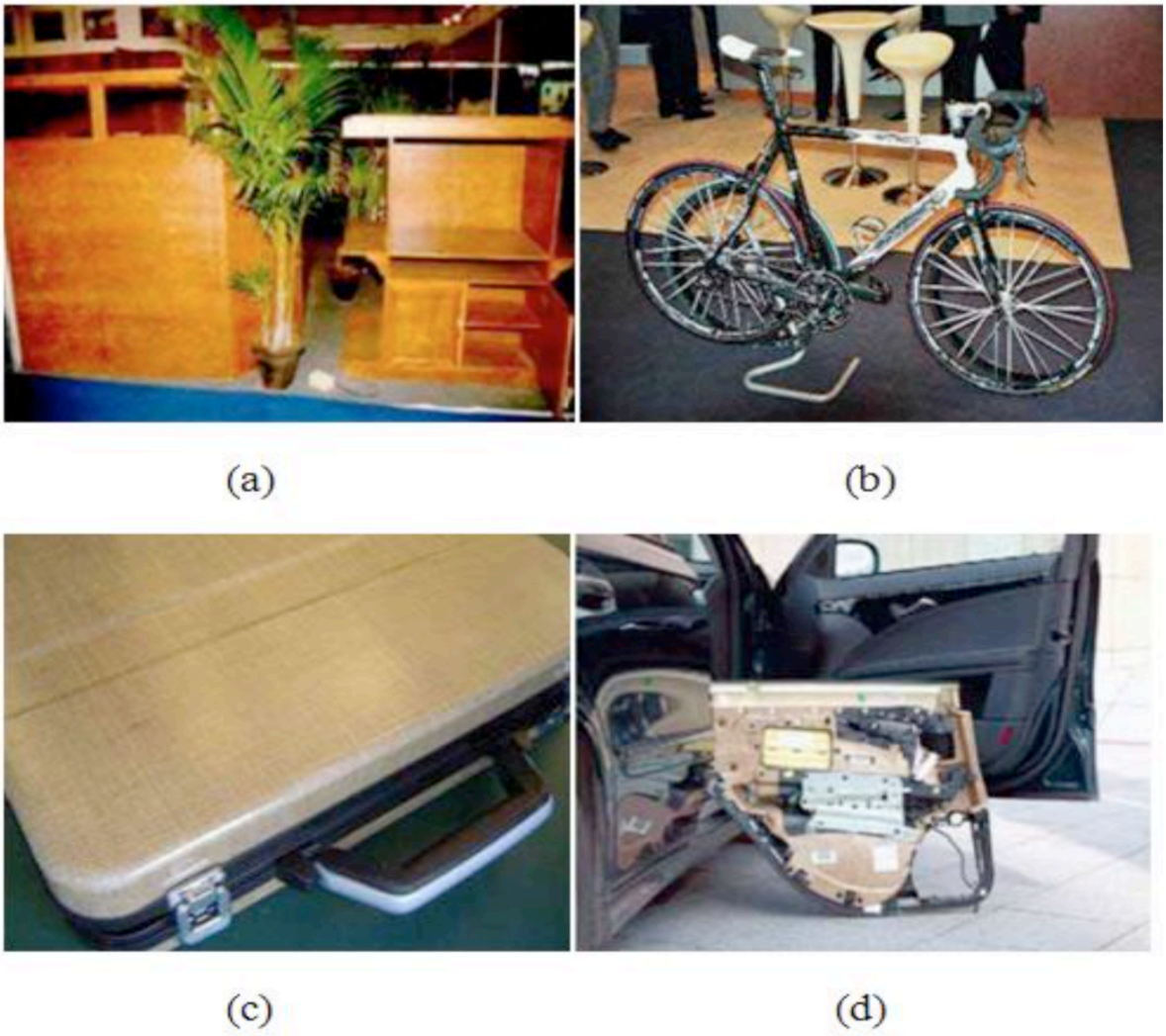

Figure 1. 2: Natural fiber products: (a) panels; (b) bike; (c) suitcase; (d) inner door panels adopted from [7].

Biodegradable polymers are a very attractive alternative for Disposable products that are used once and for short time. Starch based polymers represent the most extensively studied biodegradable polymer. Figure (1.3) shows different disposable products made of starch such as drinking cup (a) made by water stream foaming and pressing process; lawn cutting and leaf bags (b) made of corn starch by blow molding; green pens (c) produced by injection molding and foamed trays (d) made of thermoplastic starch [8].

Figure 1. 3: Starch based products: (a) drinking cup; (b) bags; (c) pens; (d) foamed trays cited from [8].

Many companies have decided to change into biodegradable polymers in packaging and food services. According to money.cnn.com in 21 March 2018, Starbucks is offering $10 million to turning into new recyclable cups in a way to reduce its environmental impact because its conventional cups have a thin layer of plastic that will take 20 years to decompose. The same environmental attitude is followed by Dunkin' Donuts (DNKN) that said it will eliminate polystyrene plastic foam cups by spring of 2018 and get rid of foam cups altogether by 2020. They will be replaced by recyclable paper cups, according to the company. McDonald's (MCD) also said earlier this year that it would eliminate foam cups and replace them with renewable or recyclable materials in all packaging by 2025.

1.4 Objective

The objective of this research work is to prepare a completely biodegradable, biocompatible, environmentally friendly, and affordable natural fibers composite reinforced with a Nano-filler; the composite is made of commercial corn starch-based matrix reinforced with both date palm and halloysite nanotubes. To achieve this objective, experiments were carried out to determine the effective content for the halloysite nanotubes that gives the effective mechanical properties. Also thermal stability and water uptake tests of the biodegradable composites were carried out.

Chapter (2) Literature Survey

2.1 Biodegradable polymer

A polymer is a macromolecule composed of repeated units linked together by a specific bond, while, the term biodegradable polymers refers to those that can break down after the period of its intended purpose to use had ended. In contrast, conventional polymers will persist for many years after disposal. The degradation results minerals, biomass, water, gases, humic matter that will come back to nature. During the degradation process the polymer loses its structure that will affect its integrity, weight, and mechanical properties. This degradation is due to microorganisms present in soil naturally, such as: bacteria, fungi, and algae. The importance of the biodegradable polymer comes from their environmental role in the recycling process (Figure 2.1).

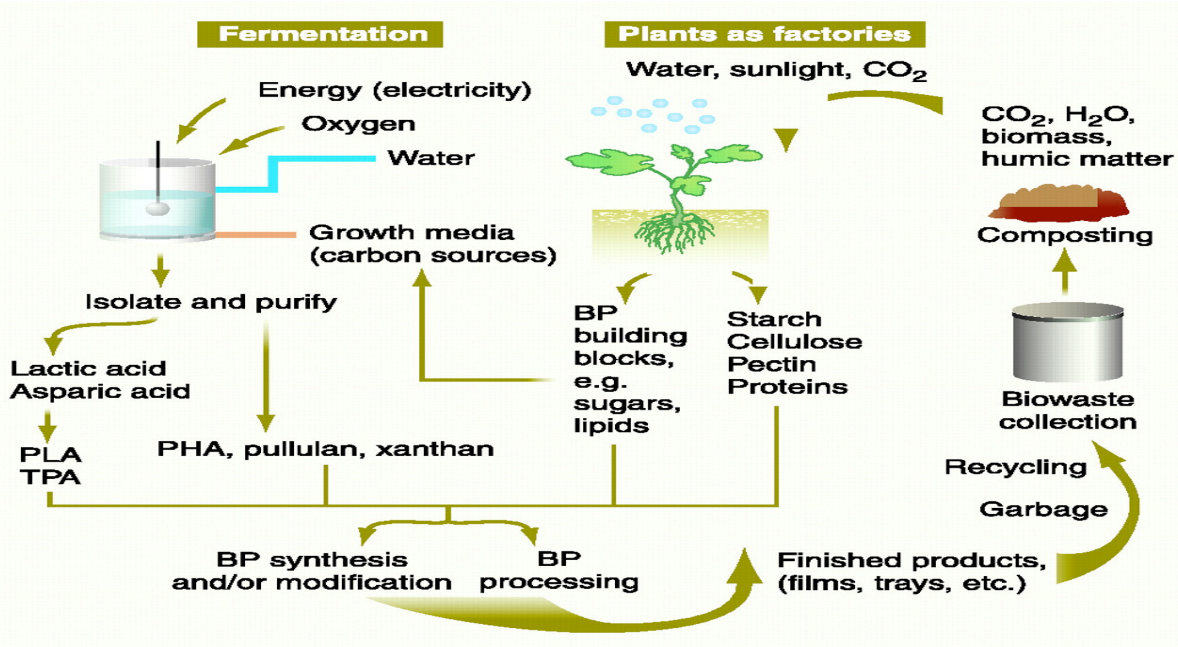

Figure 2. 1: The cycling process of the biopolymers (BPs)

where they are obtained from agricultural products. After disposal they will be degraded by microorganisms into Co_2, H_2O, biomass, and humic matter. The new agricultural plants will use the biomass and humic matter to fix atmospheric Co_2 and produce new biopolymers again (adopted from [9]).

2.1.1 Classification of Polymers

Generally, polymers can be classified according to their resources into: polymers from renewable resources and polymers from petroleum resources. In addition, polymers can be classified according to biodegradability into: biodegradable and non-biodegradable or polymers can be classified as a bio-based or fossil-based (figure 2.2)

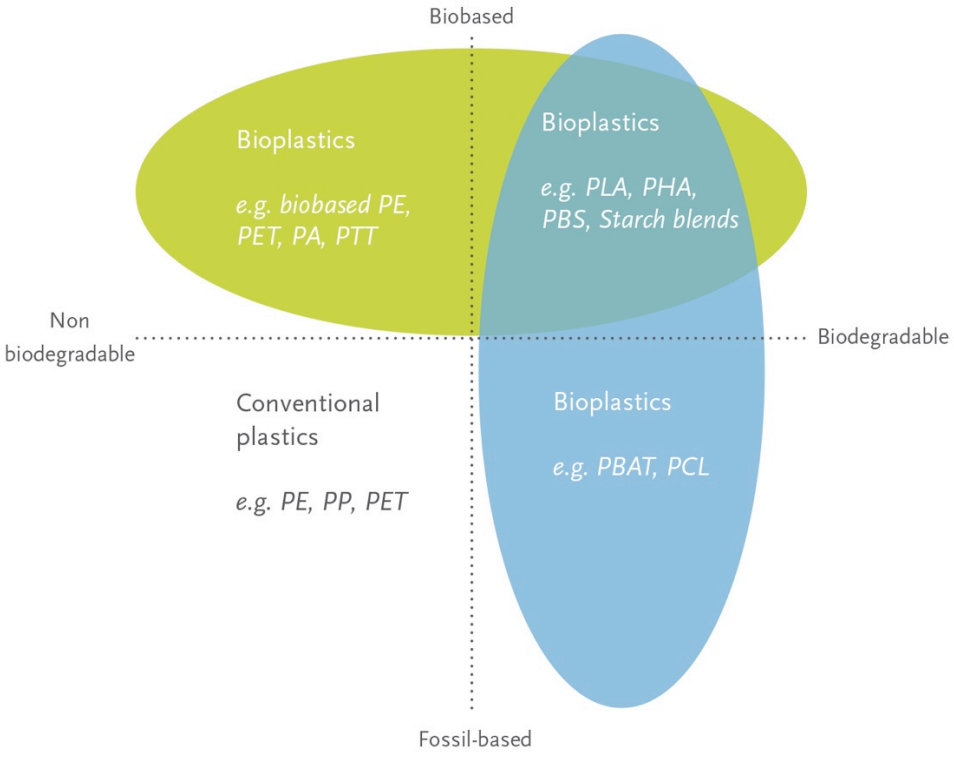

Figure 2. 2: Bioplastic are bio-based or biodegradable or both (adopted from [10]).

Bioplastics are not just one single substance, they comprise of a whole family of materials with differing properties and applications. According to European Bioplastics, a plastic material is defined as a bioplastic if it is either bio-based, biodegradable, or features both properties.

The term 'bio-based' means that the material or product is (partly) derived from biomass (plants). Biomass used for bioplastics stems from e.g. corn, sugarcane, or cellulose. On the other hand, biodegradation is a chemical process during which microorganisms that are available in the environment convert materials into natural substances such as water, carbon dioxide, and compost (artificial additives are not needed). The process of biodegradation depends on the surrounding environmental conditions (e.g. location or temperature), on the material and on the application [10]. The property of biodegradation does not depend on the re- source basis of a material but is rather linked to its chemical structure. In other words, 100

percent bio-based plastics may be non-biodegradable, and 100 percent fossil based plastics can biodegrade [10].

As previously stated there is a variety in sources of biodegradable polymer such as agro polymers, microbial and chemically synthesized, and here some of the most famous biodegradable polymers that can be used as a matrix resin.

- **Agar**

Agar is a well-known natural polymer obtained from red algae like *Gelidium amansii* (Gelidaceae). It is a gelatinous material composed of agarose and agropectin. Agarose is a linear polymer composed of repeated disaccharide called agrobiose which is made up of D-galactose and 3,6-anhydro-L-galactopyranose. Agropectin is a mixture of acidic molecules which have poor gelatinous ability. Agar is used in chromatography of protein purification, DNA separation, gelling agent, emulsifying agent, surgical lubricant and medium for bacterial culture [11].

- **Poly-hydroxyalkanoates (PHA)s**

PHAs are a family of natural polyesters produced naturally by bacterial fermentation of sugar or lipids and can be produced from recycling materials. Bacteria produce this polymeric structure mainly to store their needs of carbon and energy. They have a high Ultraviolet (UV) stability and low water penetration relatively to other biopolymers [12]. PolyHydroxybutyrate (PHB) is a simple type of PHAs which is stiff and brittle by nature due to its high crystallinity, leading to difficulties in processing. This problem can be overcome by using plasticizers as with starch like Polyvinyl-acetate (PVA) and steric acid [13].

- **Poly-lactic acid (PLA)**

PLA is a completely biodegradable thermoplastic aliphatic polyester derived from renewable resources like corn starch and sugarcanes by bacterial fermentation. PLA

can be processed in different ways such as injection molding, extrusion and blow molding where a plasticizer is recommended to be used to overcome its brittle nature [14].

- **Natural Rubber**

Natural rubber is a linear polymer of isoprene monomers (C5H8). It is derived from white latex of trees. Natural rubber is normally very stretchy and flexible and regains its original shape after being deformed. Also it is extremely waterproof and has good resistance to chemical attack [15].

2.2 Starch

Starch is a carbohydrate polysaccharide polymer composed of glucose units linked together by glycosidic linkage. Starch is produced by all green plants as the principle storage food, especially present in seeds (like rice, wheat, and corn) and underground parts (like potato, and carrot). The native starch is composed chemically from two polymers (Figure 2.3), namely Amylose (a non-branched helical chain of Glucose units linked together by α-1, 4 glycosidic linkage) and Amylopectin (a highly branched polymer of glucose units which gives a branch every 24-30 glucose units and glucose units are linked by both α-1, 4 and α-1, 6 glycosidic linkage) [11&16]. Native starch appears a milky, tasteless, and odorless in solution. In addition, native starch is semi-crystalline with crystallinity of about 20-45% [17]. Native starch is not very applicable in research or industry because of their internal swelling and rapid enzymatic degradation; However, has relatively poor mechanical properties [18]. Therefore, this leads to the use of modified starch or its derivatives (like dextrin) that stay longer before degradation and can crosslinking to form copolymers [16]. The properties of polymerized starch can be enhanced by different ways such as; blending with more hydrophobic thermoplastics, graft co-polymerization and chemical modification. Starch is one of the most extensively studied biodegradable polymers

[19].

Native starch is a carbohydrate consisting of a large number of discrete and partially crystalline granules of glucose units associated together by covalent bonds that also join the glucose molecule to the other groups, this bond is called glycosidic bond [20]. The extended network of the associated long carbohydrates molecules form repeated monomer units called polysaccharide. Physically, most native starches are semi-crystalline and having a crystallinity of about 20–45% [21].

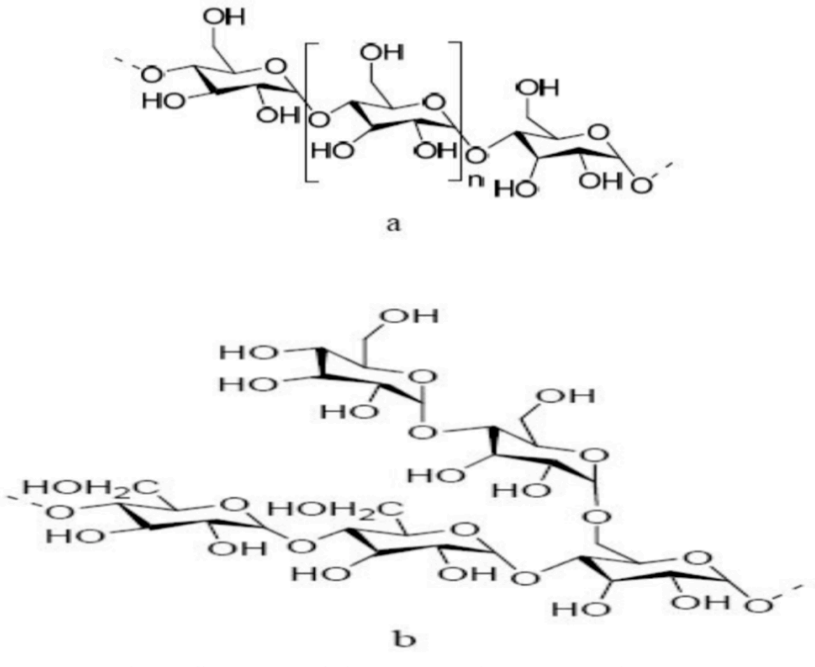

Figure 2. 3: Structure of a) Amylose and b) Amylopectin (adopted from [17])

Plant species that native starch can be obtained from is the main factor that controls the percentage of native starch constituents and its granular shape and size. For example, rice starch has spherical granules with small size (about 2μm) while potato and wheat starch have larger granules (up to 100μm). Generally, most starches consist of spherical granules about 2–100 μm in diameter [20&22].

Although the detailed microstructures of starches are still under study, it has been established that Starch consists of two types of molecules: the linear amylose and the branched amylopectin depending on the plant species. Starch generally contains 20 to 25% linear amylose and 75 to 80% branched amylopectin. The native starch crystallinity is attributed mainly to the amylopectin short-branched chains while intra

and intermolecular hydrogen bonds between the hydroxyl groups in starch molecules increase the crystallinity of native starches [22&23]. Table (2.1) includes some characteristics of most common native starches [24&25].

Table 1. 1: characteristic of native starch adopted from [24&25].

	origin	Particle size (µm)		Amylose %	Crystallinity %
Potato Starch	Tuber	5-10	Avg. 50	25	25
Corn Starch	Seed	6-21	Avg. 16	25	39
Wheat Starch	seed	5-40	Avg. 20	30	36

Amylose has a molecular weight about 10 times higher than conventional synthetic polymers, while amylopectin molecular weight is much greater than amylase. Also amylose has much smaller molecules than amylopectin and the number of amylose molecules is much greater than amylopectin [20&22]. The previous reason and the branched structure of amylopectin reduce the mobility of the polymer chains, and reduce the tendency to become oriented closely to create high level of hydrogen bonds. This prevention of amylopectin chains to associate with each other easily due to the presence of amylase is the main reason behind the native starch incomplete crystallinity. Crystalline regions are present in the form of double helices with a length of approximately 5 nm [22]. The chemical structure and a schematic representation or amylase and amylopectin can be seen in (figure 2.2).

2.2.1 Thermoplastic Starch (TPS)

Thermoplastic Starch (TPS) is the name of the transformed materials that result from thermal processing of starch and adding small amounts of other substances known as plasticizers. Thermal processing in presence of plasticizer is used to disrupt and transform the semi-crystalline structure of starch granules to a homogeneous and amorphous material called thermoplastic starch, where plasticizer also enhances the processability and the mechanical properties of TPS [22].

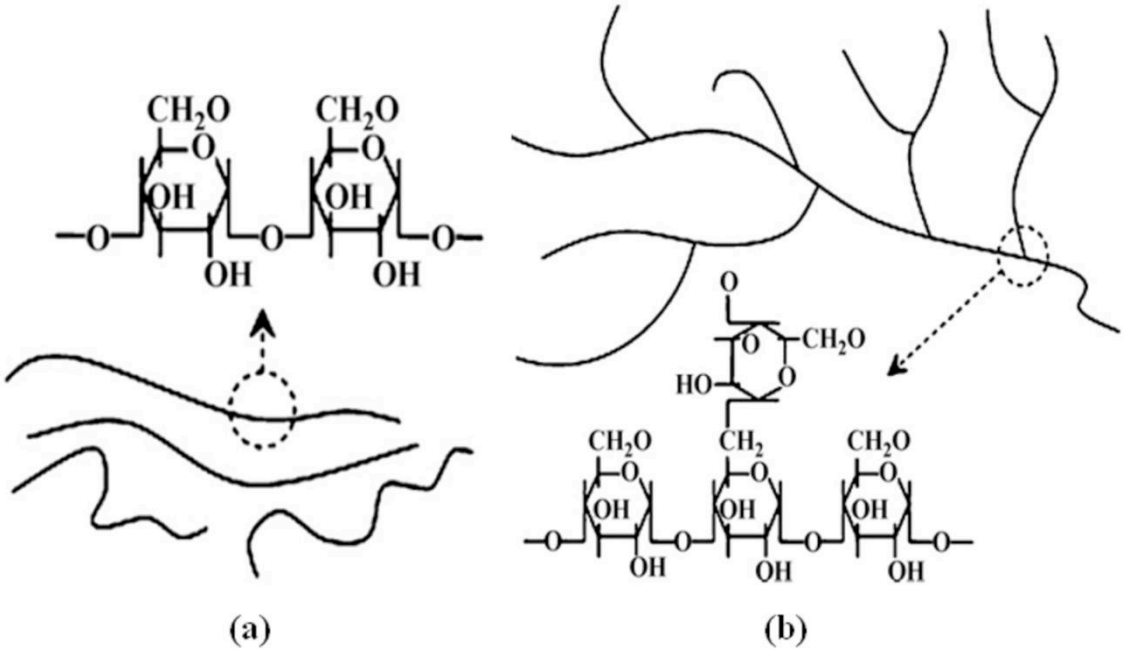

Figure 2. 4: Native starch chemical and schematic representations; (a) linear amylose; (b) branched amylopectin, adopted from [22].

2.2.2 Starch Gelatinization

Gelatinization is an endothermic process and considered the basic phenomenon of converting starch to thermoplastic starch in which the semi-crystal structure of native starch is destroyed to amorphous state before transforming to another crystal type [22]. Adding water to native starch makes the starch granules swell and burst, the semi-crystalline structure is lost and the smaller amylose molecules start leaching out of the granule, forming a network holds water and increases the mixture's viscosity. Supplying heat to this process facilitates the swelling and granules destruction process leading to significant loss of crystallinity [26&27].

Gelatinized amylopectin initially remains in an amorphous state before gel balls of short branched chains are formed. On the other hand, amylose partly leached out of the amylopectin and with cooling forms V-type single helix crystals which results in higher modulus and yield stress for extruded starch [28]. The aging of gelatinized starch causes the V-type crystals to rearrange in more crystalline structure, this process named retrogradation that leads to starch embrittlement [22]. A schematic

representation of starch gelatinization and retrogradation processes can be shown in figure (2.3).

Gelatinization can be divided into two stages; the initial gelatinization (from 20 to 85 ^{o}C) depending on the degree of cross-linking of the amylopectin. In this stage a lower mobility is found for water to interact with the hydroxyl groups. The other stage is at higher temperatures where more free hydroxyl groups is disrupted and attract water molecules, resulting in more swelling and dissolution of crystals [26&29].

Many researches on starch gelatinization showed that with high water content (70%w/w), amylose and amylopectin partially separated without the need to heating or shear stress [30].

In conclusion the process of gelatinization depends mainly on water content and temperature while applying shear stress enhance gelatinization by improving amylose leach out of the amylopectin.

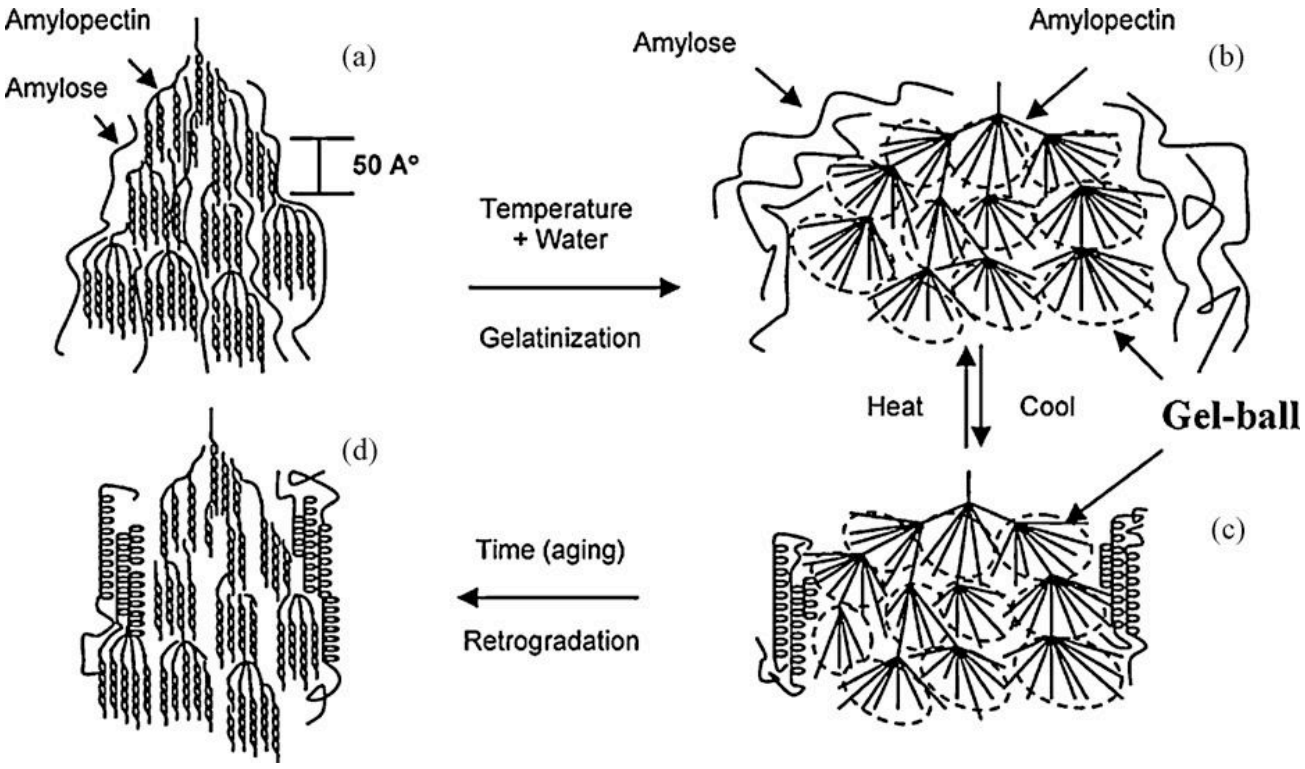

Figure 2. 5: Schematic representations of starch gelatinization and retrogradation adopted from [28].

2.2.3 Starch Plasticization

Most natural polymers are brittle and have poor processability, besides being water sensitive, causing their properties to deteriorate. This is normally overcome by adding plasticizers such as (water and glycerol) to enhance their performance and properties. Plasticizers increase the flexibility of the polymer product and also decrease the viscosity of the polymer melt. Water and glycerol are the most suitable plasticizers for starches, where they make starches flow easily and reduce the glass transition temperature (Tg) and melting point. The mechanical and heat energy supplied during preparation destroy starch internal hydroxyl bonds. Water is not preferred to be the only used plasticizer due to its volatility, so glycerol is preferred to be used [3&31].

Adding plasticizers can also influence the aging of starch-based polymers induced by retrogradation, and consequently cause a reduction in the final product embrittlement caused by retrogradation. This can be interpreted as; plasticizer lowers the number of crosslinks between starch chains, which hinders the rate of retrogradation. This was suggested to be caused by the interaction between plasticizer and amylose as well as with amylopectin. However, specific interactions between plasticizer and starch chains are difficult to elucidate [3&32].

Glycerol is the most common used plasticizer for starch. Wollerdorfer et al [33] added Sorbitol and glycerol as plasticizers to the moist starch. A co-rotating twin screw extruder was used to plasticize starch at 115°C and 50 rpm. Sorbitol to moist starch ratio was (1:6.4) while 13% of glycerol was added.

2.2.4 Factors Affecting Thermoplastic Starch Properties

a) Starch type

As previously stated it was reported that amylose is the responsible of the majority of the crystalline structure after the gelatinization process, which give the starch its strength and embrittlement. And amylopectin creates the entanglements of the

amorphous structure [23]. Also it was found that starch type (origin) controls the content of amylose and amylopectin. Thereby the type of starch used has a significant effect on the final biopolymers properties especially the mechanical properties such as; tensile strength and impact strength [25].

b) Plasticizer content

Plasticizers have been added to starch to improve processability and to enhance the mechanical properties by inhibiting retrogradation process after processing. Various researchers studied the effect of increasing the plasticizer content on the thermal and mechanical properties of starch-based polymers. Van Soest et al [34] showed that increasing glycerol content in waxy maize starch gel significantly reduces the retrogradation rate.

Godbole et al [35] investigated the thermal stability of potato starch/ Poly hydroxyl butyrate (PHB) blend with and without plasticizer (glycerin). They found that blend with the thermoplastic starch (TPS) has the greatest thermal stability. Also the glass transition temperature (Tg) was increased by plasticization, but the melting temperature was not much affected by blending neither with starch nor TPS. Table (2.2) shows these results.

Table 1. 2: PHB/starch thermal stability adopted from [34].

Starch Type	**PHB/Starch ratio (W/W)**	**Melting Point (ºC)**	**T_g (ºC)**	**Thermal Stability (ºC)**
----	1.0/0.0	168.1	63.1	223.3
Starch	0.5/0.5	167	75.9	219.7
TPS	0.5/0.5	156.4	145	259.9
Starch	0.7/0.3	167.0	71.3	217
TPS	0.7/0.3	165.5	147.4	260.3

TPS: Thermoplastic starch; **PHB**: Poly hydroxyl butyrate

Forssell et al [36] changed the plasticizers content in barley starch to study the thermal behavior of the thermoplastic starch mixtures. Barley starch and plasticizers (water and glycerol) were mixed and stored overnight before melt mixing. Glycerol content varied from (14 to 39 %w/w) and water content from (11 to 30 %w/w). Two glass transitions (lower and upper) were detected in barley starch glycerol-water mixtures by DSC. Increasing either glycerol content or water content lowers the lower and upper glass transition temperatures. For example, at (Glycerol 20%w/w and water 9.2%w/w) at relative humidity RH of 54% the lower and upper glass transition temperatures were -69 ^{o}C and 21^{o}C respectively. They also found that for mixtures having less that 20% water Amylopectin crystallization did not occur within 1 week of storage even with low glycerol content, which imply that glycerol interacted with starch, inhibiting crystallization of amylopectin.

Janssen et al [37] studied the effect of glycerol on glass transition temperature (Tg), tensile strength and impact strength of different types of injection molded starches (potato, wheat, waxy maize and pea). They found that increasing glycerol content reduces starches' glass transition temperature (Tg) and tensile strength, but increases the impact strength what means a reduction in the brittleness of the starches-based polymers.

c) Water content

Water is the most popular plasticizer used in thermal processing of starch-based polymers, where it plays an essential role in the gelatinization process of starch. It is clear that increasing water content enhances the gelatinization process, also water has an effect on the mechanical and thermal properties of the final material. Many researches focused on this topic. It was obvious that increasing water content lowers the glass transition temperature (Tg) of thermoplastic starches [18&36]. If water content is too high, the crystalline amylose might be pulled apart be the great swelling and start to polymerize in a water mediated entanglements, leading to reduced mobility. And if the water content is limited, complete gelatinization will not occur in the usual temperature ranges where the swelling forces will be much less [38].

Hulleman et al [39] studied the effect of water content on the stress and strain at break of compression molded thermoplastic starch with 30 %w/w glycerol. They confirmed that neither high water content nor limited water content gives the highest strength and strain but there is a range of water contents to get the optimum values for each stress and strain depending on starch type. For example, maximum strain at break for corn starch was at about 20% water content and no significant increase in tensile strength was observed. On the contrary potato starch showed different behavior, where increasing water content increased the tensile which can be due to its low mobility and high degree of polymerization. These results can be shown clearly in figure (2.4).

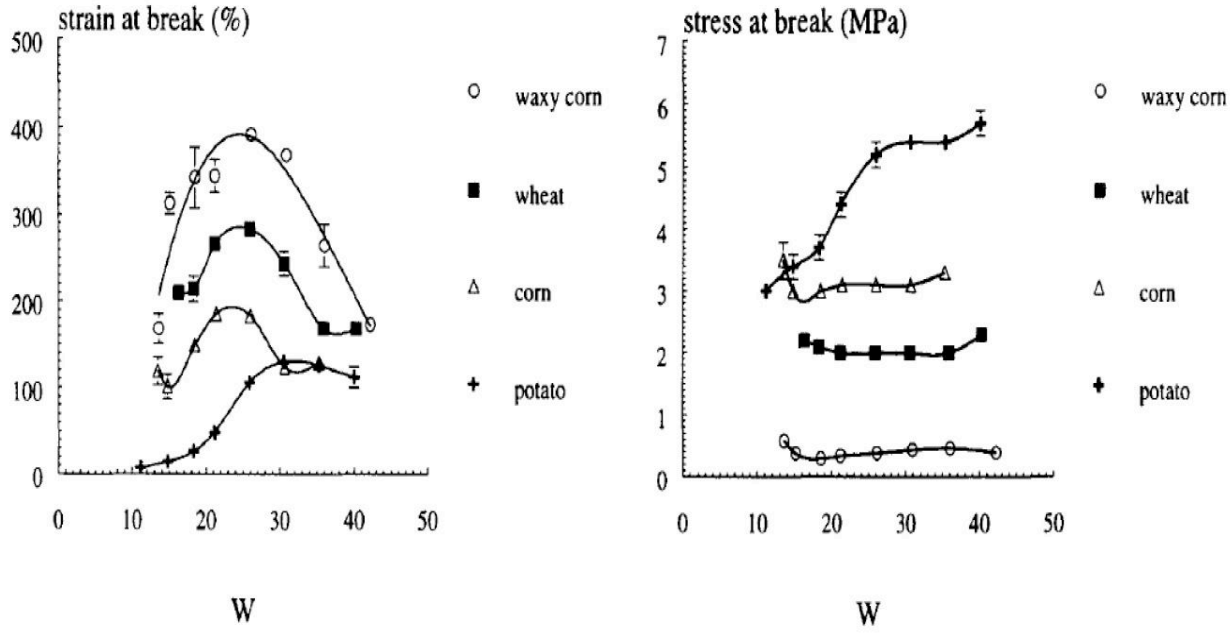

Figure 2. 6: Strain at break (εb) and nominal stress at break (σ b) versus water content during compression molding (W) for potato, corn, wheat and waxy corn starch, adopted from [39].

d) Processing conditions and techniques

Starch exhibits multiphase transition, thereby the microstructure and mechanical properties of starch-based polymers strongly depend on the processing techniques and conditions [22]. Applying shear stresses during thermoplastic starch preparation process (gelatinization and plasticization) allowing faster transfer of water into the interior molecules, where shear forces tear apart the starch granules [40]. The greatest disruption of molecular bonds of starch occurs during extrusion process because of the

intense shear applied [41].

Storing glycerol plasticized starch at room temperature for days reduces amylopectin crystallinity and affects the molecular mobility due to the interaction between glycerol with amylose and amylopectin, thereby this may enhance the flow properties and reduce resistance to shear during processing [36].

Changing processing technique will lead to changes in the resulted starch-based polymer properties. For example, the compression molding of potato starch leads to brittle materials, since the amylopectin crystals in the native powder remained largely preserved. Injection molding results in superior mechanical properties, since it increases the amorphous structure. On the other hand, aqueous gels result in disintegration of starch granules structure, then the formation of new semi-crystalline structure [42].

Starch rheological properties are more sensitive to changes in pressure than conventional petroleum-based polymers [22]. Kokini et al. [43] found that increasing pressure for 20% water content amioca starch from 15 to 200 psi (0.1 to 1.4 MPa) increased the gelatinization temperature by 57 ^{o}C. Also increasing processing temperature increases the mobility of starch granules and the melting of the crystalline regions, making starch show a visco-elastic behavior [44&45].

2.2.5 Starch Modification and Enhancing Behavior

Final products made from pure starch have unfavorable properties such as poor mechanical properties and high moisture sensitivity. In an effort to overcome these poor properties, plasticizers were used to improve the thermal and mechanical properties. Also a great attention was focused on the blending of starch with biodegradable and non-biodegradable synthetic polymers such as Polylactic acid (PLA), Polycaprolactone (PCL) and Polyethylene (PE). The blend has better mechanical and chemical properties than starch-based polymers [3&22].

In case of blending thermoplastic starch (TPS) with non-biodegradable polymer like Polyethylene (PE), TPS granules act as filler resulting in an increase in modulus, but

also in further loss of ductility with increasing TPS content [18&46]. Furthermore, if the amount of the TPS is large and after removal of biodegradable component by the effect of microorganisms under normal composting conditions, the remaining amount of synthetic polymer should disintegrate and vanish. This partial degradation leads to effective reduction in the volume of plastic waste [47]. Unfortunately, there is a great difference in the chemical properties of starch and synthetic polymers where they have totally different polar characters, so most of the synthetic polymers like (LDPE and PP) are immiscible with starch at the molecular level. This thermodynamic incompatibility often leads to poor properties of these blends [48]. So many efforts have been exerted to enhance the compatibility of the blend such as the modification of starch, where Starch was converted to a hydrophobic derivative named (stath) by phthalation [49]. Another effort exerted in the modification of LDPE, where Maleic Anhydride (MA) was grafted onto LLDPE to work as a compatibilizer between starch and LDPE [48].

Another effort focused on enhancing thermoplastic utilization in composite technology by coating Thermoplastic starch made of corn starch with a new coating to overcome its hydrophilicity. The coating made of amorphous carbon by chemical vapor deposition (CVD) using plasma of methane and subsequently with sulfur hexafluoride (SF6). A homogenous and very hydrophobic surface was resulted [50].

2.3 Natural Fibers as a Reinforcement

Cellulose is considered to be the most abundant renewable organic compound derived from biomass. The worldwide production of this biopolymer is estimated to be between 10^{10} and 10^{11} ton each year [51]. Cellulosic natural fibers have some unique properties that make them receive considerable attention as substitutes for synthetic fiber reinforcements (fiberglass) such as being low cost, renewability, availability, low density, good thermal insulation properties, acceptable specific strength and being less abrasive to tooling and not causing as many health problems during processing [52&53]. Because of these advantages, the use of natural fibers based composites has spread to various sectors like automotive, aircraft and construction [3&4]. The natural fibers reinforced polymers to synthesis the car cabinet, tables, and kitchen shelves. Flax fibers have the predominance market share of the used natural fibers in the automotive industry, due to their superior strength. They represented about 65% of German automotive industry in 2005 [6].

Natural cellulosic Fibers can be classified with respect to the part in the plant they obtained from as shown in figure (2.5). For example, kenaf fibers are extracted from kenaf stems see figure (2.6), while banana fibers are extracted from banana leaves.

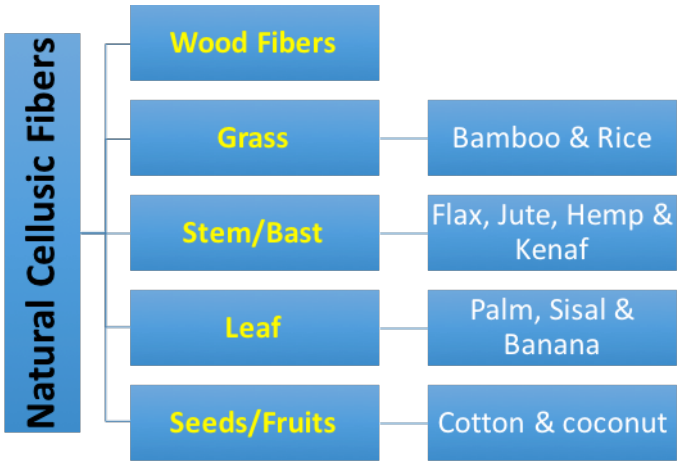

Figure 2. 7: Classification of natural fibers according to plant part adopted from [7].

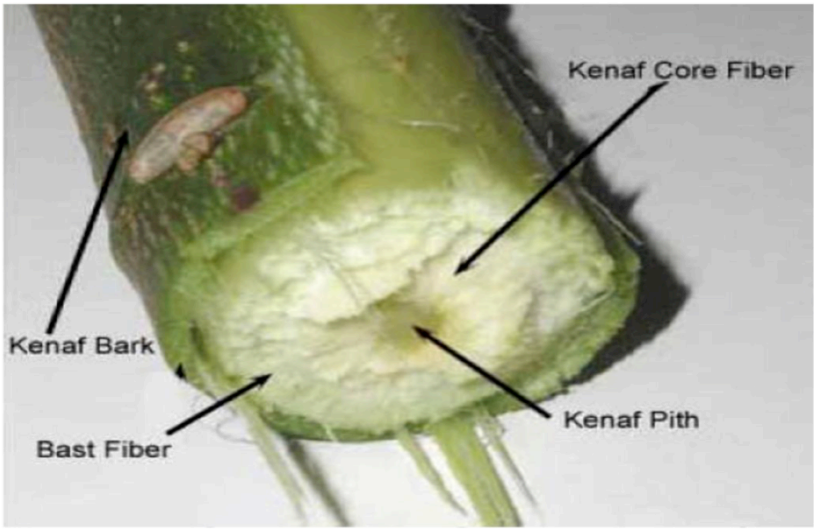

Figure 2. 8: kenaf stem cross-section adopted from [54].

The structural components of plants are formed primarily from cellulose. Thus lignocellulosic natural fibers consist of cellulose micro-fibrils surrounded by amorphous lignin and hemi-cellulose. The fibers structure is made by several fibrils run all along the length of the fiber forming various walls [55&56]. A schematic representation for the fiber structure can be shown in figure (2.7).

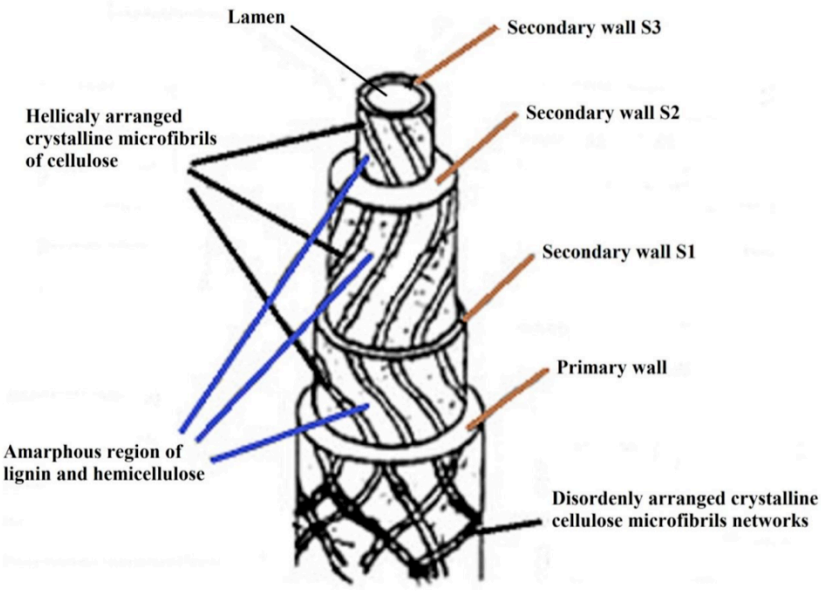

Figure 2. 9: structure of natural fiber adopted from [55].

The main chemical structure of cellulose shows a repeated dimer sugar called cellobiose that forms amorphous and crystalline parts alternatively to form one cellulose microfibril. The cellulose microfibrils are collected together to form a microfibrillated cellulose which are collected again to form a cellulose fiber [51], see figure (2.10). Chemical composition (Cellulose and lignin content) and properties vary from plant to another as shown in table (2.3). Natural fibers also exhibit variation in properties and composition for fibers from the same species due to the fluctuations in the environmental conditions (moisture, soil, temperature, etc.) in which these natural materials grow [57].

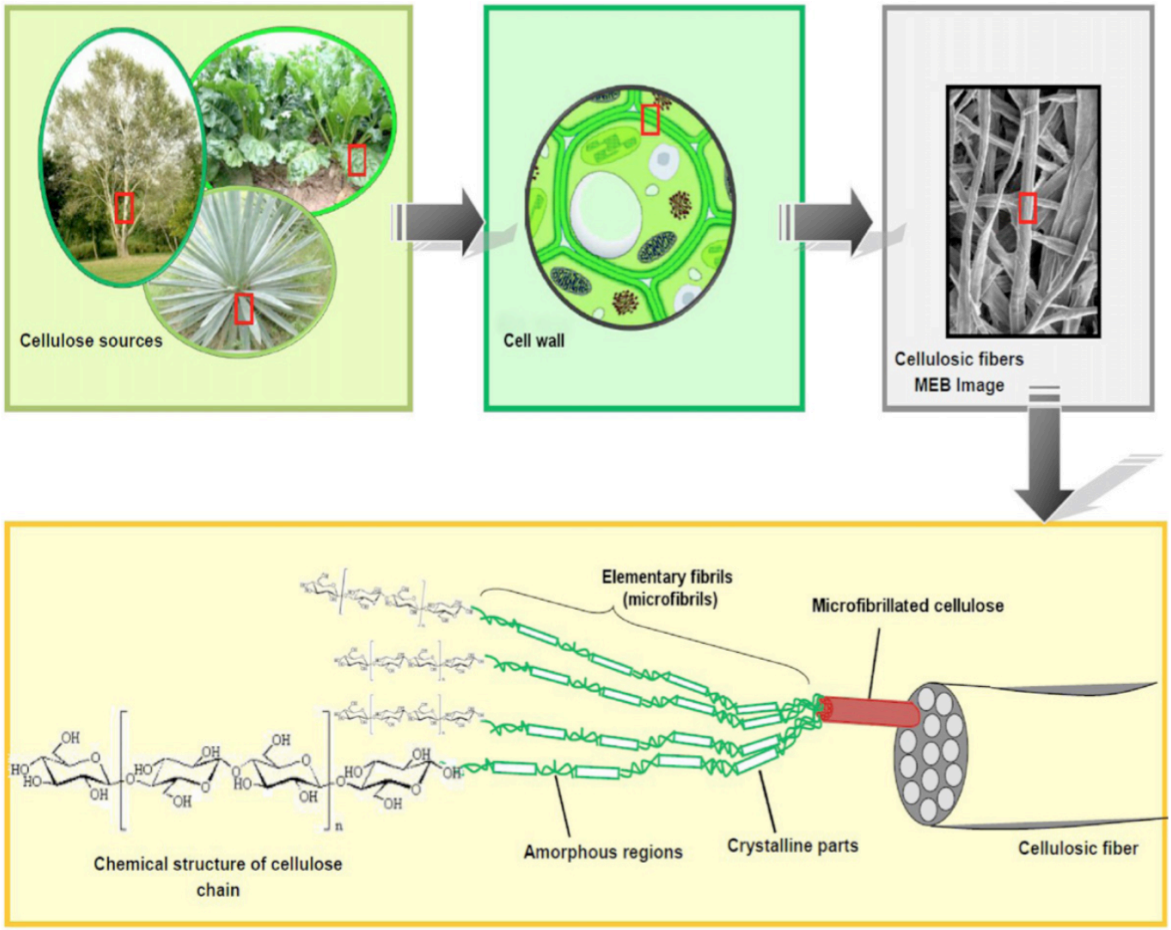

Figure 2. 10: from cellulose source to the molecular structure of cellulose adopted from [51]

Table 1. 3: chemical composition of some natural fibers adopted from [57].

Bast fibers					
Fiber type	**Cellulose %**	**Legnin %**	**Hemicellulose %**	**Pectin %**	**Ash %**
Fiber flax	71	2.2	18.6-20.6	2.3	-
Kenaf	31-57	15-19	21.5-23	-	2-5
Jute	45-71.5	12-26	13.6-21	2.3	0.5-2
Hemp	57-77	3.7-13	14-22.4	0.9	0.8
Ramie	68.6-91	0.6-0.7	5-16.7	1.9	-
Core fibers					
Fiber type	**Cellulose %**	**Legnin %**	**Hemicellulose %**	**Pectin %**	**Ash %**
Kenaf	37-49	15-21	18-24	-	2-4
Jute	41-48	21-24	18-22	-	0.8
Leaf fibers					
Fiber type	**Cellulose %**	**Legnin %**	**Hemicellulose %**	**Pectin %**	**Ash %**
Abaca	56-63	7-9	15-17	-	3
Sisal	47-78	7-11	10-24	10	0.6-1

Natural fibers exhibit large variation in properties depending on species and environmental conditions, this variation is due to differences in composition and the structure. Celluloses are polymers of repeated glucose units bonded together that gives fibers the strength. On the other hand, lignin is amorphous, hydrophobic, highly

complex matrix that is intermeshed in the plant secondary walls which repels water, allowing the plant to transport water up through its system. Hemicellulosic polymers are branched, fully amorphous and have a significantly lower molecular weight than cellulose. Hemicellulose is partly soluble in water and hydrophilic [58&59].

2.3.1 Fibers Surface Treatment

The final mechanical properties of natural fibers reinforced composites depend on the matrix, fibers and their interfacial bonding. They are highly affected by the adhesion between matrix and the reinforced composite, where the stress transfer between matrix and fibers and fibers wettability improve with good adhesion, leading to higher mechanical properties of the composite [60]. In the contrary poor adhesion leads to internal porosity, strains and poor mechanical properties also increase water absorption rates [61].

Chemical modifications such as introduction of coupling agents and chemical treatments (alkaline, peroxide) make the fibers more compatible with the hydrophobic polymers (polyethylene) by removing the large amount of hydroxyl group in cellulose the responsible of fibers most hydrophilicity, leading to improvement in adhesion, hence the mechanical properties of the composites are improved [57].

Different types of surface Modification of fibers are used to improve the interfacial interaction with matrix. Surface modification typically involves one of four methods chemical, physical, physical–chemical or mechanical. Chemical methods are the most common used in natural fibers surface modification. It involves treatment with chemicals to leach and make delignification of the fiber surface leading to rougher fiber surface [3]. Delignification is the removal of the structural polymer lignin from plant tissue [58].

Most of the chemically treated fibers showed a loss of fibers brittleness and a considerable reduction in the tensile properties which is attributed to the degradation of cellulose chains, disintegration of noncellulosic materials and the breakage of the bond structure during the chemical treatment. But no significant change occurs in the elongation of the chemically treated fibers [62].

Alkaline treatment (mercerization) is one of the most used chemical treatments of natural fibers when used as reinforcement in thermoplastics and thermosets, where alkali treatment processes are cost effective and have been widely used to improve natural fiber surface properties, and thus, composite properties [64].

In the alkaline treatment disruption of hydrogen bonding in the network structure occurs, thereby increasing surface roughness and fibrillation. This treatment removes a certain amount of lignin, wax and oils covering the external surface of the fiber cell wall. Removing lignin and wax reduces fiber diameter, thereby increasing the aspect ratio leading to good adhesion [63]. Also addition of aqueous sodium hydroxide (NaOH) to natural fiber promotes the ionization of the hydroxyl group leading to increase in the number of possible reactive sites and allow better fiber wetting [64]. The following equation [62] shows the mercerization reaction of natural fiber.

$$\text{Fiber-OH} + \text{NaOH} \rightarrow \text{Fiber-O}^{-}\text{Na}^{+} + \text{H}_2\text{O}$$

The alkali treatment of jute fibers produced a drop in both tensile strength and Young's modulus of the fibers. This was due to the excess extraction of lignin and hemicellulose that play a cementing role in the structure of the fiber, also the cell walls of the fibers exposed to damage. The same results were found for flax fibers with changes in flax fiber polymerization and molecular orientation [62&65].

Vilaseca et al [66] found that the NaOH treatment of jute strands increased the tensile and flexural strength of composites and the impact strength as well, where composite with fiber volume fraction equal to 30% showed that the tensile strength increased from 22.2 MPa to 26.3 MPa for untreated fibers and NaOH treated fibers respectively. This enhancement caused by means of a mechanical anchoring and the formation of hydrogen bonds at fiber–matrix interface, this was proven by Ph-NCO modified jute strand composites that blocked OH groups at the fibers surface what reduced the availability to form hydrogen bonds at fiber-matrix interface, so at fiber volume fraction 30% the tensile strength of Ph-NCO treated jute fibers reduced to 11.5 MPa.

Cao et al [67] studied the effect of NaOH concentration on the mechanical properties of bagasse fibers and bonding properties with starch based matrix. The best used

concentration to remove the lignin and hemicellulose without destroying the fiber was 1% concentration.

2.3.2 Date palm fibers

Usually, the used palm fibers in research are oil palm fibers and date palm fibers (DPFs) obtained from either leaves of the tree or mats that surround the tree stems. The date palm tree can grow for more than 100 years. It is widely spread in the Middle East, United States, Pakistan and India. There are more than 100 million date palm trees all over the world. Different parts of the date palm tree can be utilized to be used in different applications such as; ropes and baskets. Most of the wastes of date palm tree are used in low value products. Few studies focused in using fibers obtained from date palm tree as reinforcement in polymers [63].

Properties Palm tree stem is surrounded by mesh made of single fibers. This part of the tree is removed annually and used to make ropes. Date palm fiber (DPF) is polar by nature. The structure of (DPF) is a collection of multicellular fibers (2-5 μm in diameter and containing a central lumen). The shape of DPF is almost cylindrical and the outer surface is covered by lignin and impurities. Figure (2.11) clearly show the DPF structure [68].

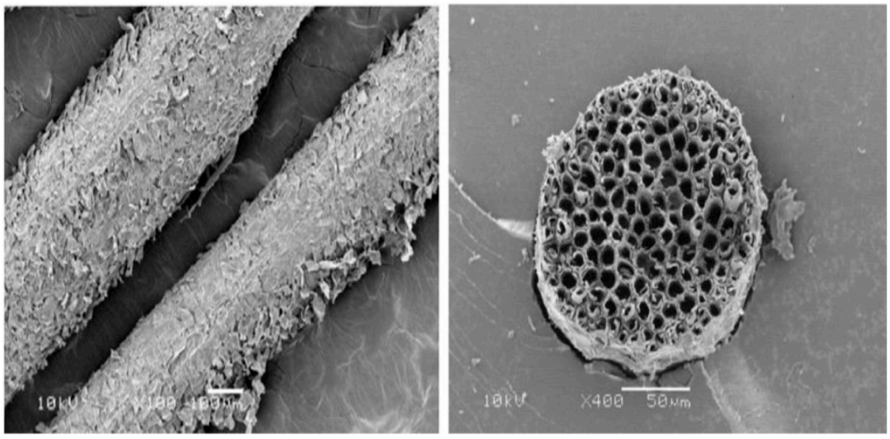

Figure 2. 11: SEM investigation of raw DPF adopted from [68].

The chemical composition of raw date palm fiber (DPF) is affected by plant's origin and agricultural parameters. Cellulose represents about 46% of its weight, but raw DPF has a higher amount of lignin (20%) when compare with other natural fibers, it has hemicellulose of about (18%) similar to other natural fibers. The rest is about 5% water and 11% of other impurities. The diameter of date palm fiber (DPF) is ranged from 0.1 to 1 mm, which is larger than most of other natural fibers [63]. The raw DPF has a density about 0.917 g/cm3 and thermal stability until 250°C. It has tensile strength varies from 60 to 275 MPa and young's modulus from 2 to 12 GPa [63&68].

2.3.3 Date Palm Fibers Preparation

Alkaline treatment is widely used to modify palm fibers surface. NaOH treatment for DPFs results in the largest increase in composite tensile strength and greatest thermal stability when compared to all chemical treatment methods. The maximum PDF tensile strength, the best fiber treated surface and better fibrillation achieved with 5% NaOH concentration for 2 hours at 100 ^{o}C [68].

The Alkaline treatment cleans the fiber surface and removes lignin from surface besides causing fibrillation. Due to severity of reaction of the alkaline solution, Increasing NaOH concentration increases the number of pores on the surface [63], this is clearly shown in figure (2.12).

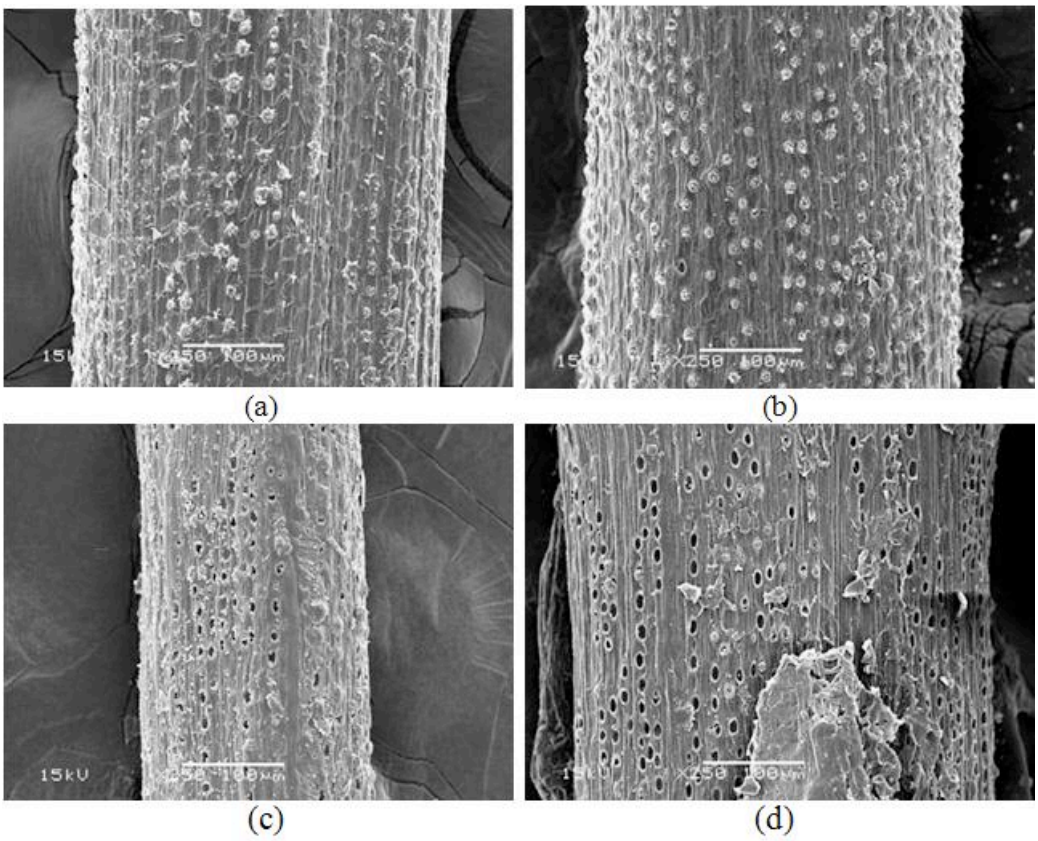

Figure 2. 12: SEM of NaOH treated DPF (a) 0.5%, (b) 1%, (c) 2.5% and (d) 5% adopted from [59].

Sreekala et al [69] studied the effect of different fiber surface modification methods such as (mercerization 5% NaOH, latex modification, Acrylation and Permanganate treatment etc.) on the mechanical properties of the oil palm fibers and her composite with phenol formaldehyde resin. IR-spectroscopy showed increase intensity of OH peaks what revealed that alkali treatment leaded to removal of hydrogen bonds. Almost all modifications reduced the fiber and composite mechanical properties but drastically increased the impact strength. The acrylated fibers had the greatest tensile strength and Modulus of 275 MPa and 11.1 GPa respectively. The maximum composite strength was recorded for the permanganate method with tensile strength of 40 MPa and mercerization method had the highest modulus of 1.3 GPa. The impact strength increased from 48 kJ/m^2 for untreated fibers composite to 190 KJ/m2 for latex modified fibers composite.

Alawar et al [63] studied the effect of alkaline treatment with concentrations 0.5%, 1%, 1.5%, 2.5% and 5% of NaOH, and acid treatment with 0.3, 0.9 and 1.6 N of HCL on date palm fibers (DPF) mechanical properties. All treatments were performed at 100

°C for 1 hour. The acid treatment caused deterioration in the tensile strength of PDF, while the alkaline treatment enhanced the mechanical properties of PDF, while maximum tensile strength of alkaline treated PDF was at concentration of 1% NaOH. It was about 3 times the tensile strength of raw PDF.

Bendahou et al [70] used untreated short palm tree fibers obtained from tree leafs as reinforcement in polypropylene (PP) and low density polyethylene (LDPE) with using maleic anhydride copolymers (MAH-g-PP and MAH-g-PE) as a compatibilizer for each matrix. They found that using compatibilizer improve the adhesion between matrix and fibers see figure (2.13), leading to better mechanical properties until fiber weight fraction less than 10%, where with more fiber content the mechanical properties start to decay again.

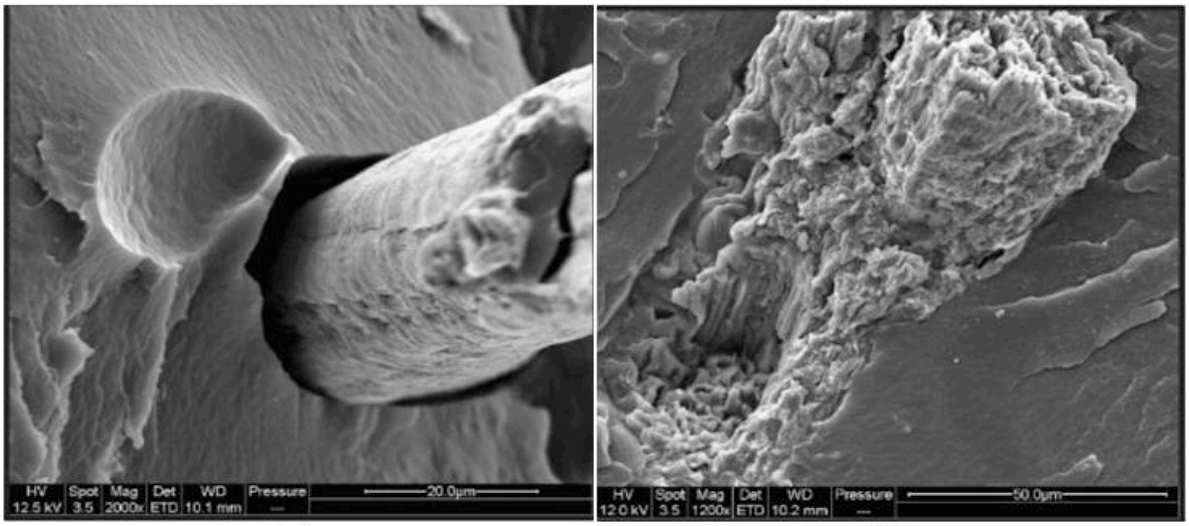

Figure 2. 13: SEM micrograph of PE-LD fracture surface: (a) without compatibilizer; (b) by using compatibilizer adopted from [70].

Bleach solution ($NaClO_2$) chemical treatment was reflected in the mechanical and physical characteristics as well as in the fiber's behavior during processing and wearing [16]. Bleach solution ($NaClO_2$) contains ClO ion which is found in chemicals widely used for bleaching pulp and paper.

Studies have been conducted wherein sodium chlorite ($NaClO_2$) was used in fiber surface treatment for composites. Mishra et al. [18&19] dipped untreated sisal fiber, for use in sisal–PS biocomposites, in sodium solution with a liquor ratio of 25:1 at 75°C for 2 h. Tensile strength

of bleached sisal fiber–PS composite was less than other chemical treated fiber composites which may be due to the fact that delignification of the fiber. But it was reported that flexural strength was better for bleached fiber composite because of lower stiffness and more flexible character of fibers after delignification. After delignification, the polymer replaces the role of lignin in fibers and makes composites more hydrophobic and tougher [18&19]. Similar result on tensile strength of bleached composites using sodium chlorite was also reported by Li et al. [20] on flax fiber–PE composites lowered its tensile strength.

2.3.4 Composites Reinforced with Natural fibers

The development of material with properties to meet the desired requirements for a specific application sometimes demands a compromise between different objectives. This can be performed by combine two or more different materials together to create a superior and unique material named composite material [3].

Composite's strong and stiff components are often the reinforcements that are embedded in softer component named the matrix. Reinforcements serve as the principal load-carrying members. The performance of composites, for example, the mechanical properties depends on the mechanical properties of its individual components, reinforcement shape (almost fibers) and content, fibers aspect ratio, fibers distribution and orientation. Also the interfacial compatibility between fibers and matrix is decisive in final composite mechanical properties, where it plays an important role on transformation of load from matrix to the fibers [5&71].

Reinforcements can be particulate, fibrous or structural. The fiber reinforcements can be (continuous-long fibers), (aligned and discontinuous fibers) or (randomly oriented and discontinuous fibers). Natural reinforcements from agricultural products almost have the fibrous shape and many of the natural fibers are short fibers. The aligned fibers result in superior mechanical properties but it is very difficult in conventional manufacturing processes to keep the fibers well aligned especially for short fibers [72].

2.3.5 Composites preparation and processing Methods

The most common processing methods used to prepare polymeric composites are screw extrusion, injection molding and compression molding.

Screw extrusion and injection molding methods are suitable for complex shaped products that need high shear stresses during processing. But the reinforced natural fibers are short and randomly oriented [3&5]. On the other hand, natural fibers compression molding can be used with short, long continuous fibers even with mats and fabric, besides being an inexpensive method for the production of lightweight and high-class interior parts in cars. Despite the limitations in shapes and designs that can be produced by compression molding, it is the dominant method in the production of natural fibers composites in the automotive industry [6].

Composite preparation is the mixing process, either mixing different constituents to the matrix (starch based blend), or mixing the prepared matrix material with the fibers. Mixers commonly used to mix natural fiber with biopolymers at elevated temperatures before compression or injection molding. For example, flax fibers were mixed with starch biopolymer at 150°C for 10 min with fiber mass fraction up to 30%, and then granulated in blade mill before injection molding [73]. Natural fibers mixing and compounding can be achieved by extruder where the fibers were fed manually into extruder with starch before processed into tensile specimen by injection molding [33].

Guimaraes et al [74] prepared the matrix using two types of mixers; a ball mill and mechanical mixer, and then the fibers were mixed homogeneously with starch in ball mill. Later a vibratory mill was used with mixing time of 1-3 hr. finally the mixture was subjected to pressure of 3-7 ton in steel mold at temperature between 110 and 170 °C.

Most of conventional mixing or extrusion methods of fibers with matrix cannot be used to produce high fiber content composite where the maximum fiber content that can be achieved is less than 50% [73&74].

Emulsion type resin is very suitable for high fiber content composites so higher strength and thermal stability can be obtained. Ochi [74] used the emulsion resin technique to add unidirectional Manila hemp fibers with volume fraction varied from 30% to 70%. First, the previously prepared starch resin was put on the surface of fibers and dried. Then the composite was set in metallic die and hot pressed at 10 MPa and 130°C for 10 minutes before it was preheated at 130°C for 5 minutes. Composite with fiber content of 70% had the highest tensile and flexural strengths of 365 MPa and 223 MPa respectively.

Takagi et al [76] reinforced 70% w/w cellulose microfibrils nanofibers in a starch-based dispersion type biodegradable resin. Nanofibers and matrix resin were mixed for 20 min using a home-use mixer, and then the composite excess water was removed with subsequent drying at 105°C by using filter paper before compression molding at 140°C and pressure of 10-50 MPa.

Shibata et al [77] fabricated Bio-based polymer composites made from longitudinal and transversal kenaf and bamboo fibers reinforced in biodegradable resin (corn starch-Polycaprolactone). The fibers were put into a cylindrical steel mold then the resin was added. The press forming was performed at 160 °C, 10 MPa for 10 min. The flexural modulus increased with increasing fiber volume fraction up to 60% for kenaf and 72% for bamboo.

Molding pressure has a considerable effect on the resulting physical and mechanical properties of biodegradable composites. Increasing molding pressure cause higher density composite, where applying high pressure, closes voids and improves adhesion between matrix and fibers, leading to improvement in the mechanical properties of the composite. For example, increasing molding pressure from 10 MPa to 50 MPa for starch resin / cellulose nanofibers composite increased the composite density from 1.03 g/cm^3 to 1.3 g/cm^3 respectively, there by the composite flexural strength and flexural modulus drastically increased from (29 MPa and 2.8 GPa) for molding pressure of 10 MPa to (49 MPa and 5.8 GPa) for molding pressure of 50 MPa [76].

2.3.6 Characterization of Biodegradable Composites

Characterization of any new developed material gives us an overview about its physical, mechanical and chemical properties under different conditions that allow us to enhance its properties and utilization. They also enable us to find the suitable areas of applications for this new material.

There are different properties that are very important for the understanding of biodegradable composites; these include density, thermal behavior (decomposition temperatures), water absorption, biodegradation behavior (degradation time) and of course the mechanical properties. Many factors affect the biodegradable composite properties such as processing conditions and techniques.

The mechanical properties of starch-based biodegradable composites depend on the type of fiber, its content, form and shape and orientation. They also depend on the matrix composition (plasticizers content).

2.3.6.1 Mechanical Properties

Many studies focused on how to improve the mechanical properties of lignocellulosic based composites. A study in MAPP kneading and extruding of flax bast fibers with Polypropylene (PP) and using maleated PP (MAPP) as a compatibilizer revealed that the flexural strength and flexural modulus increased from about 45 MPa and 1.5 GPa respectively at zero fiber content to reach about 100 MPa and 5.5 GPa at 50% fiber weight content [78].

Wollerdorfer et al [33] investigated the influence of adding lignocellulosic fibers such as (flax, jute, oil palm and ramie) on the mechanical properties of biodegradable polyester, polysaccharides and a blend of Thermoplastic starches (TPSs). The composites were produced by extrusion process followed by injection molding process. The maximum fiber content they succeeded to add was about 20-35% depending on the type of the polymer. The tensile strengths of all the polysaccharides and TPSs increased. For example, the tensile strength of TPS with flax fibers increased from 8.9 MPa for the zero fibers to 36.4 MPa for the 20% composite. However, no enhancement took place in polyester composites due to the chemical dissimilarity between polyesters and the lignocellulosic fibers.

Canigueral et al [73] studied the effect of flax fibers volume fraction % (10,20 and 30) % on

the mechanical properties of starch based composite and produced by means of high-shearing mixing followed by injection molding processing. The tensile strength and stiffness of the composite showed a lineal dependence with the amount of reinforcement, where the tensile strength increased by 42%, 83% and 112%, respectively, for those composites comprising 10%, 20% and 30% of flax strands. The tensile strength and young's modulus increased from 8 MPa and 360 MPa respectively at zero fibers content to 17 MPa and 1320 MPa respectively at 30% fibers content.

Oksman et al [79] reinforced 30 and 40 %wt of flax fibers in plasticized Polylactic acid (PLA) by using twin-screw extruder before being compression molded. The PLA-flax composite strength was about 50% better compared to similar PP-flax fiber composites. The tensile strength and modulus at 30 wt% flax fibers were higher that 40 wt% and reached 52 MPa and 8.2 GPa respectively.

Romhany et al [80] added 20, 40 and 60% of unidirectional and crossed-ply flax fibers to thermoplastic starch. The thermoplastic starch film and a layer of flax fibers were placed on one another alternately on 8 levels then hot pressed at 3 MPa and 140 ^{o}C. The tensile strength increases by increasing flax fiber content. At 60 wt % flax fiber content the strength and modulus were 78 MPa and 9.3 GPa respectively which is much greater than the mechanical properties of the pure matrix (24 MPa and 0.095 GPa).

Phattaraporn et al [81] used palm pressed fiber (PPF) as reinforcement in rice starch (RS) films at 10, 20, 30 and 40 % w/w of starch weight with different fibers diameter values (125, 177, 250 and 420 μm). Increasing palm fibers content improved the tensile strength, water resistance and thermal stability of the palm fibers/rice starch films (PPF/RSF). Fibers with diameter of 420 μm showed the best properties of all other diameters, where the tensile strength of 40% PPF at 420 μm was 16.26 MPa about 3 times the 0% rice starch film. This increase in tensile strength was combined by reduction in film elongation percent from 40.54% to 1.69% for (0% PPF/RSF) and (40% PPF/RSF) respectively.

2.3.6.2 Thermal Behavior

Thermal analysis is a set of techniques in which a physical property of a substance is measured as a function of temperature. Physical property can be (weight, temperature, dimensions, enthalpy, etc.). Thermo-Gravimetric Analysis (TGA) is the technique in which the weight loss of tested material is plotted against temperature. Differential Thermal Analysis (DTA) is another technique where the temperature difference between the substance and the reference is plotted against temperature. The difference in temperature almost displayed in micron volt resulting from the thermocouple signal voltage. DTA is used to investigate glass transition, recrystalization, melting, decomposition temperatures and decomposition behavior (endothermic or exothermic) [82].

Thermal degradation of starch-based composites is an important issue. TGA shows two major weight loss phases for native corn starch, the first till 100 ^{o}C for evaporation and hydration of water content while the second phase for the decomposition of starch at temperature around 300 ^{o}C [22].

Guimaraes et al [74] studied the thermal behavior of plasticized corn starch with 30% glycerol. TPS lost about 86% of its weight during the endothermic decomposition process between 315 and 495 ^{o}C.

Prachayawarakorn et al [83] found that the modification of thermoplastic rice starch (TPRS) with cotton fibers improved the decomposition temperature of the TPRS and for the composite as a whole. Where the decomposition temperature of TPRS with 5% cotton fibers increased from 301 to 305 ^{o}C, which may be resulted from the hydrogen bonding between TPRS and cotton fibers.

Soda treatment is known to enhance the thermal resistance of natural fibers. Al-Khanbashi et al [68] found that the alkaline treated date palm fibers (DPF) have the highest thermal stability among different chemical treatment methods as shown in figure (2.14).

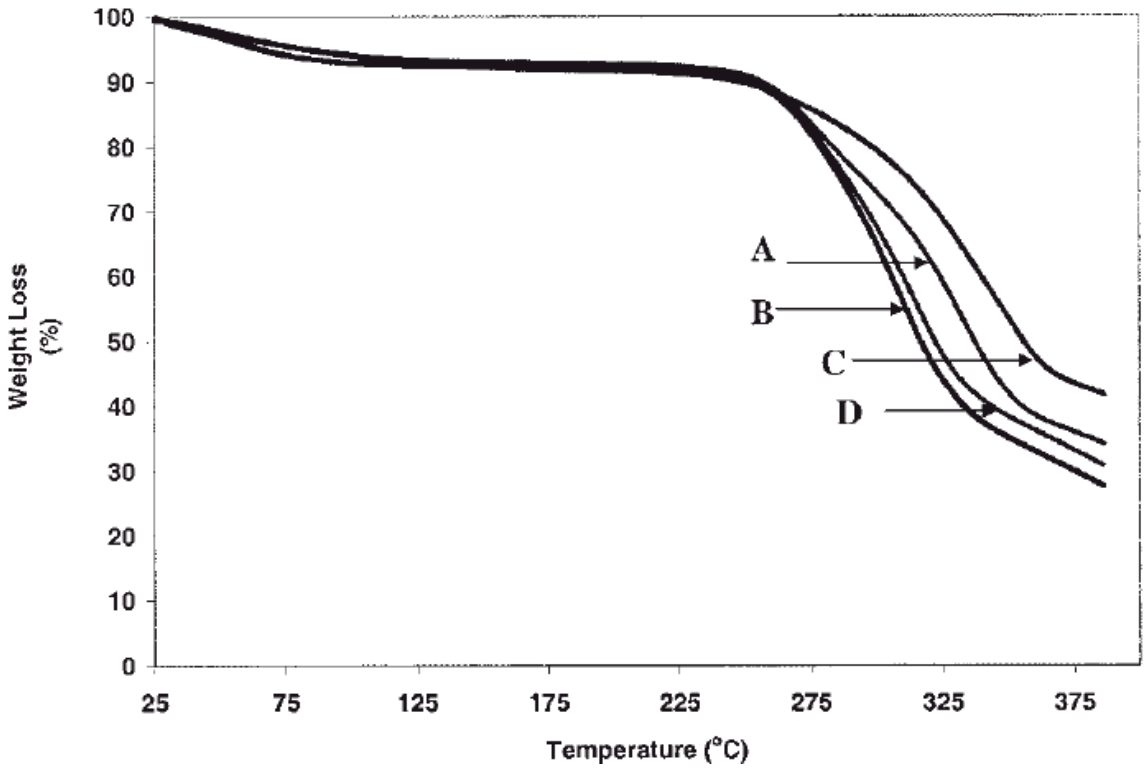

Figure 2. 14: thermal stability of DPF; (a) raw DPF, (b) detergent-treated DPF, (c) Soda-treated DPF; (d) dioxin-bleached DPF adopted from [68].

2.3.6.3 Water uptake

One of the major drawbacks in the use of lignocellulosic and starch-based composites is their water absorption tendency, where absorption of water badly affects the properties composite materials. For example, the difference in water uptake behavior of composite components makes poor dimensional stability (dimensional changes), thus weakness in the adhesion between the matrix and fibers takes place leading to poor mechanical properties [71].

Adding cotton fibers to thermoplastic starch was found to reduce the water absorption of the thermoplastic rice starch because of the less hydrophilicity of cotton fiber in comparison to starch hydrophilic property [83].

Guduri et al [84] tested the water uptake of polypropylene (PP)-short flax fibers composite with using and without using compatibilizer. The specimens were immersed in distilled water at room temperature for 24 hours. Moisture uptake measured daily for 3 weeks. After 500 hours the water weight gained percent of 20% and 30% fiber mass fraction were 1.4% and 2.5% respectively. Compatibilized composite had better mechanical properties and lower water uptake.

Gaspar et al [85] used saturated solutions of K_2CO_3, Mg $(NO_3)_2$.6H2O, NaCl, KNO_3 and distilled water to obtain relative humidity (RH) of 43, 54, 75, 91 and 100% respectively. They reduced the rate of water absorption in compostable Thermoplastic starch (TPS) by adding 10 v/v% polycaprolactone but without any improvement in the mechanical strength, where at 100% RH and after 14 days water uptake reduced from 60% for unfilled TPS to about 50% for 10 v/v% polycaprolactone filled TPS. Also applying hemicellulose and zein as additives enhanced the mechanical strength and produces a close structure that cause a lower water uptake.

Soykeabkaew et al [86] used conditioning jars filled by aqueous solution of LiCl, $MgCl_2$, $K2CO_3$, $Mg(NO3)_2$, and NaCl salts to have RH of 11.3, 32.8, 43.2, 52.9, and 75.3% respectively to test water absorption of flax fibers to reinforce starch foam (SCF) specimens at 25°C for one week.

2.4.4 Biodegradation

An irreversible process that leads to a significant change in the material structure that can be characterized by loss of properties such as (weight, mechanical strength and integrity) in specific time under specific environmental conditions caused by the effect of microorganisms like bacteria and fungi. Generally, the Biodegradability of composites is determined by their weight loss in soil burial. Table (2.6) shows the time for complete degradation under composting conditions for different materials.

Table 2.6: Time for complete biodegradation for various materials adopted from [3].

Material	**Time to degrade in the environment**
Cotton	1-5 months
PCL-g-MAH/starch	2 months
PCL-Starch	2 months
WG/PV A	1 month
WG/SCB	1 month
Conventional copy paper	1 month
PHB-PHB/Starch	1 month
Wool stocking	1 year
Bamboo stick	1-3 years
Chewing gum	5 years
Painted wood	13 years
Plastic	450 years
Glasses and tires	Uncertain time

PCL: Poly carpolactone; g: grafting; MAH: Maleic anhydride; WG: waste gelatin; PVA: poly vinyl alcohol; SCB: sugar cane bagasse; PHB: Poly hydroxyl butyrate.

Di Franco et al [87] buried disk shape samples (10mm diameter and 3mm thickness) in characterized soil with natural micro flora of polycaprolactone/starch blend (PCL/S) and sisal fiber-reinforced polycaprolactone/starch blends (SF-PCL/S). The samples were put into containers made of stainless-steel mesh before putting them at depth of 8 cm from the soil surface. The relative humidity was 40% and the temperature was 20°C. Biodegradation was determined by measuring samples weight loss for 9 months. In the first 5 months the weight loss of PCL/S was greater than SF- PCL/S composite, while at the eighth and ninth month the degradation of SF- PCL/S composite was much greater than PCL/S and reached 47%.

Kaith et al [88] used soil collected from the site of domestic waste water effluent to bury samples of corn starch based composites of (2 X 2 X 2.5 cm). The water level of the container was maintained to reach the surface of the soil.

Biodegradation was measured by FT-IR and SEM every 7 days. FT-IR test showed that in the first couple of weeks the cross links between chains (C=C and C–H) were broken. After 4 weeks the major degradation process was related to starch chemical groups. Finally, after 60 days all matrix chemical groups disappeared. While SEM investigation revealed that after 15 days of degradations, sample surfaces became heterogeneous and rough. After 4 weeks the reinforced fibers appeared on the surface. Finally, after 60 days the matrix totally disappeared and only fibers remained. The SEM degradation progress from (a) to (d) is shown in figure (2.15).

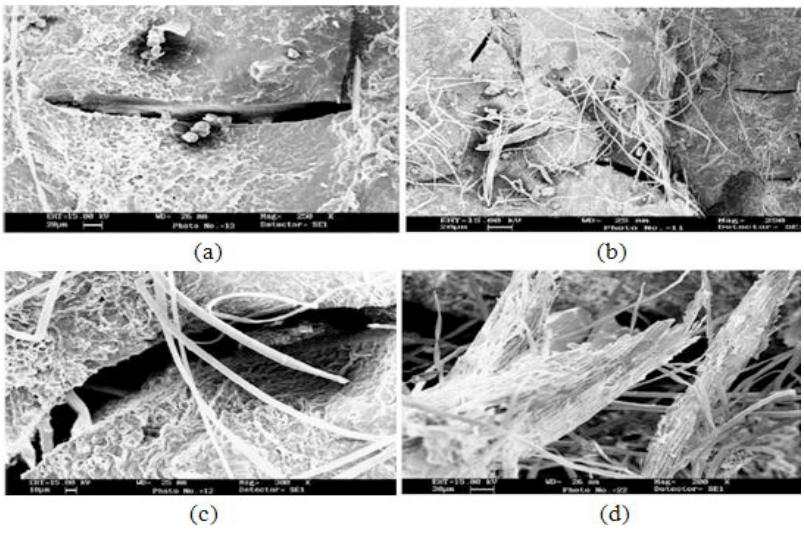

Figure 2. 15: biodegradation stages (a, b, c and d) of corn starch based composites adopted from [88].

2.4 Halloysite

The halloysite nanotubes (HNTs) are natural aluminumsilicate clay with hollow tubular structure and an empirical formula ($Al_2Si_2O_5(OH)_4 \cdot nH_2O$) that is structurally much similar to kaolinite [89]. The halloysite name is derived from the first one discovered the clay "Omaliusd Halloy" , the well-known geologist in Belgium in 1882. However, the naturally multilayer tubular halloysite, also known as hallosysite nanotube (HNT) was first described by Berthier (1826) as 1:1 dioctahedral layer silicate clay mineral of the kaolin group [90]. The publications on halloysite in the last two decades according to the Scifinder Scholar search shows increasing interest in using halloysite in research topics (Figure 2.14) [91]. Pure HNTs is usually white in color; however, depending on the type and concentration of impurities the color may transform from yellow to even brown color [92]. Generally, the using of nanotubes is considered the most effective in the nanotechnology research and applications [93].

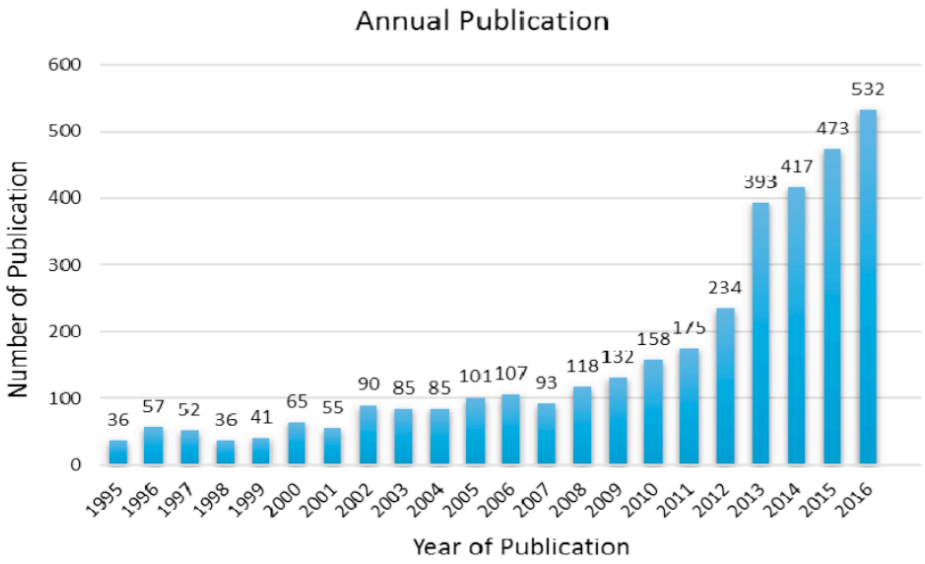

Figure 2. 16: Annual publication survey of scientific research publications on halloysite in the past two decades (using the SciFinder Scholar search system) adopted from [91]

2.4.1 Occurrence

Halloysite is often found near carbonated rocks and it is formed due to hydrothermal alteration of ultramafic rocks. In addition, halloysite is formed in volcanic rocks like rhyolite and basaltic which is formed as a weathering product by downward moving waters [94]. One of the biggest deposits of halloysite in Dunino, near Legnica in Poland that it has reserved halloysite material estimated at 10 million tons. The geologic occurrence of HNTs are found naturally deposited widely in mines in countries like china, America, Australia Brazil, France, Belgium and New Zealand [95,96,97].

2.4.2 Economic Overview

Haloysite was used in the past as a catalyst in petroleum cracking [98].

Halloysite has a great thermal stability because it is a clay mineral, so it is used to produce thin-walled porcelain or crucible products due to its high temperature resistance [99].

2.4.3 Structure

The crystal structure of halloysite was determined by Hofmann *et al.* and Mehmel [100]. The HNT hollow structure has been elucidated by the TEM micrograph in (Figure 2.17) [101]. The HNT dimensions are: the outer diameter ranges from 20 nm to 100 nm, the lumen diameter rangers from 5 nm to 30 nm, and 150 nm to 2 μm in length. This means that HNTs have high aspect ratio (length-to-diameter "L/D"). A schematic diagram in (Figure 2.18) shows the structure of the halloysite [102].

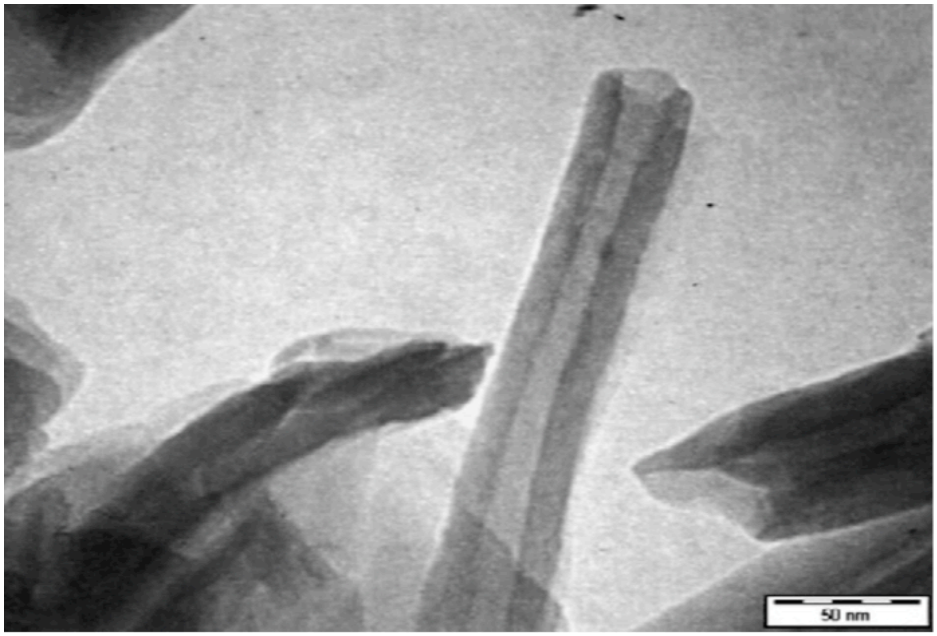

Figure 2. 17: TEM image of HNTs adopted from [101]

Halloysite as a clay mineral is made of two distinct structural units: Silicon tetrahedron and Aluminum octahedron, see (Figure 2.19). Several tetrahedrons joined together form a tetrahedral sheet and similarly an octahedron sheet is formed. The two sheets combine together by hydrogen bonds and apical oxygen sharing of the tetrahedron creating a stress on the basal oxygen. However, the presence of interlayer water molecules in the hydrated halloysite reliving the stress on the basal oxygen and will not affect the apical oxygen. To compensate this stress, Hal adopts both a rotation of the tetrahedron and a rolling of the unit layer to correct the mismatch between the plane of the apical oxygen and the plane of the inner hydroxyl and merges them into a single plane. In the rotation mechanism, adjacent tetrahedrons rotate in opposite directions to reduce the lateral dimension of the tetrahedral sheet by shrinking the distances to an equal value for the basal oxygen, silicon, and the apical oxygen in all directions in the ab plane. Generally, the natural Hal first undergoes the more efficient rolling mechanism to relieve the stress to the maximum extent and then undergoes the tetrahedral rotation to compensate the residual stress [103].

Apparently, the uniqness of halloysite is represented in its nanotubular geometry which is similar to the carbon nanotube (CNT), while its chemical composition is similar to nanoclays.

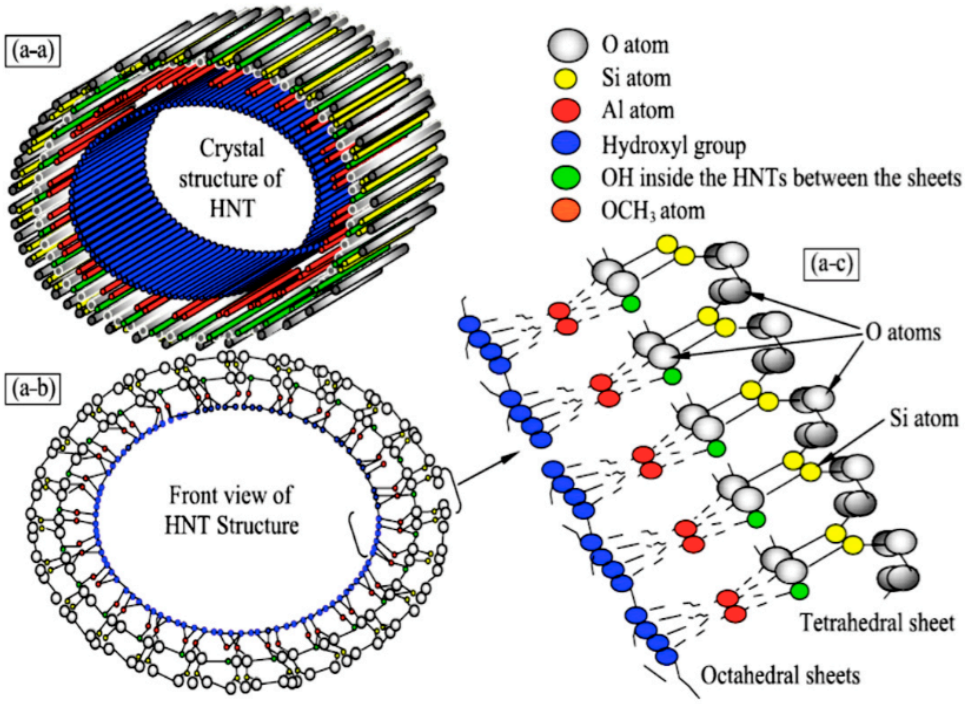

Figure 2. 18: The structure of the monoclinic unit cell of HNTs
3D view of HNTs (a-a), upper view of HNTs (a-b) & monoclinic unit cell of HNTs shows the outer tetrahedral sheets outside and the octahedral sheets inside (a-c) adopted from [102].

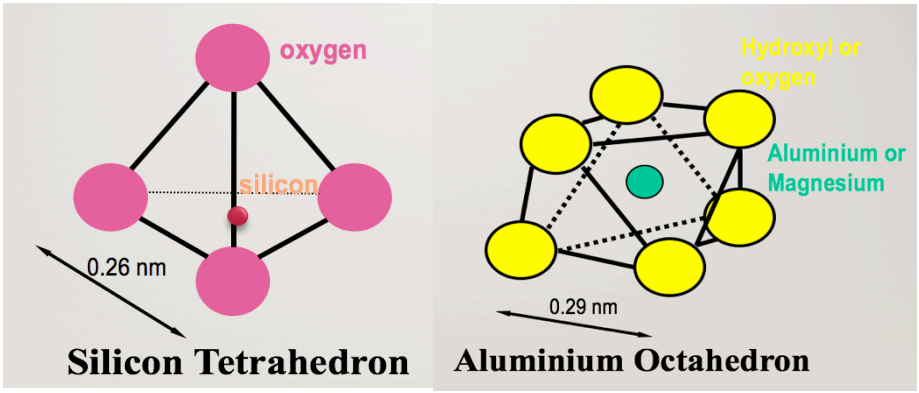

Figure 2. 19: Halloysite as a clay mineral is made of two distinct structural units: Silicon tetrahedron and Aluminum octahedron
The tetrahedron on the left has oxygen atoms at the corners, and there is a silicon in the center. Octahedron on the right has six oxygen or hydroxyl atoms in the corners, and an aluminum or magnesium ion at the center.

The tubular structure of HNTs is the most common and valuable morphology of the naturally occurring halloysite. The surface of HNTs contains siloxane (O-S-O) groups with a fewer hydroxyl groups compared to kaolinite and montmorillonites. In addition, the chemical difference between halloysite and kaolinite is that halloysite contains monolayer of water between its unit layer except that they have the same chemical formula of

($Al_2Si_2O_5(OH)_4 \cdot nH_2O$), where n represents the number of interwater layers, see (figure 2.20). Considering the hydration state of HNT, there are two hydrated forms [104]:

1- When n= 2, the d_{001}-value of the layers spacing is 10 Aº and the halloysite is named "halloysite-(10 Aº) or hydrated HNT" which means it contains one interlayer of water molecules between each layer in the hallysite structure.
2- When n= 0, the d_{001}-value of the layers is 7 Aº and the halloysite is named "halloysite-(7 Aº) or dehydrated HNT" which means it does not contain interlayer of water molecules that can be obtained by mild heating or vacuum environment and the process is irreversible.

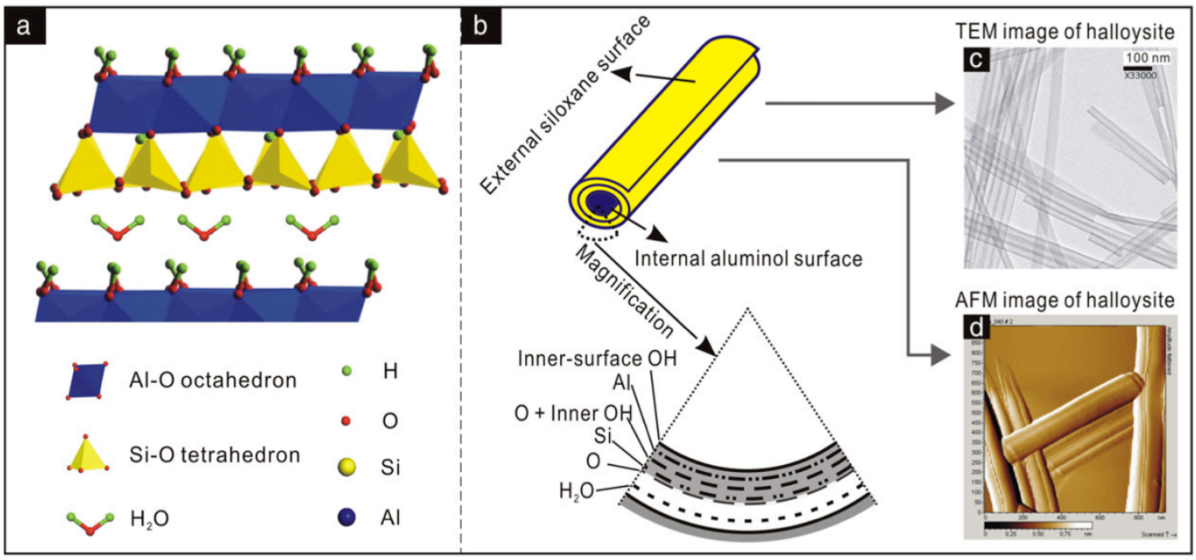

Figure 2. 20: diagram of the structure of HNTs (10 A°)
a: the crystalline structure of HNTs, b: structure of the HNTs layer represents the interlayer water, c: TEM image of HNTs and d: AFM image of HNTs adapted from [104]

2.4.4 Properties of Halloysite Nanotubes (HNTs)

a) Mechanical properties of HNTs

The halloysite nanotubes by itself as a single layer of montmorillonite has a young's modulus equal 2.7GPa according to Monte Carlo simulation [16]. When the young's Modulus of single multi-walled (15-20 layers) HNT was measured experimentally by TEM bending stage, it appeared that HNT has a young's Modulus (130 ± 24 GP) which is lower than that of single wall HNT due to the structural defect in the multi-walled HNTs [105&106]. The great mechanical property of HNTs is they are highly flexible that they can bend to 90º without

fracture [104&105]. In addition, HNTs with smaller diameter than 50 nm can reach elastic modulus 460 GPa which is three times more than HNTs with diameter ranges from 50 -160 nm which also is greater than elastic modulus of single walled HNT. This jump in elastic modulus is due to absence of structural defect and the increase in surface tension with decrease in HNTs diameter [105,107,108&109].

The introducing of HNTs as a nanofiller always improves the tensile strength, flexural properties, and impact strength by 10% than the same neat material without HNTs [110,111&112].

HNTs are green promising reinforcing nanotubes for thermoplastics because the percent of the heavy metals detected in the reinforced materials was much lower than standards of the restriction of harmful substances of the European Union [113].

b) Flame retardancy of HNTs

Inorganic clay minerals, especially those have layered structure, are the most common and effective filler at the nanoscale to enhance thermal stability and flame retardency of organic polymers. Apart from using HNTs as a reinforcing agents, Halloysite as a ceramic material can significantly increase the thermal stability and flame retardency of many polymers when it is used as a nanofiller. The properties of polymers will be expanded in many restricted applications if their thermal stability and flame retardency enhanced. Some researchers explained the improvement of flame retardancy to that halloysite acted as a barrier against heat and mass transfer, as well as from the trapping of polymer decomposition products in the lumen of the nanotubes [114&115].

For example, the limiting oxygen index (LOI) of the widely used low-density polyethylene (LDPE) has increased by 20% after dispersing 2 wt %HNTs in it [115]. In addition, Nylon 6 (PA6) that has an inherent degree of flame retardancy (limiting oxygen index (LOI) 21–25%) after adding HNTs has shown 25% and 75% decrease in total heat released (THR) and peak of heat release rate (PHRR) respectively during combustion by cone calorimeter [115]. The same improvement achieved on PA6 has also achieved on epoxy [116] and natural rubber [117]. Reinforcing polypropylene (PP) with HNTs have demonstrated significant flame retardency and have increased its burning time with minimum heat release than that of neat pp (Figure

2.21) [118]. In conclusion, HNTs may be considered an easily available, effective, and affordable mineral clay for flame retardency and thermal stability of organic polymers.

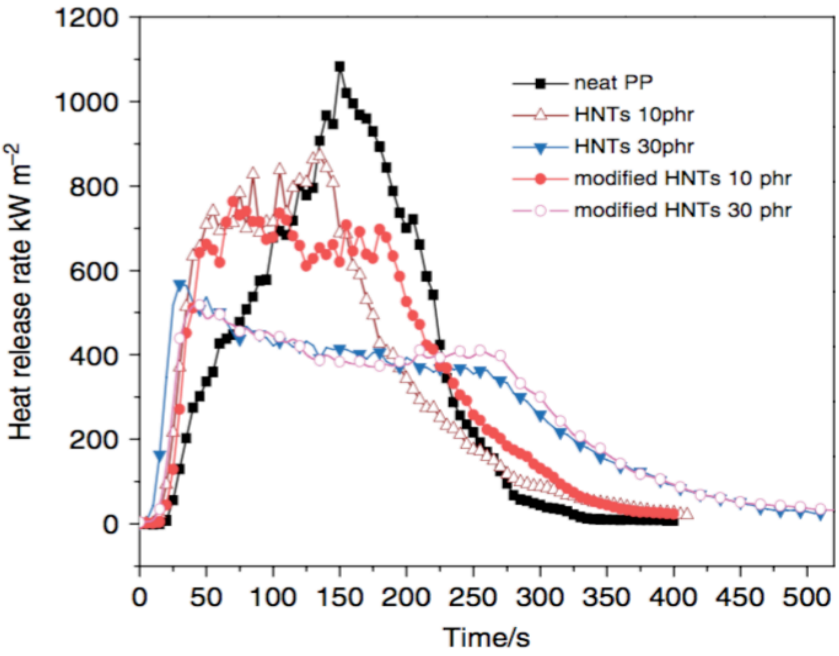

Figure 2. 21: Heat release during burning of neat pp and HNTs/pp nanocomposite adopted from [118]

2.4.5 Polysaccharide HNTs composites

The using of HNTs to reinforce polysaccharides will overcome the drawbacks of other nanoparticles or carbon nanotubes (CNTs) includes: brittleness, difficulty with fabrication, low fracture strength, high density and inadequate biocompatibility [119].

a. Surface interactions between HNTs and polysaccharides

The polysaccharides can adhere to the surface of HNTs without closing the tubes. This could be due to the interaction between the surface hydroxyl groups on HNTs and those in the polysaccharides by hydrogen bonding and covalent bonds or physical interactions [120]. By using high resolution TEM Liu *et al.* [120] elucidate the wrapping of the alginate

polysaccharide on the surface of the HNTs and partial filling of the tubes by alginate. This appears due to the increase in width of the HNTs from a maximum of about 85 nm of pristine HNTs to 115 nm for the alginate–HNTs and the presence of external layer on the HNTs surface see figure (2.22). The same phenomenon appeared in using amylose with HNTs to make a direct evidence that polysaccharides have the ability to coat the surface of the HNTs due to the interfacial interactions which means compatibility that will stabilize the composite [121].

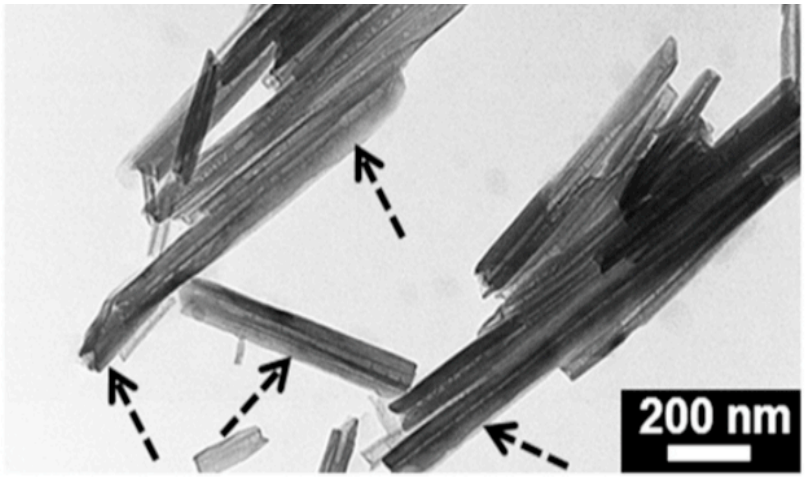

Figure 2. 22: TEM image shows the presence of alginate polymer wrapping around the HNTs [121]

b. Crystal structure of the polysaccharide-HNT composite

The crystal structures of polysaccharide-HNT composites can be investigated by X-ray diffraction (XRD). For pure CS scaffolds, a broad scattering reflection is located at ~ $20^{o}2\theta$, indicating that it is amorphous in the present preparation condition [34]. The HNTs exhibit diffraction peaks at $12^{o}2\theta$, $20^{o}2\theta$ and $25^{o}2\theta$ which are assigned to the (001), (02, 11) and (020) planes of HNTs, respectively [122]. The locations of the diffraction peaks of HNTs in the composite remained unchanged, indicating that no intercalation of CS into the interlayer of tube walls occurred. The intensity of the (001) reflection relative to the (02,11) band increased with increase in HNT loading [121].

c. Mechanical properties of the polysaccharide-HNT composites

Due to the rigid HNTs nanotubes with large aspect ratios and interfacial reactions taking place between HNTs and the polysaccharide matrix, the polysaccharide-HNT composites exhibit significantly improved mechanical properties such as tensile properties, bending flexure, compressive properties, and dynamic mechanical properties both in the dry and wet states. However, the decreased strength and Young's modulus of composites with larger HNT contents (>7.5%) are related to the presence of HNT aggregates in the composites [121]. HNTs have been used to reinforce the major polysaccharides used in biomedical engineering to enhance their mechanical properties as shown in (table 2.7)

Table 1. 4: The effect and load percent of HNTs into polysaccharides on the tensile strength and young's modulus adopted from [31].

Polysaccharide matrix	HNTs loading %	Method of composite preparation	Improvement in tensile strength and young's modulus	Reference
Starch	Polyethylene glycol modified HNTs	Solution mixing	50% increase in tensile strength	[119]
Starch	6 wt. %	Melt-extrusion	Tensile strength and elastic modulus increase up to 28% and 95%, respectively.	[123]
Chitosan	7.5 wt.%	Solution casting	Tensile strength = 54.2 Mpa Young's modulus = 1240 Mpa	[124]
Cellulose	8 wt.%	Mixing with ionic liquid 1-butyl-3-methylimidazolium chloride	Tensile strength = 60 Mpa	[125]

d. Thermal properties of the polysaccharide-HNT composites

The glass-transition temperature (Tg) and thermal stability of polysaccharides can also be affected by the Polysaccharide-HNT composites in biomedicine addition of HNTs. The Tg value of the CS-HNT composites increased consistently with increase in HNT loading [36]. The maximum Tg of the composites was 172°C for the composites with 10% HNTs, which was 12°C higher than that of pure chitosan. In addition, the intensity of the loss tangent (tan δ) peaks for composites is less than that of pure CS, as the CS can dissipate more energy applied to the sample due to its viscous response at high temperature.

The interactions between HNTs and chitosan can also affect the thermal stability of the CS-HNT composites [126]. The degradation temperature of CS is increased slightly by the addition of HNTs, while the degradation temperature of HNTs is decreased slightly compared to pristine HNTs. For example, for the chitosan sample (weight ratio of CS and HNTs = 1:4), the degradation temperatures of chitosan and HNT components were 277 and 477°C, which are 4°C higher and 6°C lower than pure chitosan and pristine HNTs, respectively. De Silva et al [127] also found that the corresponding temperatures of chitosan-HNT membranes at 50% remaining weight had increased drastically compared with pure chitosan. The increase in the thermal stability of chitosan is attributed to the effective delay in mass transport during the thermal decomposition via the addition of HNTs.

e. Biocompatibility of HNTs/polysaccharide composites

By increasing the use HNTs in biomedical applications, many studies will be required to investigate the toxicity of the HNTs on the living tissues. The viability of fibroblast and endothelial cells were tested on a scaffold of HNTs/Chitosan nanocomposite in comparison to neat chitosan scaffold that shows no reduction in cell viability and growth with good absorbance and formation of intercellular junctions which indicating normal growth of cells [121&124]. *In vivo* studies of biocompatibility of HNTs / chitosan sponge preparation were studied in wound healing ability that showed faster healing without scar formation than neat chitosan sponge preparation [126&128].

CHAPTER (3) EXPERIMENTAL WORK

The experimental work was carried out in the laboratories of School of Science and Engineering of the American University in Cairo (AUC).

A detailed explanation of experimental work will be discussed in this chapter.

3.1 Materials

Commercial corn starch

Commercial corn starch was purchased from market. It is produced by Aro Sheri Company in Egypt. The purchased corn starch moisture content was measured and equaled about 2% wt which was considered in plasticized starch preparation.

Glycerin

Glycerin with 99.7% purity was used. It was purchased from El-Gomhouria CO.

Halloysite nanoclay

HNTs powder was purchased from Sigma-Aldrich with Linear Formula $Al_2Si_2O_5(OH)_4 \cdot 2 H_2O$ and Molecular Weight 294.19

Sodium chlorite

Sodium chlorite ($NaClO_2$) extra pure (purity 80%) white powder was purchased from Loba Chemie laboratory reagents and fine chemicals.

Date palm fruit bearing branches

The fruit bearing branches of date palm trees were supplied from research institute for a sustainable environment (RICE) in the American University in Cairo (AUC).

Sodium hydroxide (NaOH)

NaOH with molecular weight 40.00 was purchased from Alamia Company for Chemicals.

Acetic acid

Glacial acetic acid with 99.9% was purchased from Teba for Chemical Industries.

Steric acid

Steric acid with assay 98% was purchased from Alamia Company for Chemicals.

3.2 Experimental Procedure

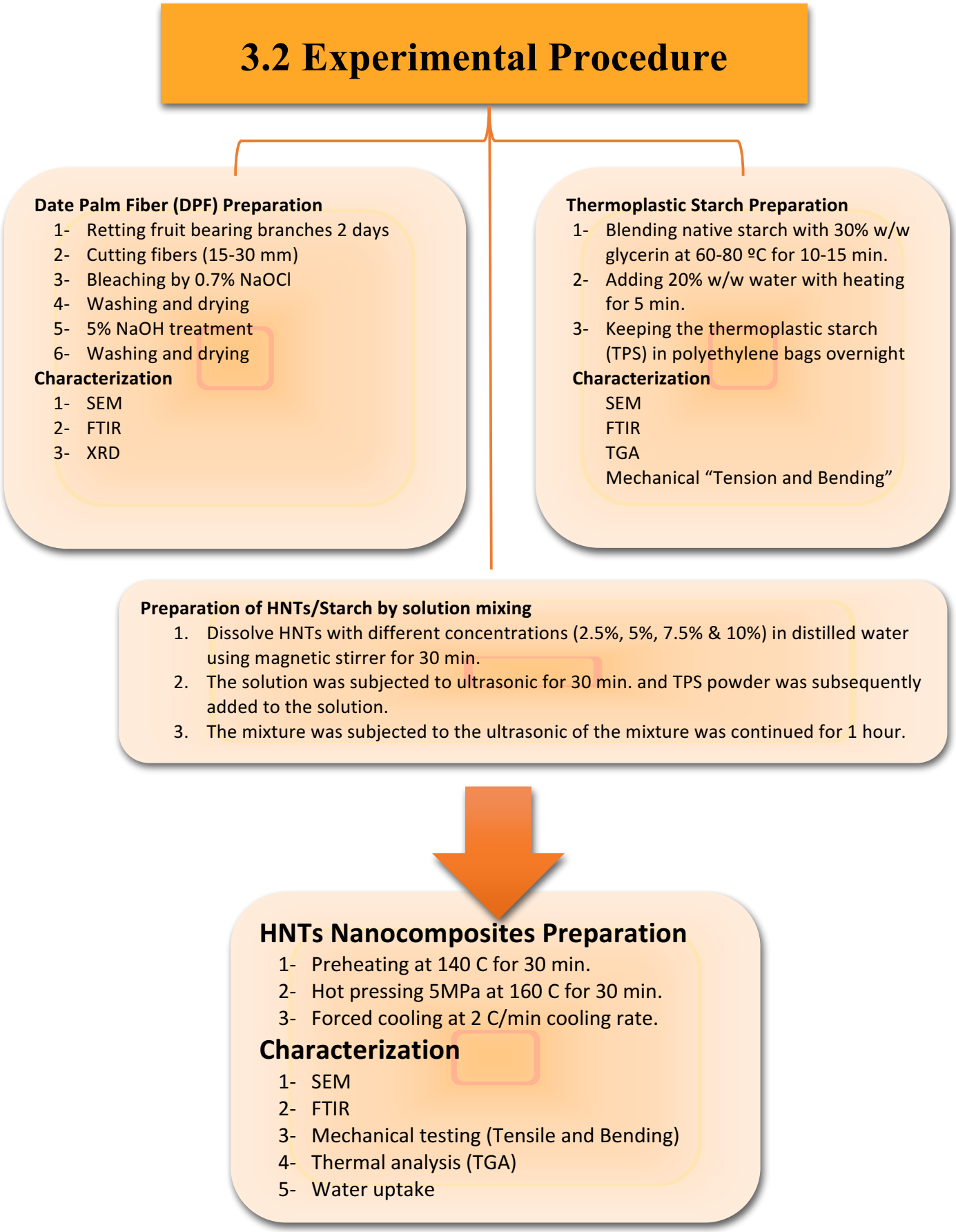

3.2.1 Date palm Fibers

a. Preparation and treatments of date palm Fibers

Fruit bearing branches is the branches that hang from the palm tree top carrying the fruits as shown in figure (3.1).

Figure 3. 1: fruit bearing branches in date palm tree.

Fibers from fruit bearing branches were processed by retting technique, where fruit bearing branches were soaked in water at room temperature for 5 days to allow bacteria to feed on lignin and hemicellulose between fibers. Then the groups of stacked fibers were separated longitudinally before being cut transversely by scissors to get small pieces with lengths from 20 to 30 mm. A batch of these pieces about 30 gm were subjected to mechanical treatment by blending them in a home use blender with 300 ml of water. Blending performed 4 times each for 15 seconds at maximum speed. The blended fibers were then dried in oven at 120 ^{o}C for 3 hours as shown in figure (3.2a).

In order to remove the lignin layer around the fibers according to literature [80], the dried dissembled fibers were then bleached by using (0.7%) (w/v) sodium chlorite solution (fiber to liquor ratio of 1:50) at P^H 4 adjusted by adding acetic acid and the mixture was boiled for 5 hours to remove the lignin and the process was repeated twice until the fibers became white. The bleached fibers were washed again then dried in oven at 120 ^oC for 3 hours to be ready for preparation of the nanocomposite figure (3.2b).

Figure 3. 2: The final shape of palm fibers after cutting and mechanical blending and b: bleached fibers

For cellulose isolation, the dried fibers were then soaked in 5% NaOH solution at 90 oC for 3 hours. Then the fibers with NaOH solution were stirred in home use mixer for 30 minutes at temperature from 80-90 ^oC. NaOH treated fibers were then washed several times by cold water in sieves to get rid of most of separated lignin, before being dipped in 5% acetic acid solution to remove any excess NaOH from the fibers surface as shown in figure (3.3). Fibers were washed again then dried in oven at 120 ^oC for 3 hours. Finally, the dried fibers were put in small blender for very short time to dissemble fibers entanglements and agglomerates.

Figure 3. 3: The final shape of palm fibers after NaOH treatment

According to literature [63], 1% NaOH solution is the concentration that gives maximum DPFs strength. This was for DPFs that were obtained from fibers surround the date palm tree stem not the fruit bearing branches as in our case. In this study the use of 5% NaOH solution gave separated and fine fibers that can be used.

b. Field Emission-Scanning Electron Microscope (FE-SEM) investigation of fibers

before SEM observation the samples were coated with gold using a putter coater (BALTEC SCD 005). The scanning electron microphotographs (SEM) of date palm fibers (DPFs) before and after treatments with NaOH and sodium chlorite were taken by using SUPRA 55 ZEISS FE-SEM operating with a vacuum pressure 1e-4 mbar and eht 8 kV.

c. XRD of fibers

X - ray diffraction (XRD) is a versatile, non - destructive technique that reveals detailed information about the chemical composition and crystallographic structure of natural and manufactured materials. XRD is an apt method to examine whether a resultant material has amorphous or crystalline nature. In crystalline solids, the constituent particles (atoms, ions or molecules) are arranged in a regular order. The interaction between X - rays of and a particular crystalline solid helps in investigating its actual structure. In the present work,

XRD patterns were recorded using X'per PRO PANalytical and Rigaku X - ray diffractometer (RINT - 2200) with CuK radiation at 0.02 / sec step interval.

The principle behind the design of powder diffraction experiments is the random orientation of crystals in a powder. If the powdered crystals are randomly oriented, then for all sets of planes (h k l) some of the crystals in the powder will be in the correct orientation (horizontal) with respect to the X - ray source to satisfy Bragg's law for the proper angle . In other words, at least a few of the mineral grains in the powder will diffract for each of the planes (h k l) during a scan through the angles.

X - ray diffraction is based on constructive interference of monochromatic X - rays from a crystalline sample. When a focused X - ray beam interacts with these planes of atoms, the beam undergoes various modifications like transmission, absorption, refraction, scattering and diffraction. The diffracted beam can provide information about the d - spacing by applying Bragg's law given by,

$$n\lambda = 2d \sin\theta \qquad (3.1)$$

where n is an integer, is the wavelength of incident wave, d is the spacing between the planes in the atomic lattice and is the angle between the incident ray and the scattering planes.

d. Fourier transform infrared spectroscopy (FTIR) of DPF

The spectra of the dried fibers were measured using NICOLET 6700 (Thermo scientific). Thirty-two consecutive scans were taken and their average were stored. Spectra were taken from 4000 to 400 cm^{-1}. Their resolution of the wavenumber was 2 cm^{-1}

3.2.2 Thermoplastic starch matrix

A home-use mixer was used in preparing thermoplastic starch blend. In order to supply heat during starch gelatinization process, a heating coil was especially fixed around the mixer vessel as shown in figure (3.4). Dry native starch was placed in the mixer vessel before adding 30% w/w glycerin on weight basis of dry starch and keeping mixing for 10 minutes at temperature range (60-80) ^{o}C. Then 20% w/w distilled water on weight basis of dry starch was added during mixing, the mixing process continued for another 5 minutes at the same temperature.

Figure 3. 4: home-use mixer with the heating coil.

The using of 30% w/w glycerin content was the most common in literature to facilitate processing without glycerin's exudation and to reach a compromise between resulted matrix strength and brittleness [36&37]. While adding 20% w/w water was to obtain the maximum strain at break with high tensile strength [39]. Thermoplastic starch (TPS) blend was then kept in polyethylene bags overnight to enhance its flow properties [36].

3.2.3 Adding HNTs and fibers to matrix

Various methods of mixing fibers and matrix were tried, including mixing short fibers with thermoplastic starch blend in home use mixer and adding fibers as two mats between layers of thermoplastic starch blend. Both methods led to uneven distribution of fibers in the matrix. Eventually, an emulsion technique was found to be a good alternative for preparing high fiber content composites. In the emulsion technique, fibers were carefully distributed in the die cavity to insure regular distribution of fibers. Preliminary experiments showed that the water content of the emulsion needs to be increased as the fiber content of the composite increases. Therefore, thermoplastic starch (TPS) blend and HNTs was emulsified in water with ratios of (TPS: water) equal (1:3) for (50 wt%) fiber content. Finally, the emulsion was poured carefully on the fibers inside the die cavity as shown in figure (3.5).

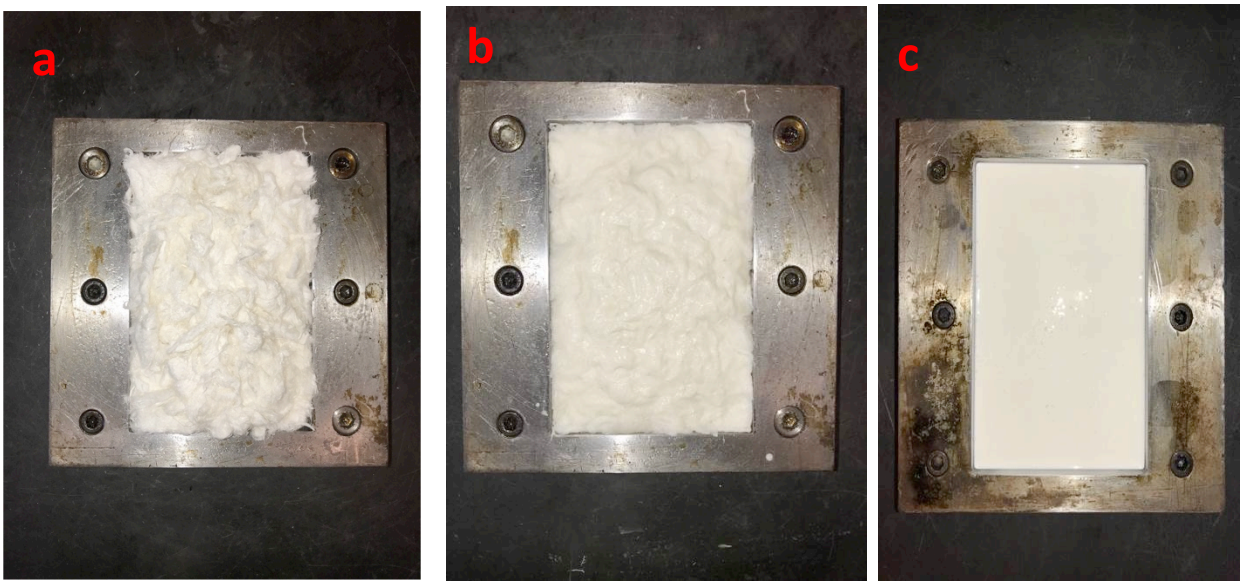

Figure 3. 5: preparation of the die for compression molding (a) fibers in die before adding emulsion; (b) after adding TPS emulsion and (c) the emulsion of HNTs/TPS poured in the die for heating and pressing.

3.3.3 Compression molding

Compression molding was chosen as a processing method because it is suitable for high fiber content and different fiber shapes, besides being inexpensive in the industrial scale relative to other processing techniques [6]. A metallic positive-type mold made of steel was made to overcome the problems of undefined actual pressure applied on the material. In the positive-type mold, the full molding pressure is exerted on the material which leads to better plasticization and suppresses the formation of voids in the specimen. The assembly drawing of the metallic mold can be shown in figure (3.6).

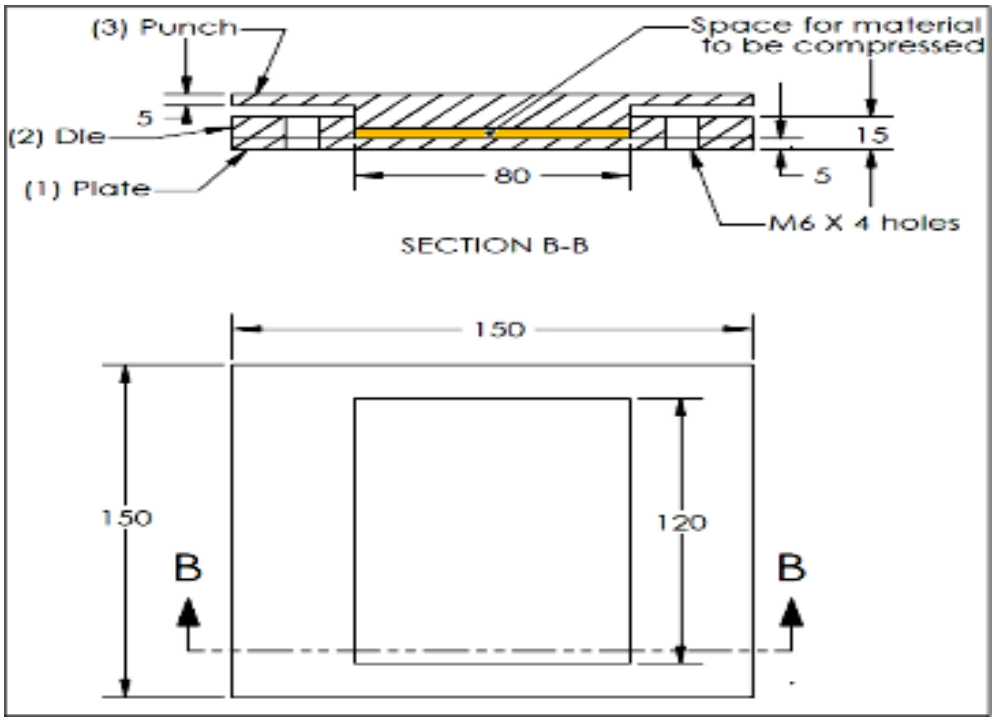

Figure 3. 6: assembly drawing of the metallic positive-type mold.

The metallic mold was coated by steric acid to work as a releasing agent in order to prevent adhesion between the composite material and the mold. After the composite materials were placed in the metallic mold as previously stated, the mold was placed on a hydraulic press figure (3.7). Then the material was subjected to preheating for 30 min at 140 ^{o}C, followed by thermal molding for 30 min at 5 MPa and 160 ^{o}C before forced cooling by fan with cooling rate equals 2 ^{o}C/min. Two thermocouples, one in each plate of the mold, were used to measure the temperature, which was maintained within ±3 ^{o}C of the specified preheating and molding temperatures.

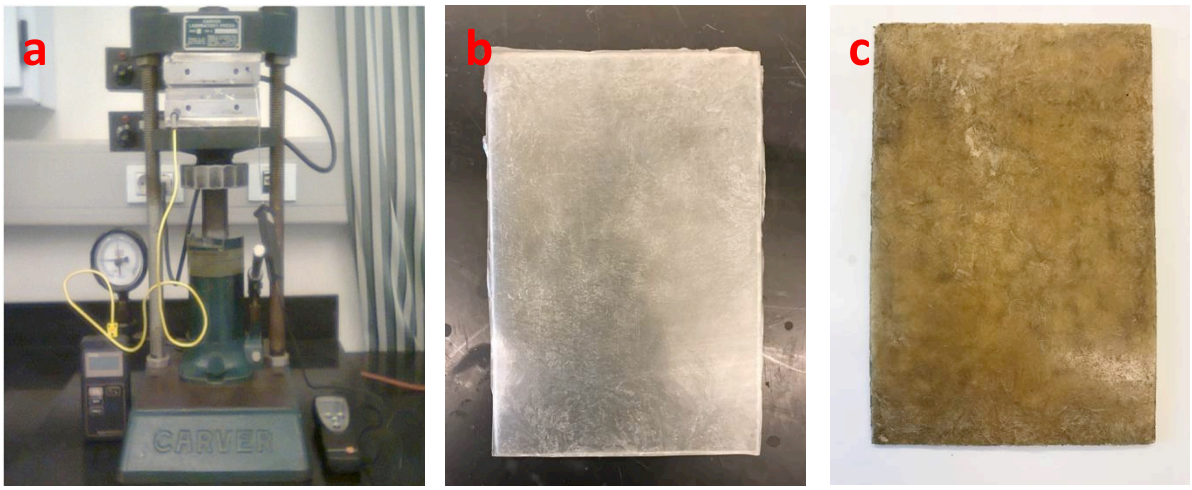

Figure 3. 7: the press used and samples produces
(a): Carver Laboratory Press Model C; (b) hot pressed HNTs/TPS nanocomposite 120x80x2 mm; (c) hot pressed HNTs/DPFs/TPS nanocomposite sample

Processing parameters (temperature and pressure) were chosen as much as possible to maximize the properties of the resulting composites. According to literature increasing molding pressure enhances the mechanical properties of the composite [76], 5 MPa was the maximum pressure that can be accomplished by the available press. Most research works in TPS was performed at molding temperature varies from 130-170 ^{o}C [75,76&108]. And in this work; when temperature exceeds 180^{o}C the TPS based matrix begins to burn.

3.5.5 Thermal Analysis

Thermo-Gravimetric Analysis (TGA) tests were carried out by 60Hz detector and under 20 ml/min flow of Nitrogen atmosphere. The tests were carried out at temperature range from 0 to 900^{o}C for matrix (zero fiber), HNTs reinforced TPS based nanocomposites (2.50, 5, 7.5 and 10 wt%), HNTs/DPFs/TPS reinforced nanocomposites (2.5, 5, 7.5 & 10 wt%).

3.5.6 Water uptake

The effect of adding fiber on composites water absorption tendency was studied. A humidity chamber (desiccator) was set up at 100%RH using distilled water figure (3.8). The samples with dimensions (80x8x2) mm were dried at oven at 100 ^{o}C for 4 hours, weighted and were then placed in the humidity chamber. The test was carried out at room temperature. The weight difference was measured daily until the mass of the samples were almost constant.

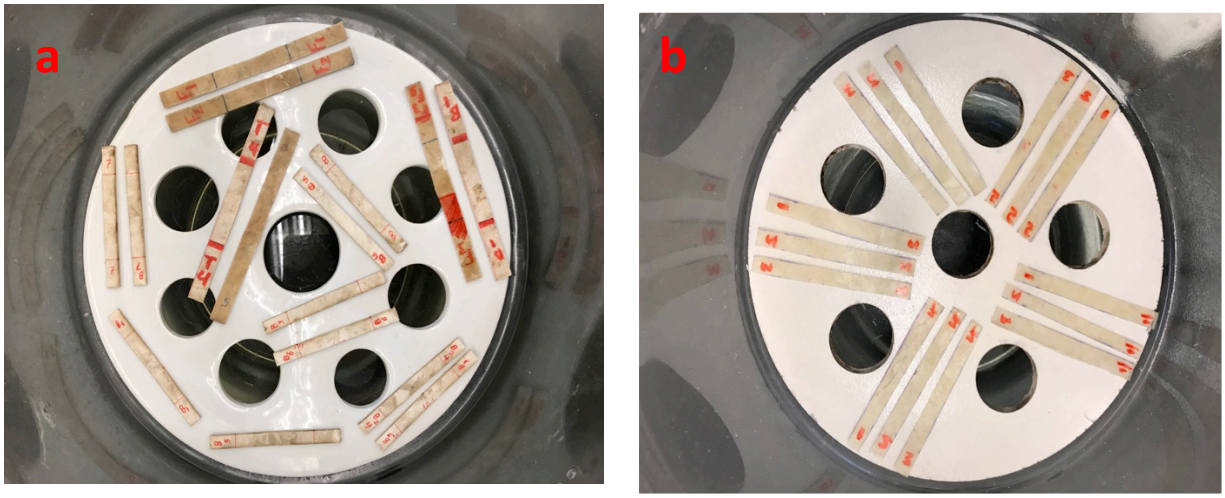

Figure 3. 8: the humidity chamber with samples inside it.
(a) HNTs reinforced TPS based nanocomposites and (b) HNTs/DPFs/TPS reinforced nanocomposites

CHAPTER (4): RESULTS AND DISCUSSIONS

4.1 Fiber characterization

4.1.1 SEM Investigation

To study the effect of both alkaline treatment and bleaching sodium chlorite ($NaClO_2$) on the surface of date palm fibers, untreated and treated fibers were investigated using SEM.

Figure (4.1) shows untreated date palm fibers. The raw palm date fiber is cylindrical in shape. Most of fiber surface is covered by lignin and impurities that hinders the direct contact between matrix and the strong cellulosic part. Figure (4.2) is for the DPF subjected to mechanical treatment that shows an improvement in surface morphology. The mechanical treatment cleaned the fiber surface and caused surface fibrillation so the mechanical anchoring will improve the mechanical properties.

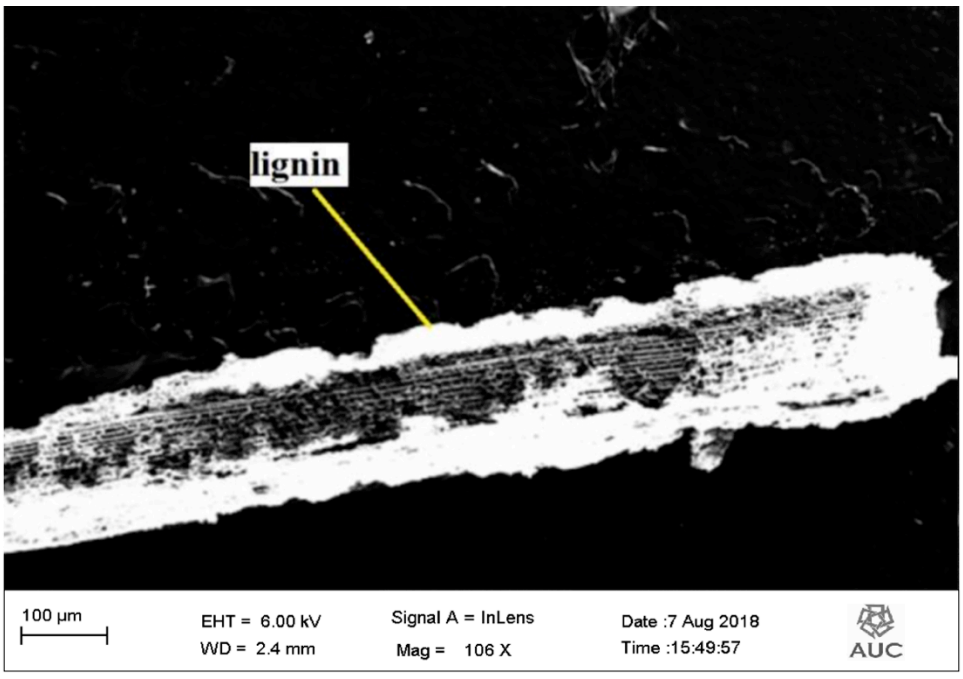

Figure 4. 1: SEM investigation of untreated DPFs.

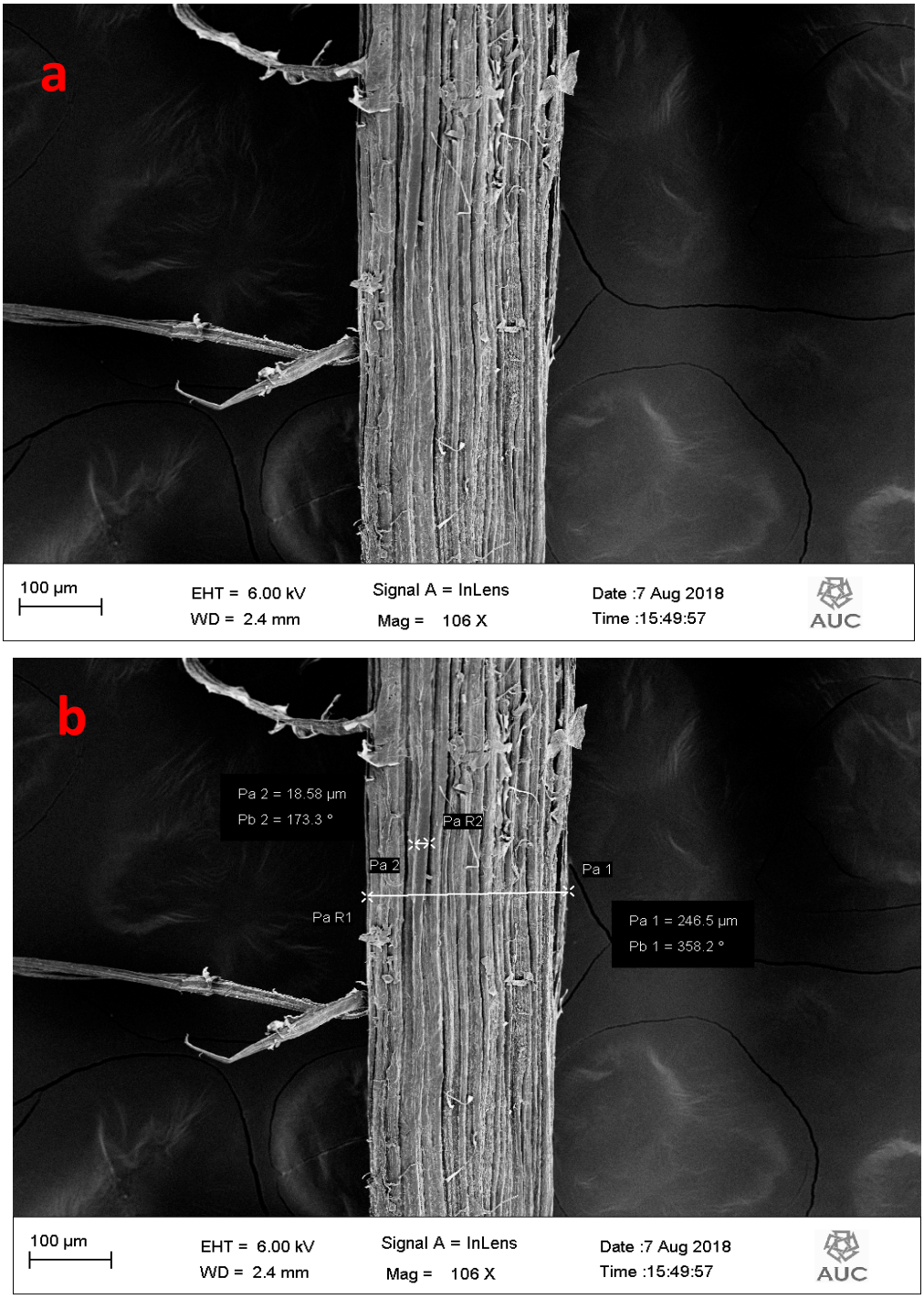

Figure 4. 2: SEM investigation of treated DPFs with mechanical treatment
a: Delignified DPF shows the fibrils that are still attached due to the interfibrils lignin, b: shows the width of the DPF and one microfibril.

As can be seen in figure (4.3) that the Date palm fibers after bleaching by sodium chlorite ($NaClO_2$) and NaOH treatment. Sodium chlorite ($NaClO_2$) bleaching causes clear delignification and fibrillation due to the removal of the interfibrils lignin which will disrupt this the fiber complex structurel. The fibers treated by NaOH to remove lignin completely and partially hemicellulose that will cause more fibrillation of the DPF because hemicellulose is not in a crystalline state and acts as a bridge between cellulose and lignin [129].

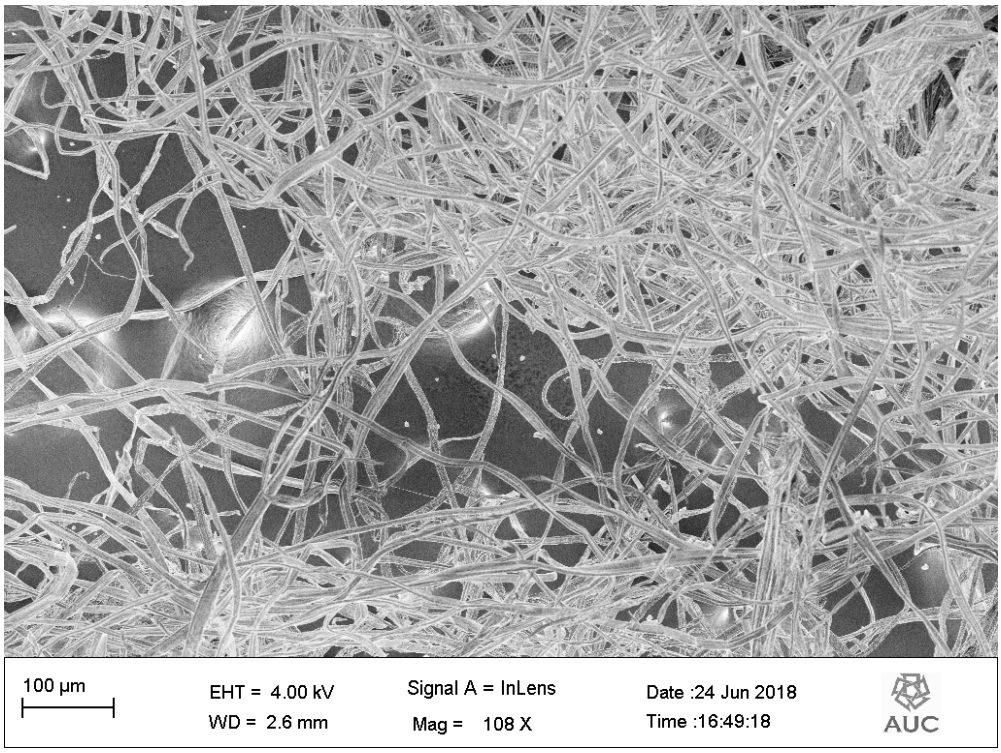

Figure 4. 3: shows the final shape of DPF after bleaching by sodium chlorite and NaOH treatment.

4.1.2 Fourier transform infrared (FTIR) spectroscopy

FTIR spectroscopy is an indispensable technique used extensively for studying and tracking changes in the chemical structures of the fibers after the various chemical treatments as shown in figure (4.4). Table (4.1) contains the most significant absorbance bands assigned to the functional groups of cellulosic natural fibers [125].

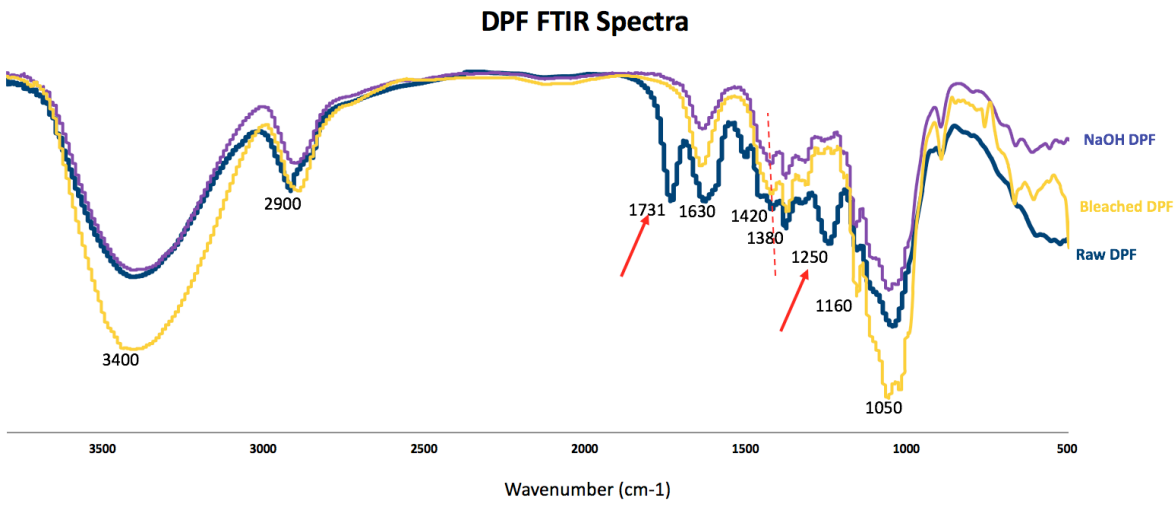

Figure 4. 4: shows the FTIR spectra of raw DPF and after bleaching by sodium chlorite (NaClO2) and NaOH treatment

Table 4. 1: Positions and assignments of the IR vibration bonds appear in DPF spectra.

Peaks (cm^{-1})	**Assignation**
3300 – 3450	-OH bond
2890 - 2900	aliphatic saturated C–H stretching vibration
1630	Absorbed water "bending" vibration
1420	CH_2 symmetrical bending
1380	bending vibrations of the C–H and C–O groups of the aromatic rings in polysaccharides
1160	-C – O bond stretching of the C ▪O ▪H bounds
1050	-C – O stretching

The prominent peak at 1,731 cm^{-1} in the spectrum obtained for the raw fiber (pointed by red arrow) was assigned to the C=O stretching of the acetyl group and uranic ester groups of the hemicellulose or to the ester linkage of the carboxylic group in the ferulic and p-coumaric acids of lignin and/or hemicellulose [130]. The peak at 1,250 cm^{-1} (pointed by red arrow) corresponds to the C–O stretching of the aryl group in lignin. These last two peaks were completely absent from the spectra of the alkali-treated fibers and bleached fibers. Taken together, these findings indicate that most of the hemicellulose and lignin were removed [131].

In addition, the characteristic band at 1424 cm–1 (the CH2 scissoring band for cellulose I) shifts to 1418 cm–1, indicating the destruction of the intramolecular hydrogen bonds and the formation of cellulose II. This shift is attributed to the change in the form of the hydroxyl rotamers in positions “3” and “6” (co-rotations around bonds C3–O3 and C6–O6) [132].

4.1.3 X ray Diffraction

The crystal structures of cellulose from DPF under different treatments can be investigated by X-ray diffraction (XRD) in figure (4.5). All the diffractograms were typical of semi-crystalline materials, displaying an amorphous broad hump and crystalline peaks.

Three well-defined crystalline peaks typical of cellulose I were present at around 2θ = 16°, 22 °, and 34.5°. As expected, the magnitudes of these crystalline peaks increased upon purification of cellulose and removal of amorphous lignin and hemicellulose

The regenerated cellulose exhibits three characteristic peaks at around 2θ = 12.5° which corresponds to (1 1 $\bar{}$ 0) plane, whereas the sharper peaks at 2θ = 20.5° and 2θ = 22 ° correspond to (110) and (2 0 0) planes respectively. These peaks are consistent with a transformation of cellulose I to cellulose II. The intensity of the peaks increases after bleaching and NaOH treatment of the fibers which indicates successful removal of lignin and the amorphous hemicellulose.

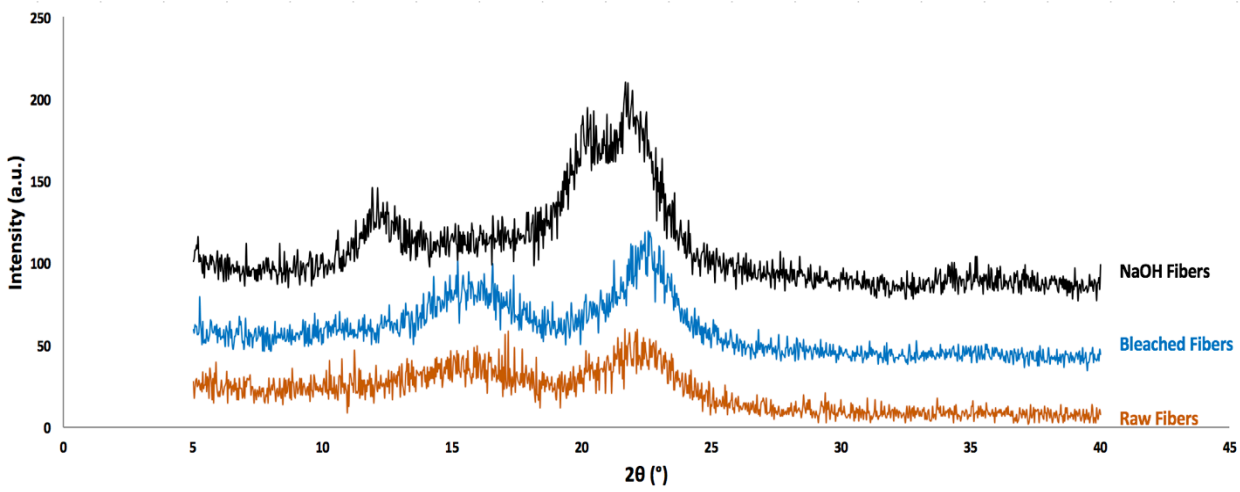

Figure 4. 5: X-ray diffraction patterns for Raw DPF, NaOH treated DPF, and Bleached DPF

The crystallinity (I_c) was determined by means of Eq. (1) using the height of 2 0 0 peak ($I_{2\,0\,0}$, 2θ = 22°) and the minimum between the 200 and 110 peaks (I_{am}, 2θ =12.5°). $I_{2\,0\,0}$ represents both crystalline and amorphous material while I_{am} represents amorphous material.

$$I_c = \left[\frac{I_{2\,0\,0} - I_{am}}{I_{2\,0\,0}}\right] \times 100 \qquad (4.1)$$

The crystallinity index of untreated DPF (calculated by Segal formula) was approximately 35%. The increase in crystallinity index was due to complete removal of lignin and the peeling reactions that take place in the amorphous areas during the NaOH treatment and bleaching. These findings confirm that the non-cellulosic amorphous polysaccharides were efficiently decreased by the treatment [132].

Generally, cellulose in natural fibers comes in four types of cellulose that are classified as types I, II, III, and IV. The major distinction between the two forms of cellulose I and II lies in the layout of their atoms: cellulose II has antiparallel packing, whereas the chains in cellulose I run in a parallel direction. It is interesting to note that the untreated DPF shows typical cellulose I structure, based on the fact that there is no doublet in the main peak at $2\theta = 22^{\circ}$ [133]. After treating the DPF with sodium hydroxide and bleaching, the crystalline peak appears as a doublet at $2\theta = 20.5^{\circ}$ and $2\theta = 22^{\circ}$, representing transformation of native cellulose from cellulose I to cellulose II. A significant variation in the direction pattern of untreated and cellulose fibers can be explained by the replacement of OH groups by ONa groups during alkaline treatment. Subsequent rinsing with water will remove the linked Na-ions and thus causing the cellulose to be converted to a new crystalline structure, which is cellulose II or regenerated cellulose [134].

4.2 TPS Matrix Characterization

4.2.1 Native and gelatinized starch SEM morphology

Granules morphology of native commercial corn starch is stone like poliedric shape and irregular sizes with particle size varied from 4.9 to 33 µm and the average size about 16 µm.. Figure (4.6) is for the blend of overnight stored plasticized corn starch (TPS) made of native starch with 30% w/w glycerin and 20% w/w water with heating. It shows that the starch particles are agglomerated and connected together by strong starch-glycerin interactions. The strong interaction is by virtue of heated mixing and storage overnight [3&36].

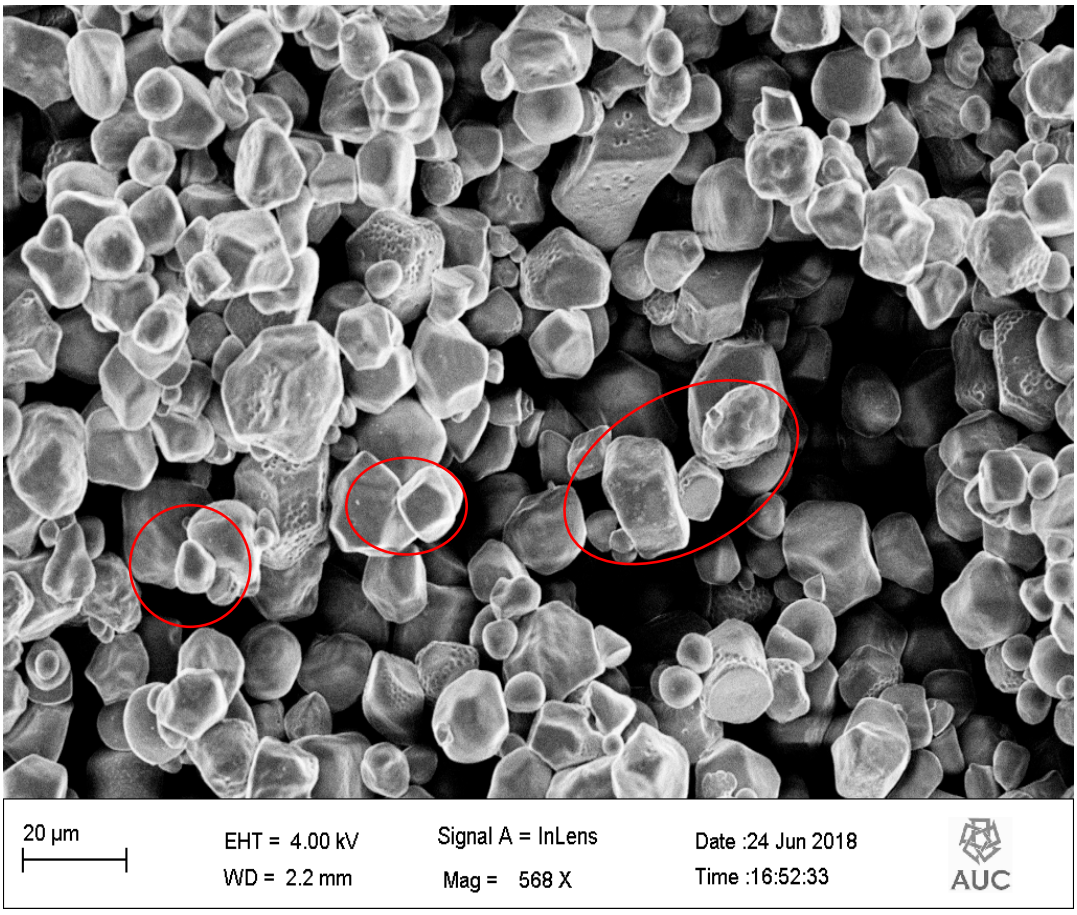

Figure 4. 6: SEM investigation for plasticized corn starch.

4.2.2 Fourier transform infrared (FTIR) spectroscopy

The FTIR spectra of TPS is shown in figure (4.7) and their assignation is reported in table (4.2)

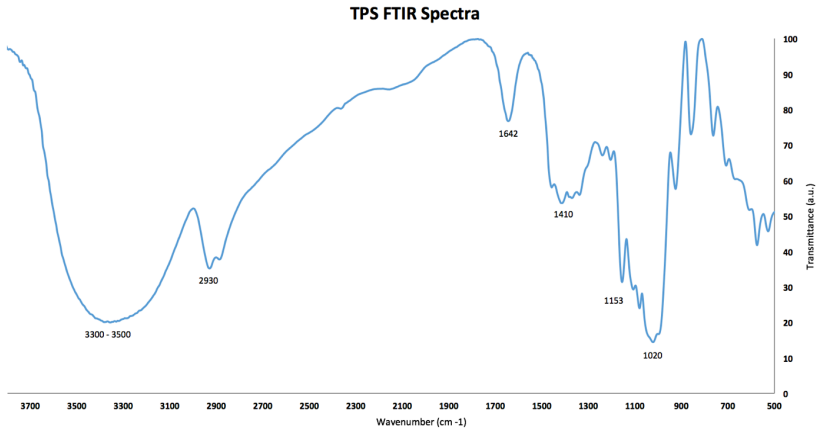

Figure 4. 7: Shows the FTIR spectra of TPS

Table 4. 2: Positions and assignments of the IR vibration bonds appear in TPS spectra.

Peaks (cm^{-1})	**Assignation**
3300 – 3500	-OH bond
2930	aliphatic saturated C–H and C–H_2 stretching vibration of glucose rings
1642	Absorbed water "bending" vibration
1420	CH_2 symmetrical bending
1153	-C – O bond stretching of the C –O –H bounds
1020	-C – O stretching in C – O – C group in the anhydroglucose ring

4.2.3 Mechanical Properties

The hot pressed TPS-based matrix by emulsion technique and compression molding was subjected to tensile and flexural testing; the mechanical properties were as shown in table (4.3).

Table 4. 3: hot pressed TPS matrix tensile and flexural properties.

	Tension Test			**Bending Test**		
	Ultimate Tensile Strength (Mpa)	**Young's modulus (MPa)**	**Max. Strain %**	**Flexural Strength (MPa)**	**Flexural modulus (MPa)**	**Strain % at Max. stress**
TPS matrix	3.8	378	5.25	6.7	685	3.4

4.2.4 Hot pressed matrix fracture surface morphology

The granular structure of the TPS is no longer visible after hot pressing. Figure (4.10) shows the fracture surface of thermoplastic starch (TPS)-based matrix compression molded by emulsion technique. The fracture surface of TPS-based matrix fabricated by the conventional technique, where 20% w/w of water and 30% w/w of glycerin mixed with starch while heating then the TPS blend was compression molded. Rough fracture surface and presence of dimples mean high material ductility.

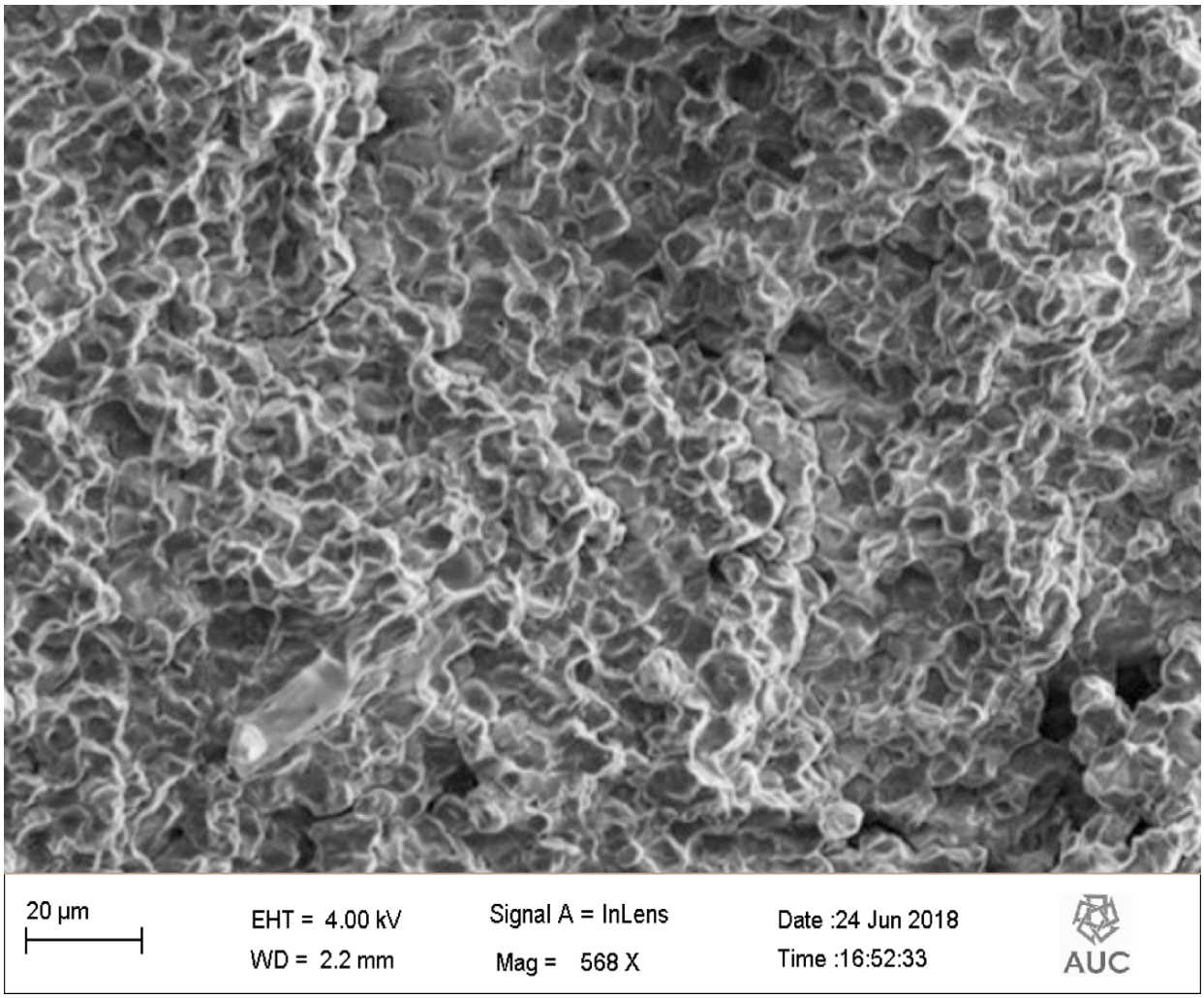

Figure 4. 8: FE-SEM fracture surface investigation of hot pressed TPS blend.

4.2.5 Thermal Gravimetric Analysis (TGA) of TPS

Thermal degradation of the thermoplastic starch (TPS)-based matrix is an important factor to identify the limits of processing, treatment or operating temperatures. Figure (4.9) shows the TGA curve obtained for the hot pressed TPS-based matrix by emulsion technique, where the percentage loss of the sample weight and the derivative of the weight loss due to the volatilization of the degradation products are monitored as a function of temperature. It can be seen that there are two main weight loss phases. The first phase is a weight loss of about 30% up to 184 ^{o}C due to the presence of hydrated/adsorbed water and glycerin. The second weight loss phase corresponds to the thermal decomposition of starch (burning of starch organic matter). The total weight loss in the second phase was about 65.8% between 185 and 580 ^{o}C, while most of starch weight loss (about 40%) was between 280 and 322 ^{o}C that was associated with T_{50} = 300 ^{o}C which is the decomposition temperature at 50% of the weight loss. Similar results of starch systems thermal Analysis were reported in [22&83]. The remaining 4.2% is due to the presence of inorganic materials in the hot pressed TPS-based matrix that included during matrix processing or sample preparation.

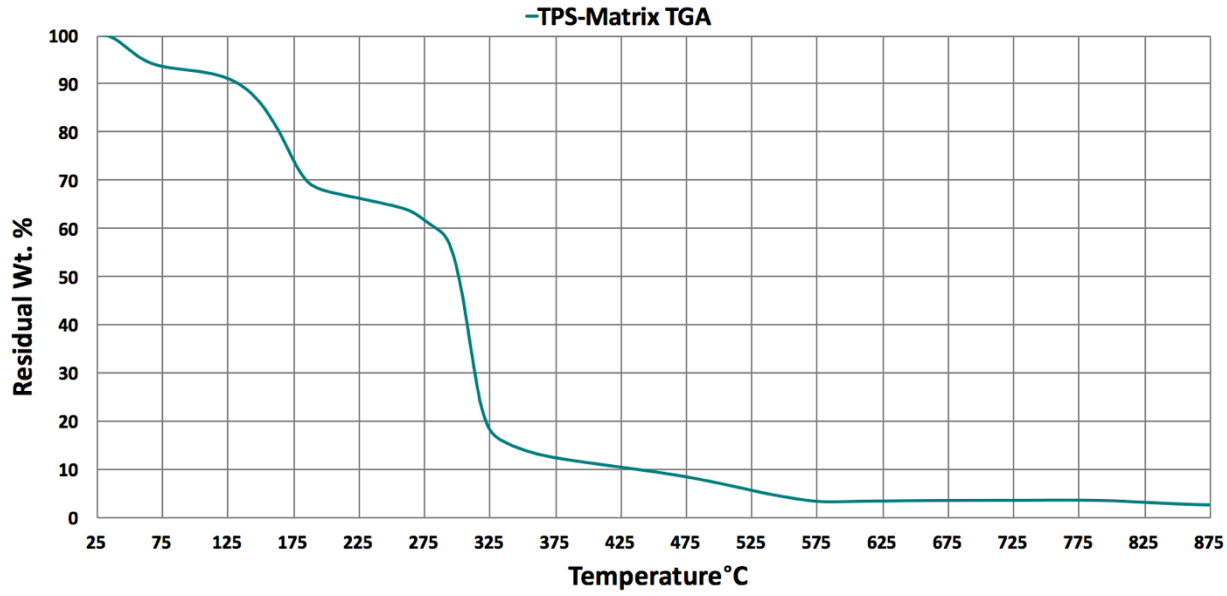

Figure 4. 9: TGA analysis of hot pressed TPS-based matrix.

4.3 Halloysite Nanotubes (HNTs) Characterization

4.3.1. HNTs SEM Morphology

Figure (4.10) shows the FE-SEM micrographs of HNTs as a powder before dissolving and dispersion by sonicator in distilled water (a) and after (b). HNTs have a cylindrical shape shows that their surface is relatively smooth, sharp, and distinguishable with a length of <1.5 μm and width ranges from 60-115 nm.

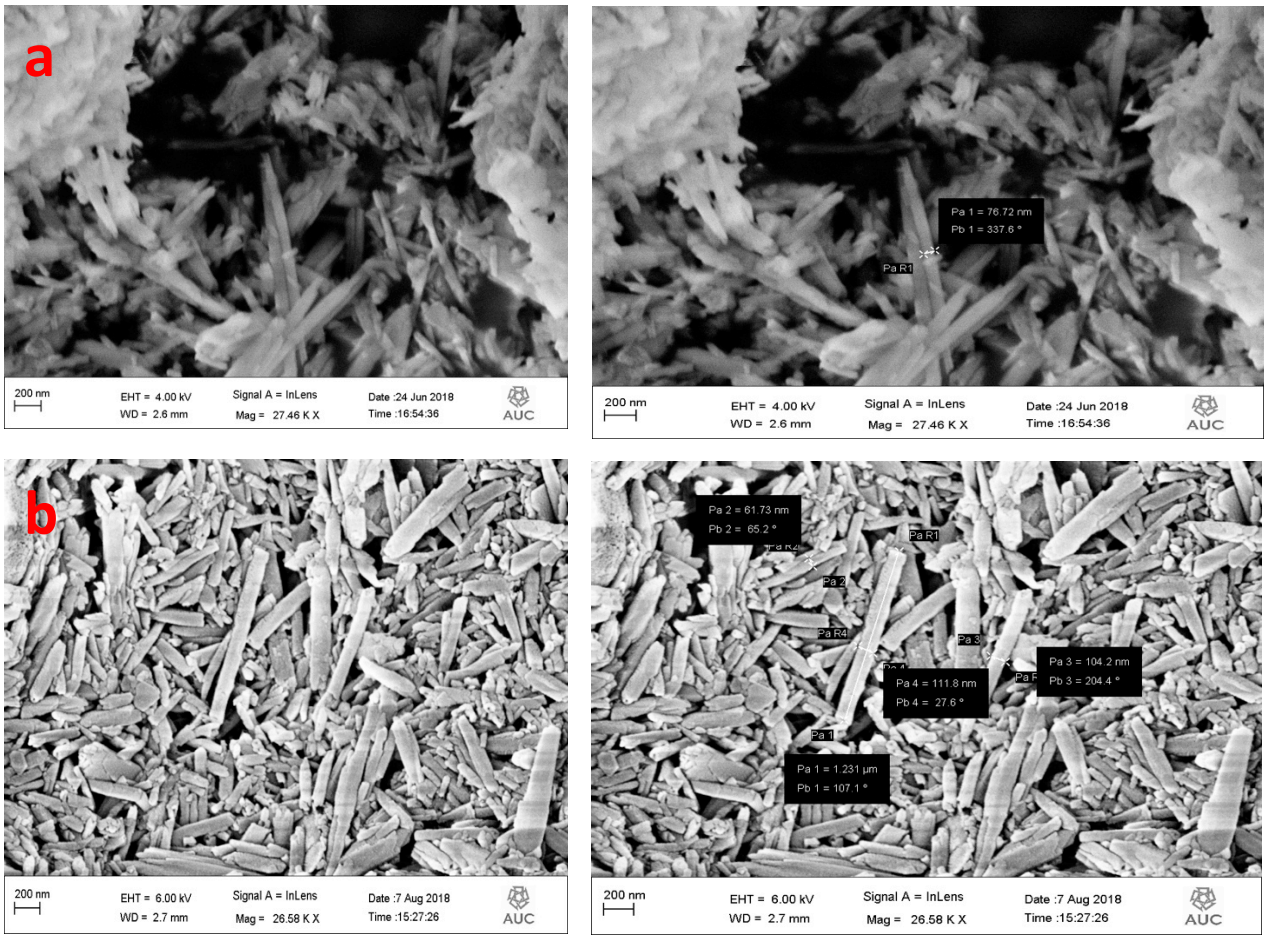

Figure 4. 10: SEM micrographs of HNTs: (a) before dispersion and (b) after dispersion

The FE-SEM has used to investigate the adhesion between the HNTS and TPS grains as shown in figure (4.11). It shows that HNTs can adhere from its lateral side to the surface of TPS grains which indicates good dispersion. This adhesion is due to the interaction between the hydroxyl groups on the surface of the HNTs and those on TPS grains by hydrogen

bonding and covalent bonds or physical interactions [120&121]. The coverage of TPS grains by HNTs increases by the increase of the HNTs concentration from 22.5% to 10% and an extensive coverage and accumulation appeared with HNTs 10%.

On the other hand, bleached DPF which get rid of lignin and the cellulosic fibers become exposed with their surface hydroxyl groups can also attract HNTs by hydrogen bonding and covalent bonds or physical interactions. As shown in figure (4.12) the surface of the DPF and TPS appeared rough due to the accumulation of the HNTs.

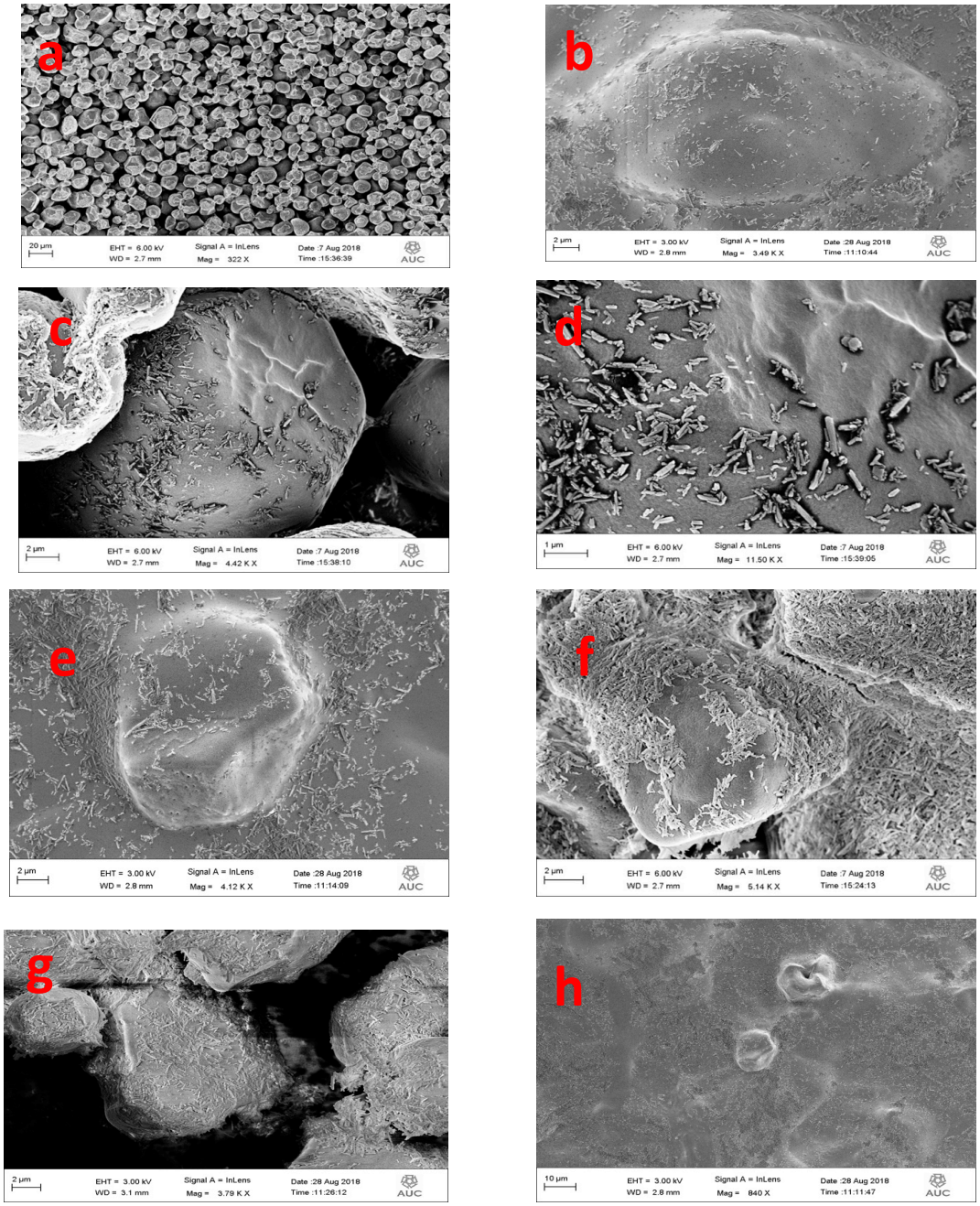

Figure 4. 11: the HNTs interaction and adhesion
(a &b), (c &d), (e) & (f &g) shows adhesion of HNTs 2.5%, 5%, 7.5% & 10% respectively on the surface of the TPS; (h) shows the adhesion and dispersion of HNTs on the surface of a thin film of TPS.

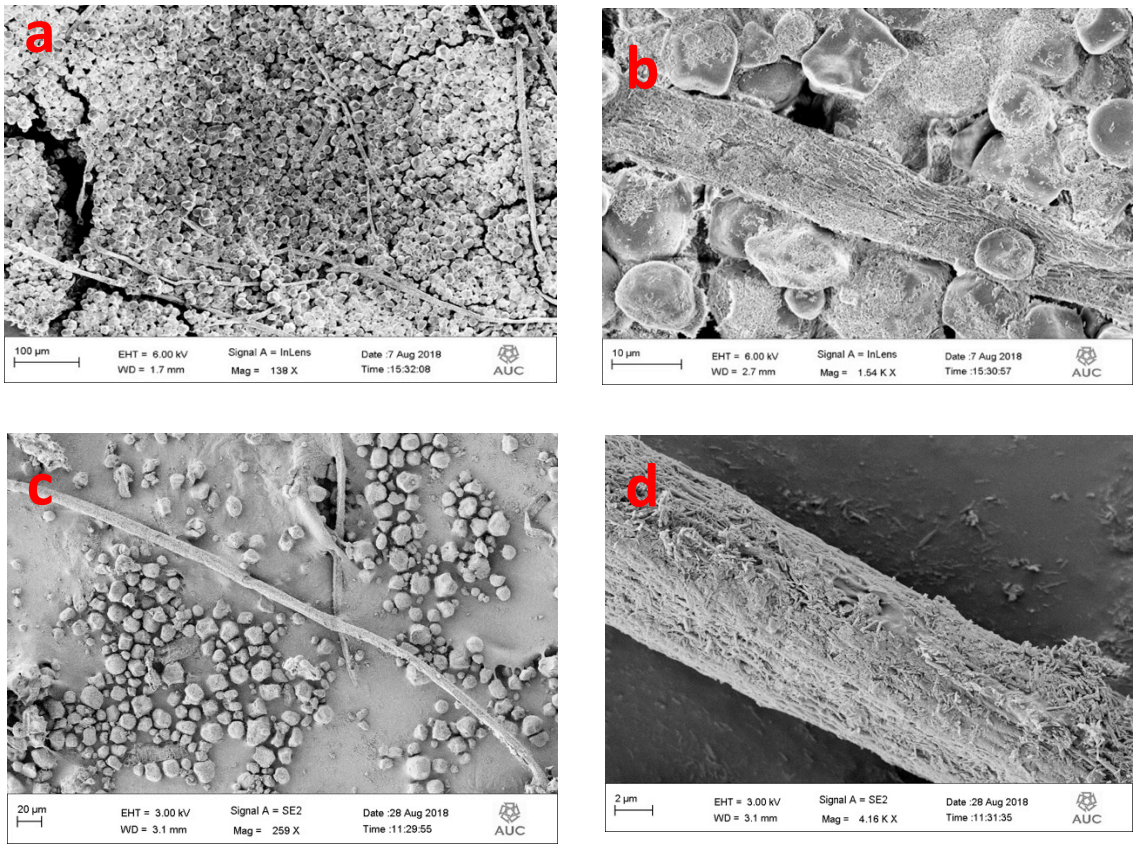

Figure 4. 12: HNTs adhere on the surface bleached DPF and it is completely coated by HNTs (a &b) with 5% HNTs & (c &d) with 10% HNTs.

4.3.2 Fourier transform infrared (FTIR) spectroscopy

The structure of the HNTs was analyzed using FTIR spectroscopy. Figure (4.13) shows the main infrared spectral differences which records the characteristic peaks of HNTs. Table (4.4) contains the most significant absorbance bands assigned to the functional groups of HNTs.

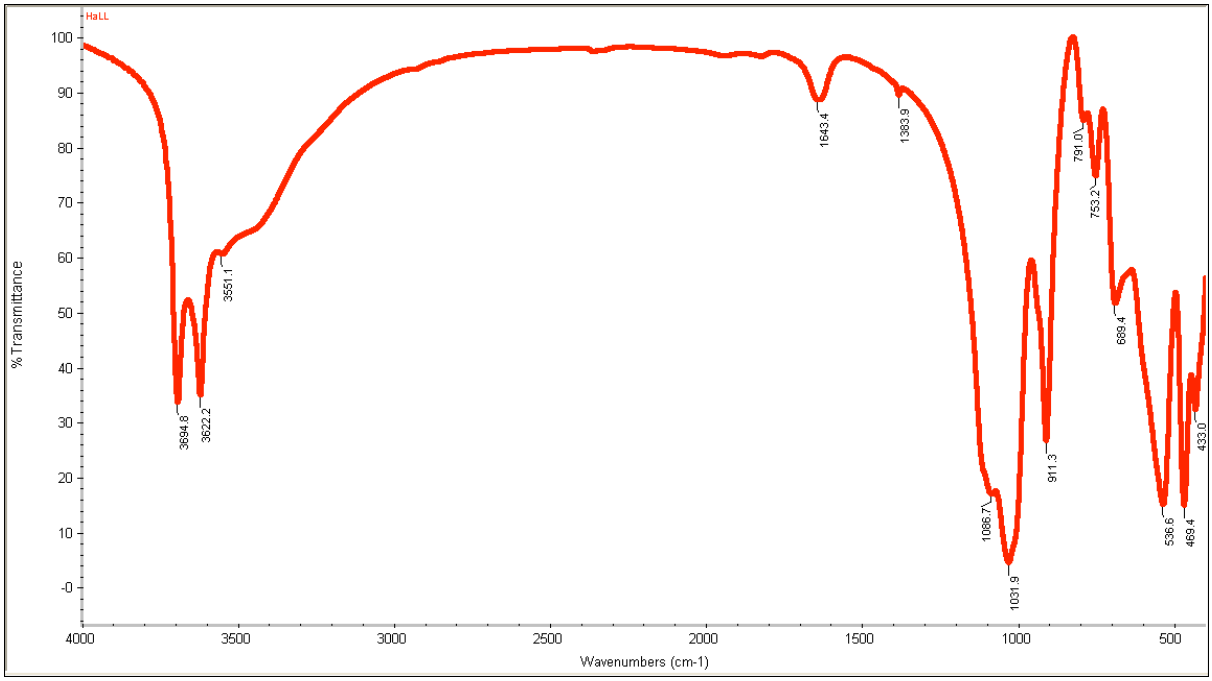

Figure 4. 13: FTIR spectra of HNTs

Table 4. 4: Positions and assignments of the IR vibration bonds appear in HNTs spectra.

Component	Peaks (cm^{-1})	Assignation
Halloysite Nanotubes (HNTs)	3700 – 3600	O–H stretching of external and internal hydroxyl groups
	3622	O–H stretching of inner hydroxyl groups
	1643	O–H deformation of water
	1032	In-plane Si–O stretching
	911	Al–O bending
	791	Symmetric Si–O stretching
	536	Deformation of Al–O–Si
	469	Deformation of Si–O–Si

4.3.3 Thermal Gravimetric Analysis (TGA) of HNTs

The Thermogravimetric Analyzer (TGA) is an essential laboratory tool used for material thermal characterization. Thermogravimetric Analysis is a technique in which the mass of a substance is monitored as a function of temperature or time as the sample specimen is subjected to a controlled temperature program in a controlled atmosphere. One of the major prominent property of HNTs is their thermal stability due to their mineral clay structure.

Figure (4.14) illustrates the thermogravimetric analysis (TGA) curve of HNTs in which there are a gradual mass loss phase and a major mass loss phases. The first gradual mass loss which is about 4% at temperature ranges from 100 to 450 ºC corresponding to the loss of adsorbed water (surface and interlayer) [135]. The second major mass loss which is about 10% at temperature ranges from 450 to 520 ºC that is assigned to the dehydroxylation of structural AlOH groups of halloysite [136]. In addition, the char residue of the HNTs at 900 ºC is 85.9%.

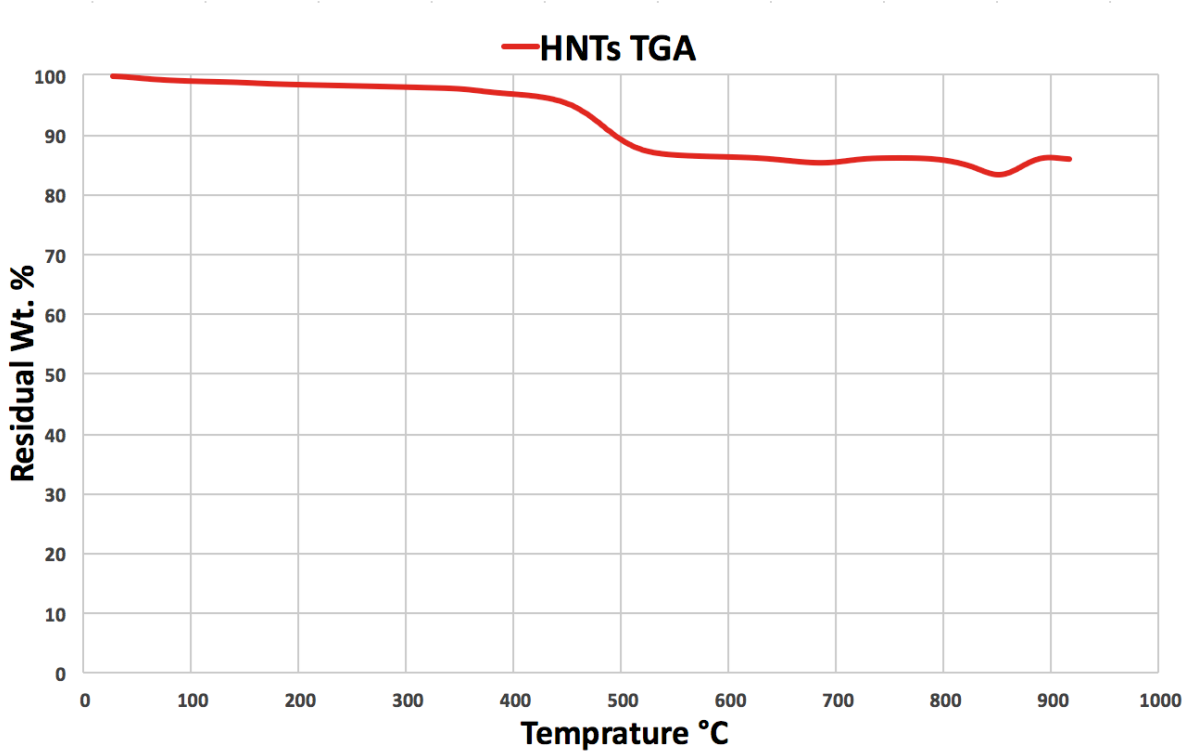

Figure 4. 14: TGA analysis of pure HNTs.

4.4 HNTs/TPS Nanocomposite characterization

4.4.1 SEM morphology of HNTs/TPS nanocomposites

Halloysite Nanotubes (HNTs) dispersion inside the hot pressed TPS was investigated by FE-SEM. Images of the HNTs/TPS nanocomposites show that HNTs are uniformly dispersed in the TPS matrix as shown in figure (4.15). Homogenous dispersion of HNTs with a majority of individual nanotubes is observed up to 7.5 wt% of HNT. However, aggregates are visible at higher loading (10 wt%) of HNTs (Fig. 1g and k, respectively). Besides, the interface between HNTs and plasticized starch matrix seems to be very good without any sign of debonding suggests that the interface between HNTs and TPS is of proper quality (Figure 4.15e).

FE-SEM used to study the surface fracture of the HNTs/TPS nanocomposite that indicated that the fracture occurred due to pulling of the short part of HNTs from the TPS. Figure (4.15f) shows many white shiny dots which represents the pulled HNTs from the matrix at the fracture surface of 7.5 wt % HNTs/TPS nanocomposite. Aggregates are visible at higher loading (10 wt.%) of HNTs in the TPS matrix.

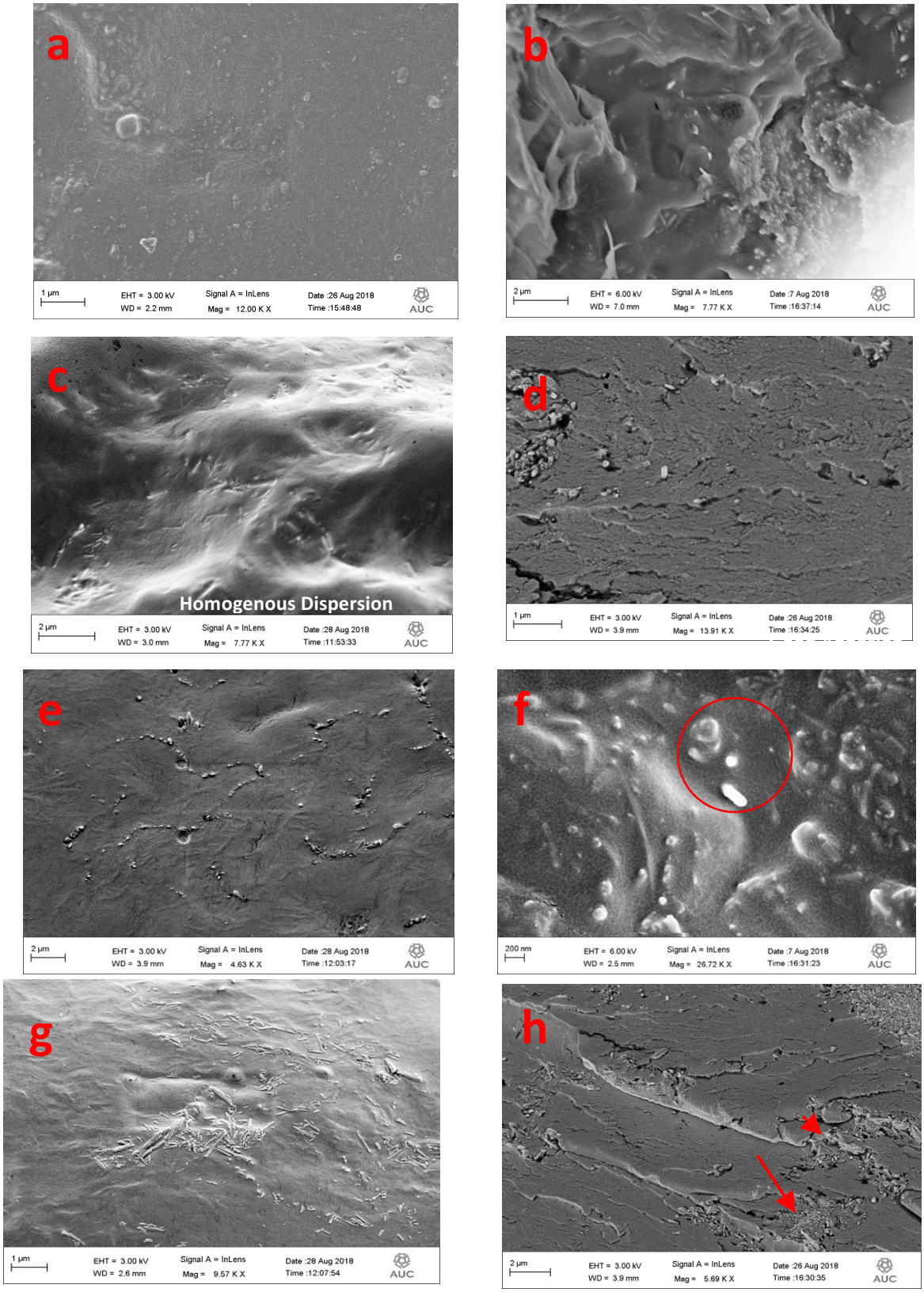

Figure 4. 15: shows the dispersion and surface fracture of the HNTs at the different concentrations images of (a, c, e & h) show the dispersion of the HNTs inside the TPS matrix after hot pressing with different HNTs percentages 2.5 wt.%, 5 wt.%, 7.5 wt.% & 10 wt.% respectively; images of (b, d, f & i) show the surface fracture of the HNTs/TPS nanocomposites after tension of the HNTs inside the TPS matrix after hot pressing with different HNTs percentages 2.5 wt.%, 5 wt.%, 7.5 wt.% & 10 wt.% respectively

4.4.2 FTIR of HNTs/TPS nanocomposites

The interaction between HNTs and TPS inside the nanocomposite verified by FTIR. The characteristic peaks and their assignation of TPS and HNTs were determined previously in figures (4.7) and figure (4.13) respectively. During plasticizing the native starch water and glycerin were added that played a key role in forming hydrogen bonds in order to plasticizing starch. Similarly, HNTs and TPS were prepared by emulsion technique in water. This will make new hydrogen bonds between surface of HNTs and TPS.

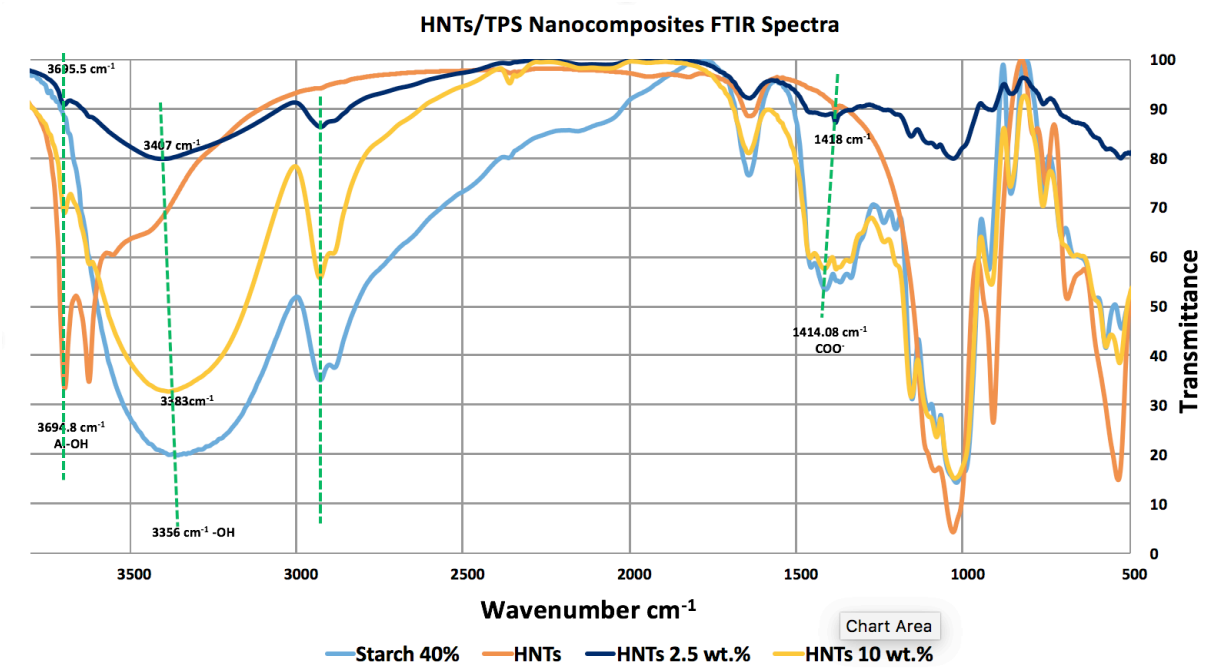

Figure 4. 16: FTIR spectra of HNTs/TPS nanocomposites

The shift occurred in the peaks of TPS and HNTs spectra is due to the formation of hydrogen bonds between the HNTs and TPS in the nanocomposite [120]. This is due to the interaction between hydroxyl groups in TPS and oxygen species of Si – O and Al – O of HNT. The shift occurred at the peaks 3694 cm-^{1}, 3383 cm^{-1} and 2923 cm^{-1} which indicating the increase in hydrogen bonds formed inside the nanocomposite. However, neither noticeable variations in the spectra of the FTIR peaks nor the appearance of new peaks by the incorporation of HNTs TPS matrix. Therefore, from the present FTIR results a physical interaction mainly the hydrogen bonds occur between HNTs and alginate, which is a benefit for the performance improvement of the nanocomposite.

4.4.3 Mechanical Properties

Tension test

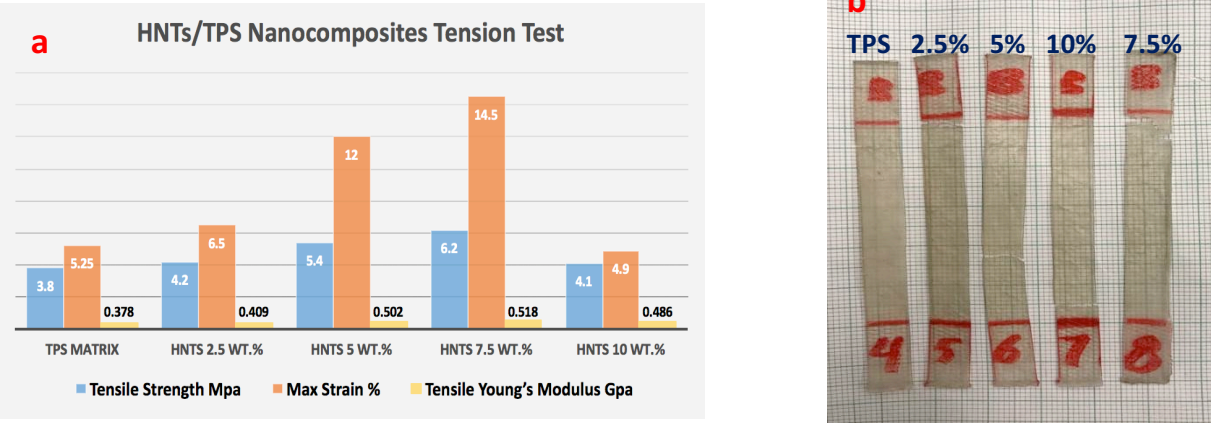

Figure 4.17: a: Composite measured tensile properties; tensile strength, Young's modulus and strain % at break; **b:** image shows the elongation of HNTs/TPS samples after tension test.

In figure (4.17) the tensile strength and modulus of the composites created by TPS-based matrix and reinforced with HNTs are shown. It shows that both tensile strength and modulus of HNTs/TPS-based composites increase when HNTs content is increased to reach maximum values at 7.5 wt.% HNTs content before decreasing at higher HNTs contents due to the aggregation of the HNTs inside the matrix. The tensile strength of 7.5 wt.% HNTs/TPS-based nanocomposites increased by about 50% compared to another work by H. Ibrahim et.al [137] that used the same method of compression molding to prepare samples of TPS.

The enhancement of the mechanical properties after adding HNTs inside the TPS is due to the high aspect ratio and the mechanical properties of the HNTs. In addition, the compatibility between HNTs and TPS matrix due to the interfacial adhesion with homologous dispersion inside the TPS matrix that will transfer the stress from the matrix to the reinforcing HNTs which will hinder the fracture due to its crystalline nature. The fracture will not find any way for complete failure except find its way in matrix or pulling HNTs out of the matrix by rupture the hydrogen bonds or the covalent bonds. However, we can conclude that the main reason for the improvement in tension is mainly attributed to homogenous distribution of the HNTs inside the TPS matrix.

On the other hand, H. Schmitta et. al. [123] prepared a bionanocomposite based on HNTs and glycerin plasticized wheat starch by melt-extrusion that could reach to 85% and 87% increase in the elongation at break for unmodified HNTs and modified HNTs, respectively. Obviously, this is due to the ductile effect of the TPS and good adhesion with interfacial interaction between HNTs and plasticized wheat starch. However, the tensile strength and Young's modulus for HNTs 8% wt.% with modified or non-modified HNTs could not exceed 2.9 MPa and 31.3 MPa, respectively.

Bending test

Flexure test is easy to run and relatively inexpensive. Also flexural strength and modulus are important properties to evaluate mechanical behavior of polymeric composites in some designs where the component is subjected to bending stresses.

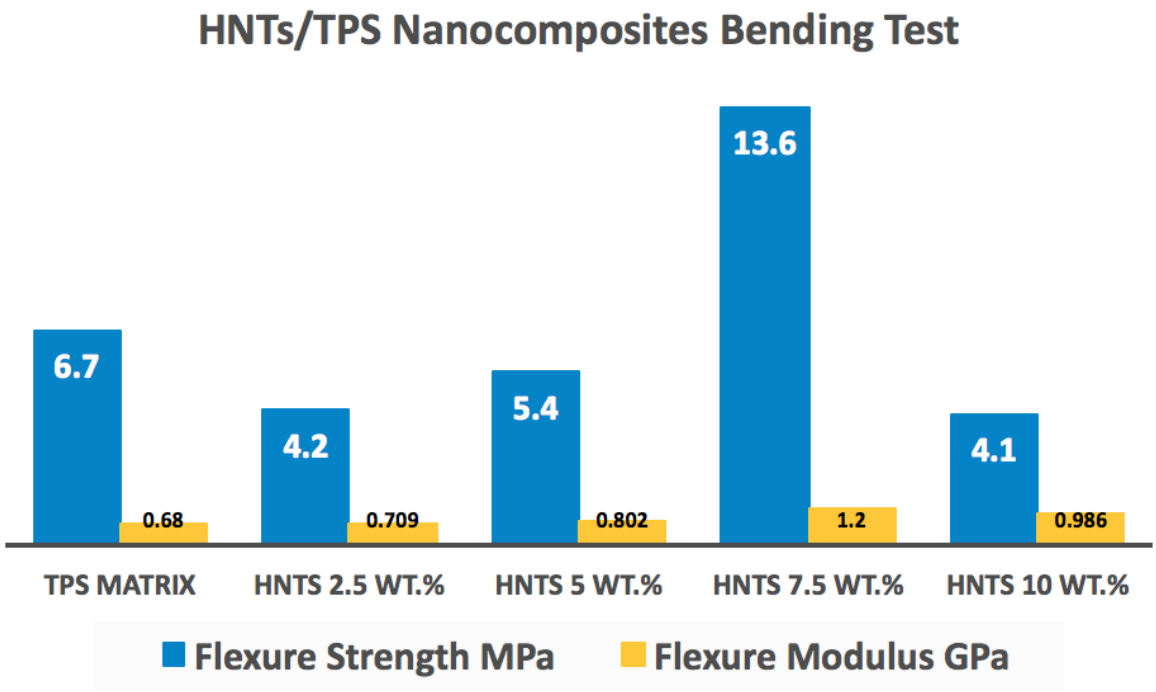

Figure 4.18: Nanocomposite measured flexure properties; flexure strength and flexure modulus.

In figure (4.18) the flexural strength and modulus of the composites created by TPS-based matrix and reinforced with HNTs are shown. The resulted nanocomposites flexural properties confirm the results of the tensile test, where the optimum flexural strength and modulus were found at 7.5 wt% HNTs content. For example, the flexural strength and modulus increased from 6.7 MPa and 685 MPa respectively at 0 wt% nanocomposite to reach 13.6 MPa and 1.2

GPa respectively at HNTs 7.5 wt% nanocomposite. Greater credence is often given to results obtained from tensile test because they provide the more conservative data.

The higher increase in flexure strgnth than tesile stregnth may be due to difference in tension mechanism where in tension test the break of specimens was caused by separation between fibers or HNTs and matrix so the pulling of the DPF or HNTs to reach failure were easier than applying bending stress on the samples to reach complete failure. Moreover, the HNTs have great mechanical property that they are highly flexible where they can bend to 90º without fracture [104&105]. However, still the main factor in increase the mechanical properties the homogenous distribution of the HNTs inside the TPS matrix.

4.4.4 Thermal Gravimetric Analysis (TGA) of HNTs/TPS

Thermal degradation of the thermoplastic starch (TPS)-based matrix is an important factor to identify the limits of processing, treatment or operating temperatures after adding HNTs. Figure (4.19) shows the TGA curve obtained for the hot pressed HNTs/TPS-based matrix by emulsion technique, where the percentage loss of the sample weight and the derivative of the weight loss due to the volatilization of the degradation products are monitored as a function of temperature.

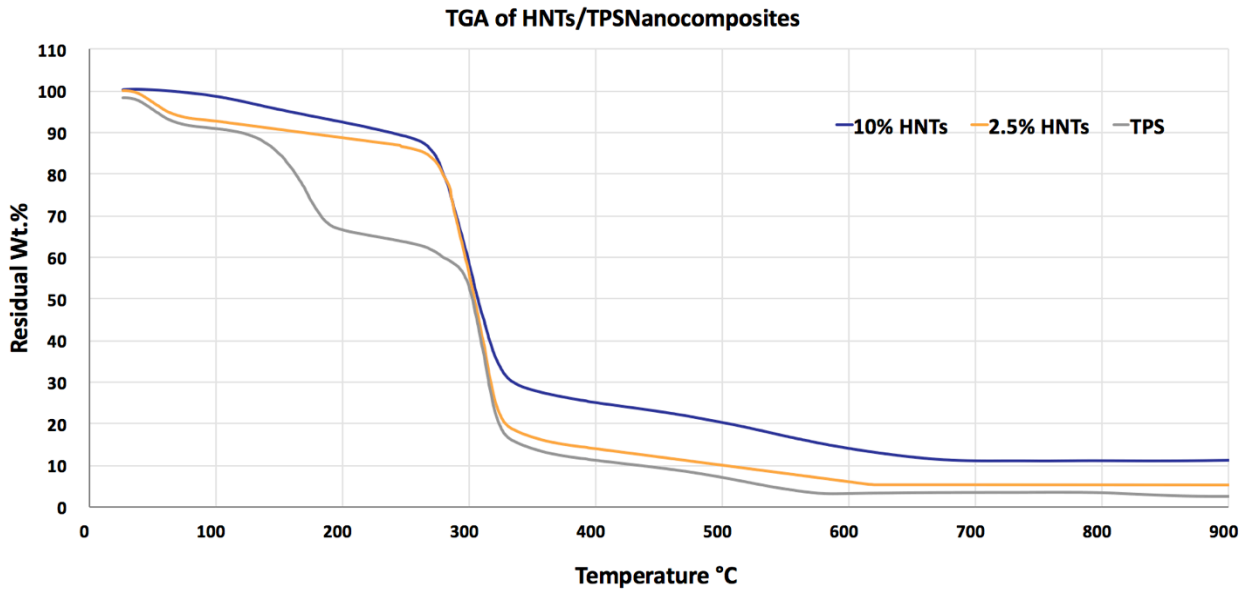

Figure 4. 17: TGA analysis of HNTs/TPS Nanocomposites

Table 4. 5: the thermal temperature of weight loss of HNTs/TPS nanocomposites

HNTs wt.%	Temp. at 10% weight loss (°C)	Temp. at 30% weight loss (°C)	Temp. at 50% weight loss (°C)	Weight% loss at 120 °C	Residual weight% at 600 °C
HNTs 0 wt.%	121 °C	183.2 °C	302.7 °C	9.9%	3.2%
HNTs 2.5 wt.%	167 °C	288.9 °C	304 °C	8.1%	6%
HNTs 10 wt.%	235 °C	290 °C	307.1 °C	2.6%	14.1%

It can be seen from the above table that the thermal stability of the HNTs/TPS nanocomposites increased by increasing the HNTs wt.%. This is because the nature of HNTs as a mineral clay. However, most of HNTs samples weight loss occurs nearly at the same temperature range from 270 °C to 335 °C which is greater than that of TPS alone. Moreover, the sample with HNTs 10 wt.% can withstand 120 °C and loss only 2.6% of its original weight that reflects the high thermal stability due to the wt.% of HNTs.

4.4.5 Water uptake

Water uptake of the HNTs/TPS nanocomposites is important factor to determine behavior and changes on the material in ambient temperature in different humidity conditions. Generally, the water uptake is attributed to the hydrophilicity of the matrix and the voids between filler and matrix [138]. Pure TPS can uptake 50% of its original weight after placing it in 100% humidity which is higher when compared to the different HNTs/TPS concentrations. This means that the addition of HNTs decreases the degree of the material to absorb water. This decrease is due to the decrease of the ratio of TPS by increasing the HNTs percent because it is a clay mineral which has a limited water absorption degree. In addition, HNTs will increase the entanglement of the TPS which will decrease the mobility of the polymer chains and water uptake consequently [120]. This is approved by decease in the water uptake by increase the HNTs percent in the nanocomposite. This could be also due to the aggregation of the HNTs which hinder the water movement in the polymer chains.

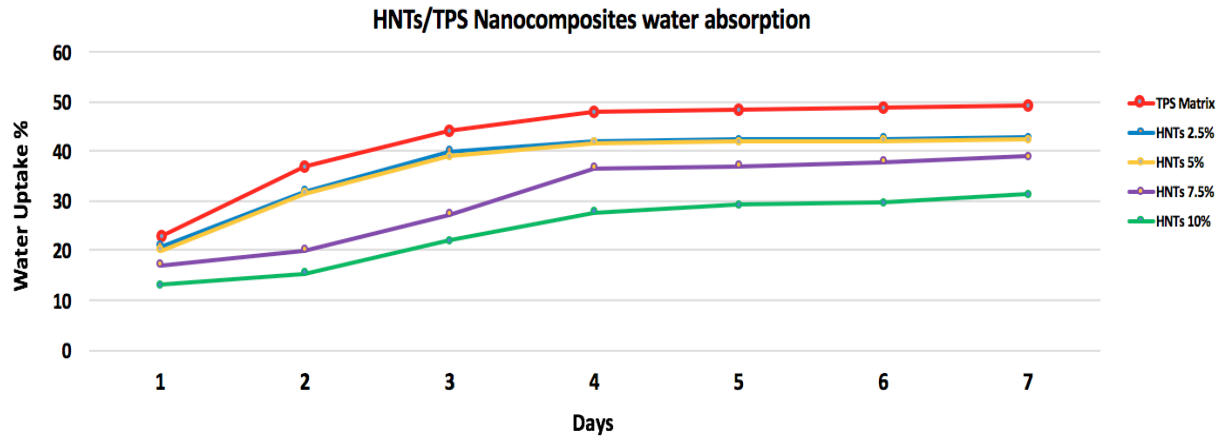

Figure 4. 18: Composite measured tensile properties; tensile strength and tensile Young's modulus.

4.5 HNTs/DPFs/TPS Nanocomposite characterization

4.5.1 FTIR of HNTs/DPFs/TPS nanocomposites

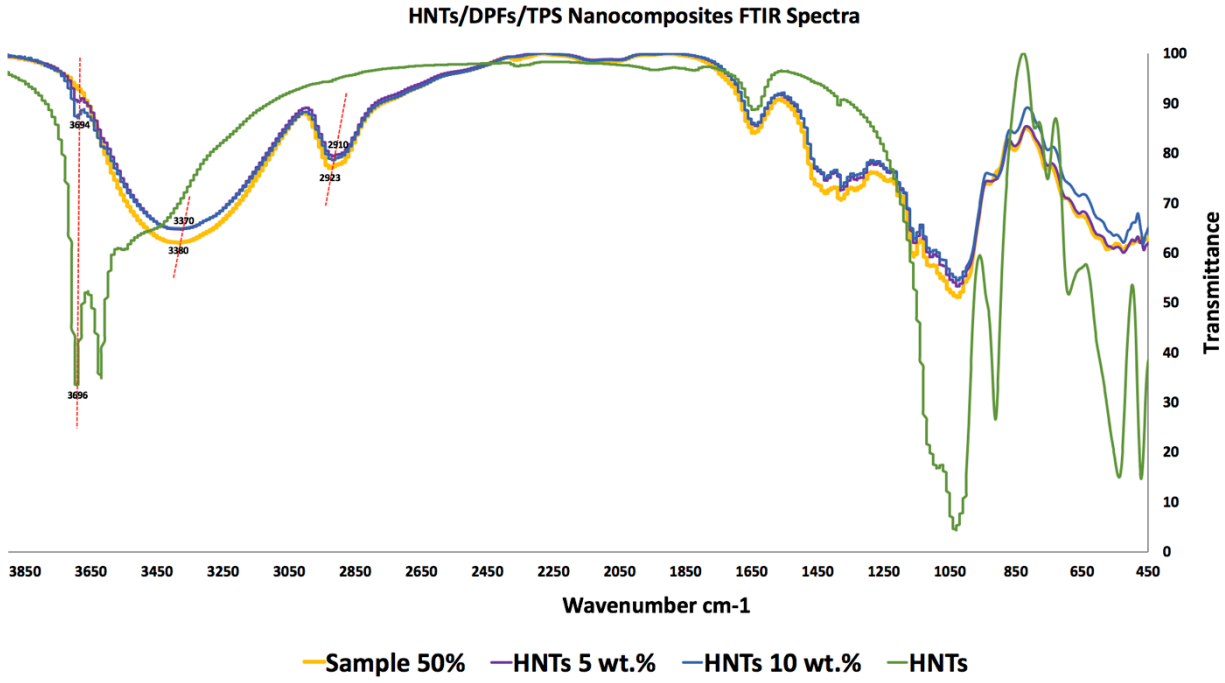

Figure 4. 19: FTIR spectra of HNTs/DPF/TPS nanocomposites

The structure of the nanocomposites of HNTs/DPF/TPS based matrix was analyzed using FTIR spectroscopy. Figure (4.19) shows the main FTIR spectral differences which recorded the characteristic peaks of nanocomposites of HNTs/DPF/TPS based matrix. The FTIR spectra of the nanocomposites show combined peaks with HNTs and DPT/TPS composite indicating the successful incorporation of HNTs into the DPF/TPS composite. The characteristic peak of HNTs at 3696 cm^{-1} shift to lower wave numbers at 3694 cm^{-1} compared to that of nanocomposites of HNTs/DPF/TPS based matrix. This is an elucidation to the formation of hydrogen bonds between the HNTs and DPF or TPS in the nanocomposite [120]. This is due to the interaction between hydroxyl groups in TPS or DPT and oxygen species of Si – O and Al – O of HNT. The same red shift occurred in the DPF/TPS composites at the peaks 3380 cm^{-1} and 2923 cm^{-1} respectively which indicating the increase in hydrogen bonds formed inside the nanocomposite. However, neither noticeable variations in the spectra of the FTIR peaks nor the appearance of new peaks by the incorporation of HNTs into DPF/TPS composites. Therefore, from the present FTIR results a physical interaction mainly the hydrogen bonds occur between HNTs and alginate, which is a benefit for the performance improvement of the nanocomposite.

4.5.2 SEM morphology of HNTs/DPF/TPS nanocomposites

Halloysite Nanotubes (HNTs) and DPF dispersion inside the hot pressed TPS was investigated by FE-SEM. Images of the HNTs/DPF/TPS nanocomposites show that HNTs and DPF are uniformly dispersed in the TPS matrix as shown in figure (4.20). Homogenous dispersion of HNTs and DPF with a majority of individual nanotubes is observed. Besides, the interface between HNTs, DPT and TPS matrix seems to be very good without any sign of debonding suggests that the interface between HNTs and TPS is of proper quality (Figure 4.20 a-d). This is approved by the adhesion between DPF and TPS matrix was excellent as shown in figure (4.20 e-i). Similarly, also HNTs was embedded in the TPS matrix covers the DPF as shown in figure (4.20 e-i).

FE-SEM used to study the surface fracture of the HNTs/TPS nanocomposite that indicated that the fracture occurred due to pulling of the short part of DPF from the TPS. Figure (4.20 i&m) shows the grooves of DPF pulled and leave with the other fractured part and a protruding fibers from the matrix which is still embedded by its large part inside the TPS matrix. Besides, the break of the TPS matrix adhering the fibers is also another cause of the fracture as shown in figure (4.20 n&o). The fracture surface morphology all wt. % HNTs/ DPF TPS-based nanocomposites is not much different. In conclusion; three types of failure mechanisms have been identified: matrix failure, fiber fracture and fiber-matrix or HNTs interfacial failure.

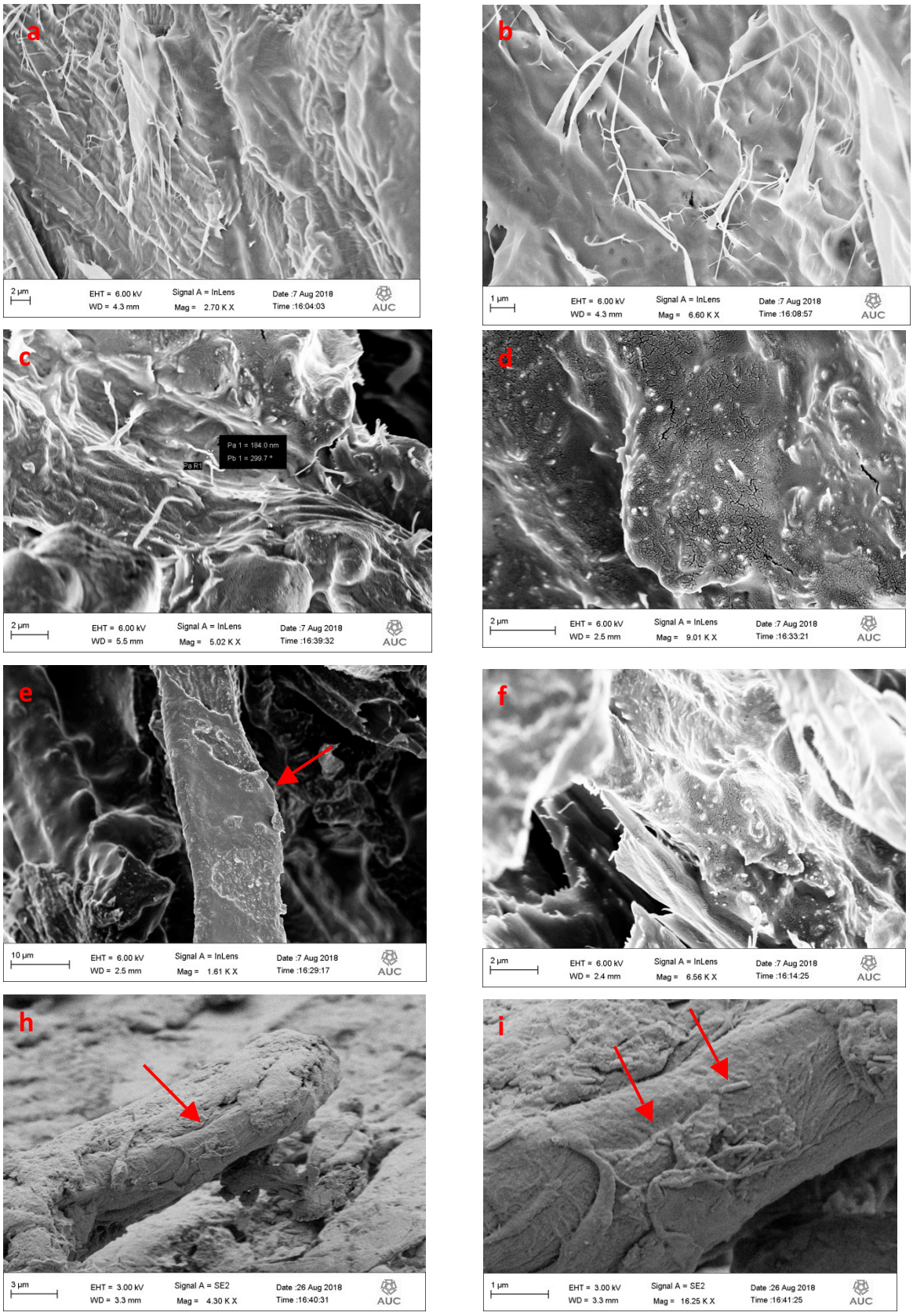

Figure 4. 20: shows the HNTs, DPF dispersion and surface fracture of the TPS-based nanocomposites.

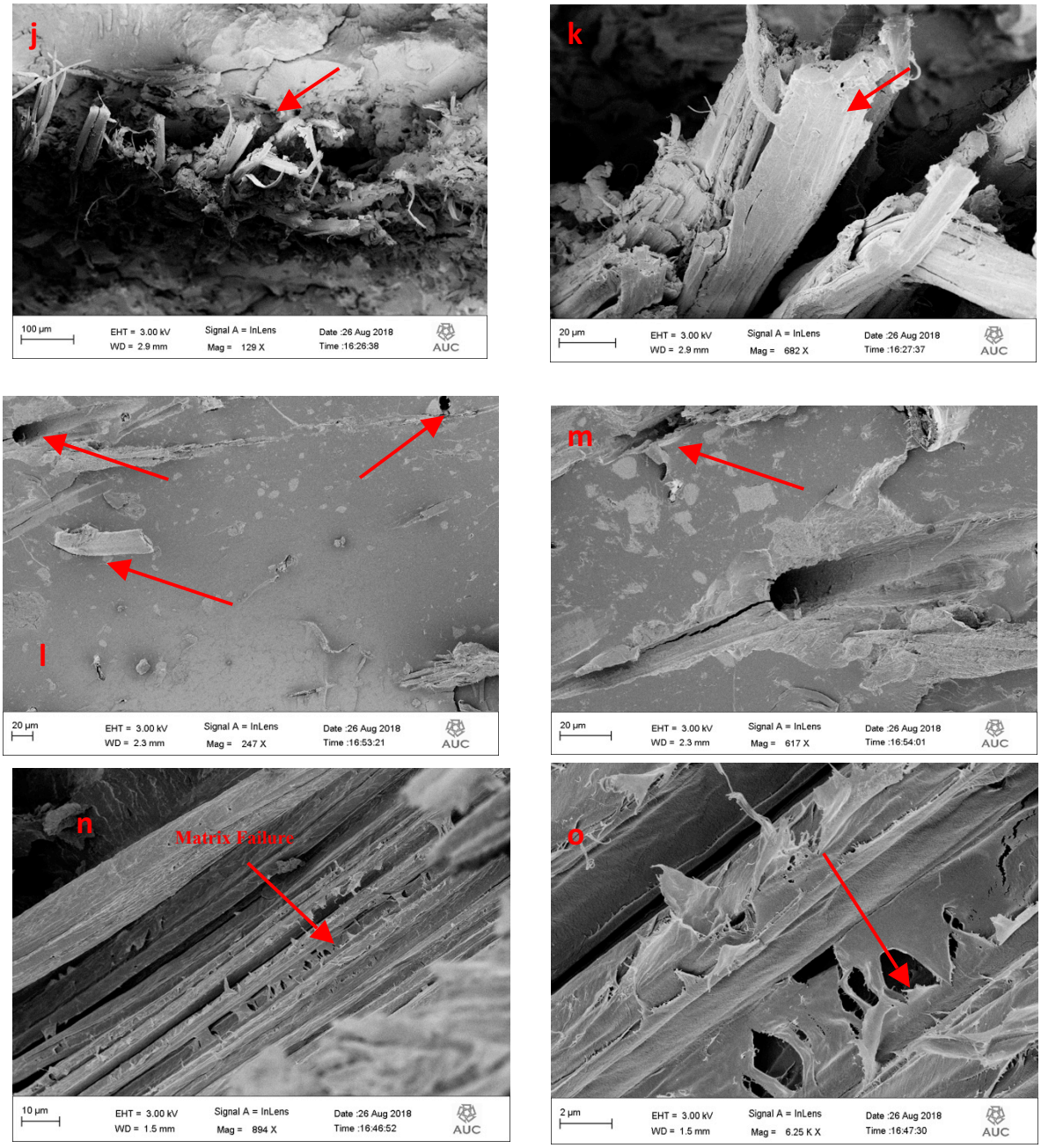

Figure 4. 21 "continued": shows the HNTs, DPF dispersion and surface fracture of the TPS-based nanocomposites.

4.5.3 Mechanical Properties

Tension test

In figure (4.21) the tensile strength and modulus of the composites created by TPS-based matrix and reinforced with both DPFs and HNTs are shown. It shows that both tensile strength and modulus of HNTs/DPFs/TPS-based composites increase when HNTs content is increased to reach maximum values at 5 wt.% HNTs content before decreasing at higher HNTs contents due to the agglomeration of the HNTs inside the matrix and a decrease in the fiber content. The tensile strength of 5 wt.% HNTs/DPFs/TPS-based composites increased by 50% compared to another work by H. Ibrahim et.al [137] that used date palm fibers only without HNTs.

The results in this work was comparable with results of Soheilmoghaddam M. et. al. [125] that was using cellulose fibers after treating it with NaOH "regenerated cellulose" to prepare regenerated cellulose/halloysites nanocomposites; However, the cellulose is linked with HNTs by ionic liquid. The results of tensile strength were very similar, where with HNTs 4 wt. % and HNTs 6 wt. % the tensile strength was 41 Mpa and 59.6 Mpa, respectively. However, the Young's modulus of the HNTs/DPFs/TPS-based nanocomposites was higher by about 115% than that of regenerated cellulose/halloysites nanocomposites.

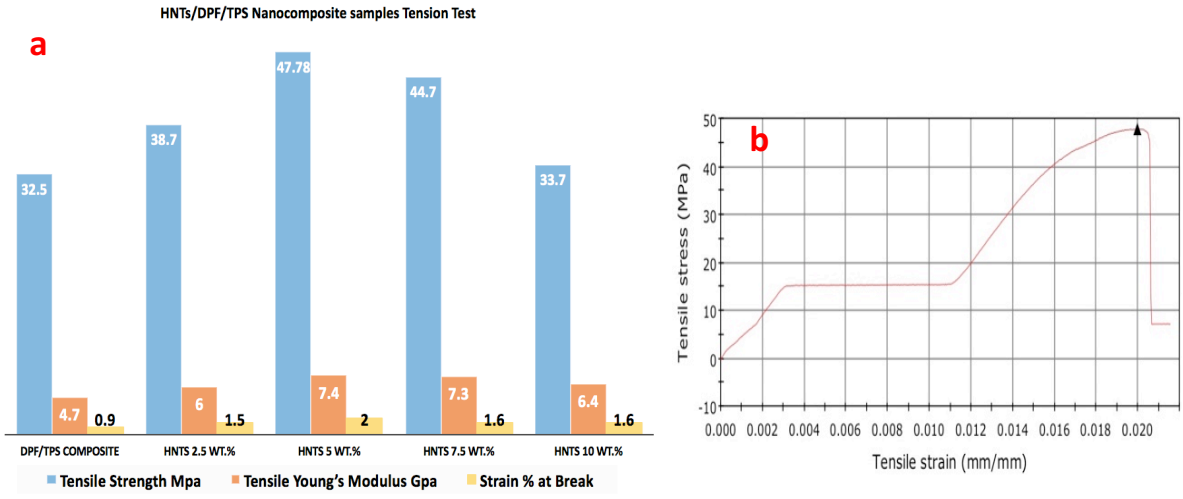

Figure 4. 22: Composite measured tensile properties
a: tensile strength, Young's modulus and strain % at break; b: the stress – strain curve obtained from the machine of sample with HNTs 5 wt.%.

Stress – strain curve

In figure (4.21 b) the strain behaviour of the 5% HNTs/DPF/TPS nanocomposite under tension is divided into two main phases. The first phase is the tension of the composite material totaly that can withstand tension stress till 15 MPa then the ductile part of the sample will appear which is due to the distension of the composite material equally to the strain rate rate of the machine tension. The second phase will begin when the material wholy loses its ductility and under the contineous tension force applied the fibers and nanotubes are pulled out from the TPS matrix which needs more force to be applied on the sample that will lead to increase in the stress applied untill the fibers and HNTs are detached from the TPS matrix. The could approve the effect of the hydrogen bonds formed between the HNTs, bleached DPF and TPS matrix. The maximum tensile stress and youngs modulus reached equal 47.8 MPa and respectively for the sample 5%HNTs /DPF/ TPS nanocomposite. The same stress-strain behaviour appeared in the other samples contains 2.5%, 7.5% and 10%.

Bending test

Flexure test is easy to run and relatively inexpensive. Also flexural strength and modulus are important properties to evaluate mechanical behavior of polymeric composites in some designs where the component is subjected to bending stresses.

In figure (4.22) the flexural strength and modulus of the composites created by TPS-based matrix and reinforced with HNTs and DPFs are shown. The resulted nanocomposites flexural properties confirm the results of the tensile test, where the optimum flexural strength and modulus were found at 5 wt% HNTs content. For example, the flexural strength and modulus increased from 73.6 MPa and 5 GPa respectively at 0 wt% nanocomposite to reach 153.6 MPa and 10.2 GPa respectively at HNTs 5 wt% nanocomposite. Greater credence is often given to results obtained from tensile test because they provide the more conservative data.

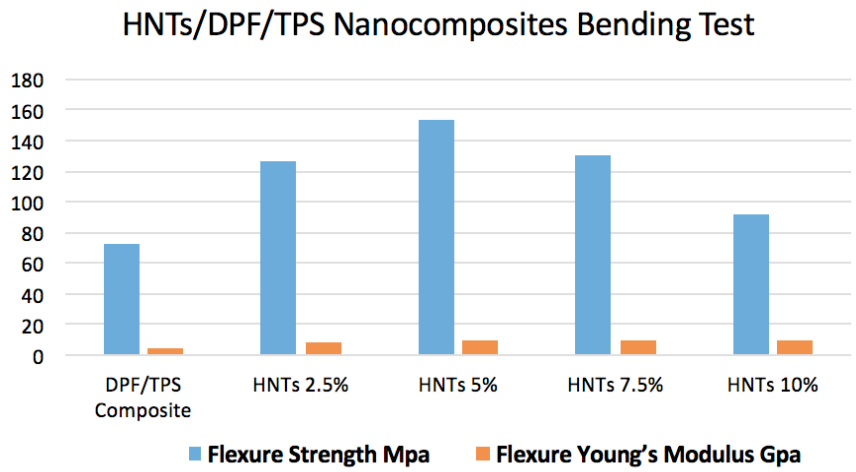

Figure 4. 23: Nanocomposite measured flexure properties; flexure strength and flexure modulus.

Flexural strength and modulus were significantly higher than tensile strength and modulus which is consistent with theories in literature. According to a statistical strength theory based on a Weibull distribution, the higher strength in bending test than tension is due to difference in stress nature. In bending test composite fail gradually and the generated stress has a gradient that results in increase in the strength of the half exposed to tensile stresses, while in tension test all composite cross section being under uniform stress [139&140].

In addition, the observations of higher increase in flexure strgnth than tesile stregnth may be due to difference in tension mechanism where in tension test the break of specimens was caused by separation between fibers or HNTs and matrix so the pulling of the DPF or HNTs to reach failure were easier than applying bending stress on the samples to reach complete failure. Moreover, the HNTs have great mechanical property that they are highly flexible where they can bend to 90º without fracture [104&105]. Clearly this great mechanical property will increase the flexure strength and flexibility of samples during the bending test. As shown in figure (4.23) the samples can return to its original shape after bending test. Especially, HNTs 5 wt.% sample withstand 153 MPa and did not reach to fracture and have the ability to return back to its original shape.

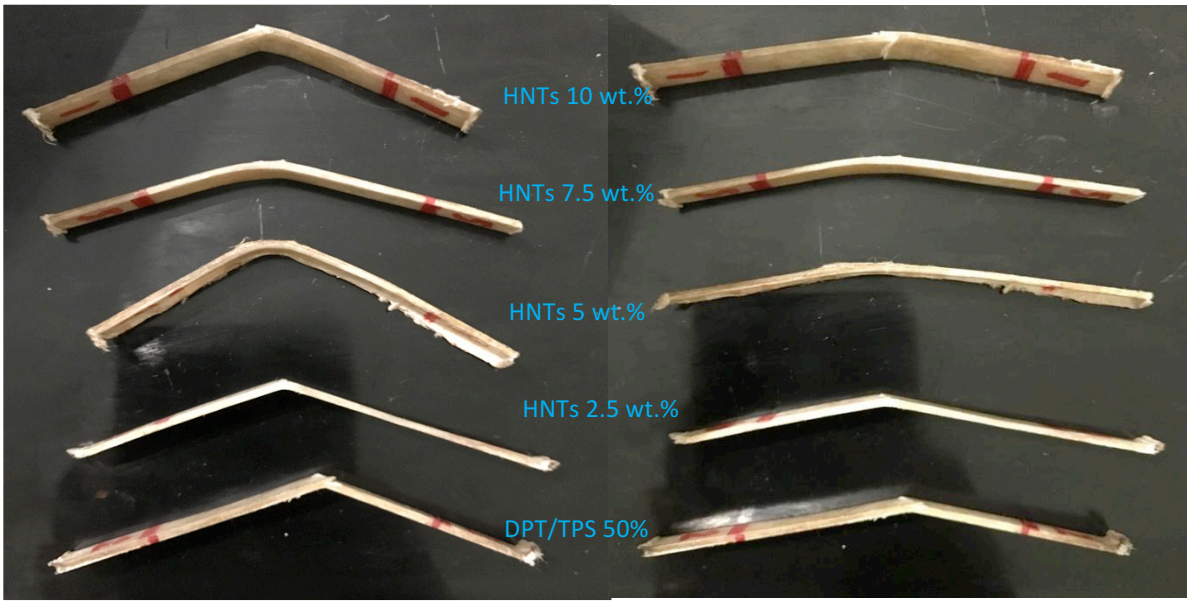

Figure 4. 24: the shape of nanocomposite measured flexure strength with different HNTs wt. %.

In conclusion, results showed that increase in HNTs percent in the composite increased the cnanocomposite flexure stregnth and modulus until HNts 5 wt. Flexural strength of HNTs 10 wt% and 7.5 wt.% nanocomposites was lower than HNTs 5 wt% nanocomposites because of the aggregation of the HNTs inside the TPS matrix. This makes failure starts and continues into areas of the TPS matrix that don't have enough HNTs to stop the failure.

4.5.4 Thermal Gravimetric Analysis (TGA) of HNTs/DPFs/TPS

Thermal degradation of the thermoplastic starch (TPS)-based matrix is an important factor to identify the limits of processing, treatment or operating temperatures after adding DPFs and HNTs. Figure (4.24) shows the TGA curve obtained for the hot pressed HNTs/DPFs/TPS-based matrix by emulsion technique, where the percentage loss of the sample weight and the derivative of the weight loss due to the volatilization of the degradation products are monitored as a function of temperature.

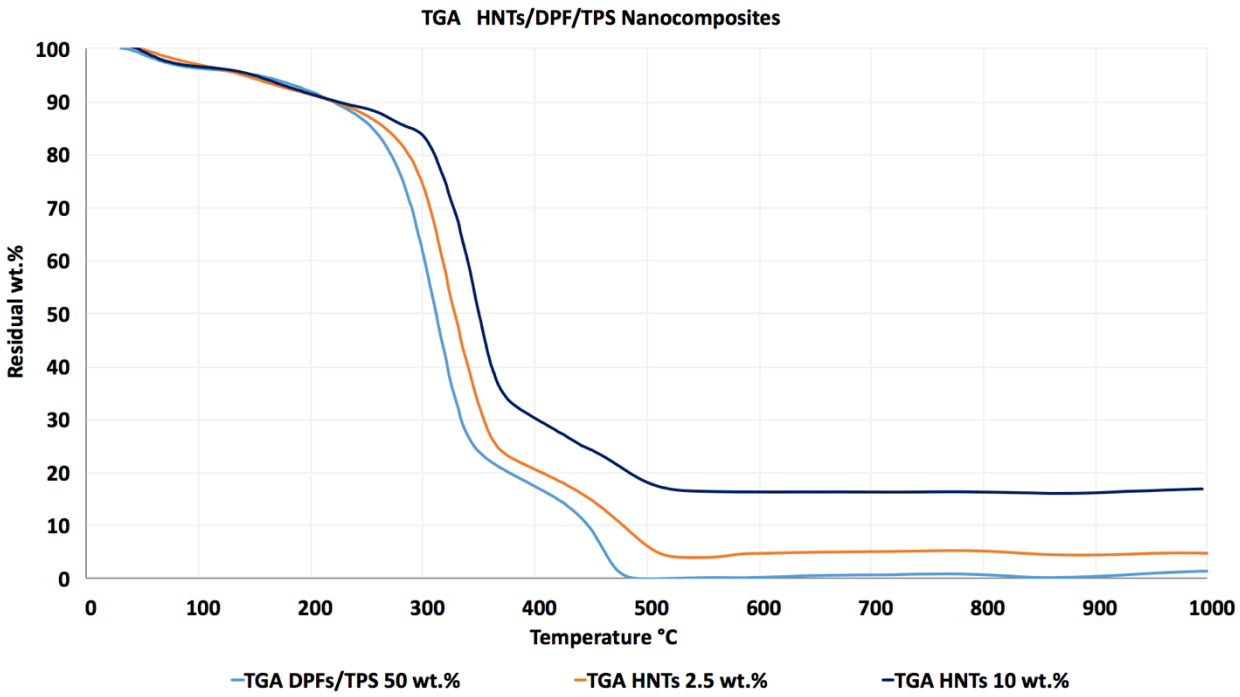

Figure 4. 25: TGA analysis of HNTs/DPFs/TPS Nanocomposites

Table 4. 6: Thermal degradation of nanocomposites with different HNTs weight content.

HNTs wt.%	Temp. at 10% weight loss (^{o}C)	Temp. at 30% weight loss (^{o}C)	Temp. at 50% weight loss (^{o}C)	Weight% loss at 120 ^{o}C	Residual weight% at 600 ^{o}C
HNTs 0 wt.%	219 ^{o}C	289.6 ^{o}C	311.4 ^{o}C	5%	0.2%
HNTs 2.5 wt.%	222.5 ^{o}C	305.7 ^{o}C	328.1 ^{o}C	4%	4.7%
HNTs 10 wt.%	224.4 ^{o}C	327 ^{o}C	349.4 ^{o}C	4%	16.2%

It can be seen from the above table that the thermal stability of the HNTs/DPFs/TPS nanocomposites increased by increasing the HNTs wt.%. This is because the nature of HNTs as a mineral clay. However, most of HNTs samples weight loss occurs nearly at the same temperature range from 300 ^{o}C to 350 ^{o}C which is greater than that of DPFs/TPS alone.

4.5.5 Water uptake

The behavior of water uptake by a composites filled by a hybrid filler at 100% RH in ambient temperature is very essential to determine the durability of the composite system. Generally, the water uptake is attributed to the hydrophilicity of the filler surface and the voids between filler and matrix [138]. The water uptake of the composite system showed a dramatic reduction in water uptake due to the addition of the treated DPF making the composite less hydrophilic see figure (4.25), Although increasing fiber content increases voids in the composite that facilitate the water absorption by the matrix, the overall water uptake of the composite decreases due to the increase in cellulosic content which is less hydrophilic than TPS matrix. In addition, the presence of HNTs will fill these voids that will hinder the movement of the water molecules through composite the system.

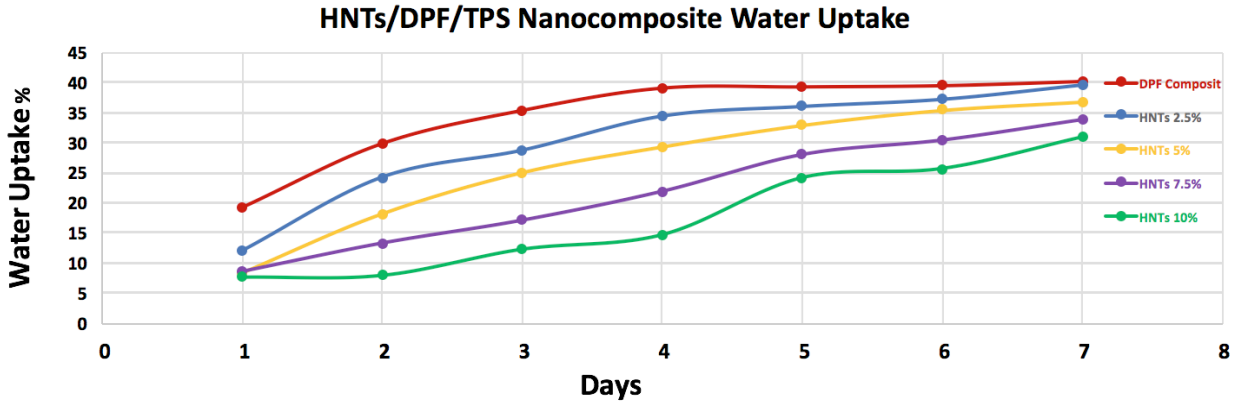

Figure 4. 26: composites water uptake of DPF/TPs composite with different HNTs concentrations.

The figure (4.25) shows that water uptake reduced from about 40% for DPF/TPS matrix to be about 31% for 5% HNTs/DPF/TPS-based composites and reaches its maximum reduction in 10% HNTs/DPF/TPS-based composites. This could be due to the decrease in fibers content and the increase in the HNTs as an inorganic filler from 2.5% to 10% at the expense of the fibers.

Conclusion

- Mechanical properties and SEM investigations showed that emulsion technique produces stronger and stiffer hot pressed TPS-based matrix with moderate tensile and flexure strength.
- HNTs/TPS based nanocomposites with 2, 5, 7.5 wt% content have low void fractions and densities close to the theoretical values, while a drastic decrease in the composite density was found at composites with 10 wt% HNTs content therefore an increase in HNTs aggregation, this was attributed to the surface charges attraction.
- Three types of failure mechanisms have been identified by SEM investigation: matrix failure, fiber fracture and HNTs or DPfs-matrix interfacial failure where with fiber contents up to 50 wt% and HNTs content up to 5% TPS-based composites with uniform distribution.
- Good DPFs and HNTs-matrix interface and good fiber wettability confirms the role of alkaline treatment in improving the adhesion between lignocellulosic fibers and matrix by causing fiber fibrillation and removing lignin and dirt from fiber surface.
- The results demonstrated that each of the tensile strength, modulus, flexural strength and modulus improved with the percentage HNTs up to 7.5 wt. % without DPFs and 5 wt. % without DPFs by means of mechanical anchoring.
- The tensile strength and modulus increased from about (3.8 MPa and 0.4 GPa) at 0% to reach their maximum values of (6.2 MPa and 0.518 GPa) at 7.5 wt% HNTs/TPS based matrix and (47.78 MPa and 7.4 GPa) at 5 wt% HNTs/DPFs/TPS based nanocomposites.
- When HNTs with DPFs content is more than 5 wt%, bad mechanical properties and more aggregations of HNTs was observed.

- As the HNTs content increased thermal stability increased remarkably, especially at low temperatures. With 10 wt.% HNTs the temperature of 10% weight loss increased from 121^{o}C to 235^{o}C for TPS nanocomposite and from 219^{o}C to 224 for DPF^{o}C HNTs/DPFs/TPS nanocomposite.
- Increasing HNTs content increased composite moisture resistance and made the composite less hydrophilic due to the increase in mineral clay content which is less hydrophilic than TPS matrix.

FUTURE WORK

- Working to improve the penetration of the matrix between HNTs and fibers in order to fabricate TPS-based composite with better mechanical properties.
- SEM investigation, IR-spectroscopy and mechanical properties are other strategies that can be used for evaluating water uptake and biodegradation rate.
- Detailed study of the effect of nanocomposite moisture content on the mechanical properties can be carried out.
- TPS-based composite reinforced with lignocellulosic fibers can be biodegradable bone plates to be used in orthopedics, so a fatigue test is needed for investigate their ability to perform repeated work regularly.

References

1. The Great Wall Of China. *The Energy Planet.* [Online] [Cited: October 12, 2011.] http://library.thinkquest.org/C004471/tep/en/cultures/chinese.html.

2. **Johnson T.** History of composites. *About.* [Online] [Cited: January 4, 2012.] http://composite.about.com/od/aboutcompositesplastics/a/HistoryofComposites.htm.

3. **Satyanarayana KG, Gregorio GC. Arizaga, Wypych F.** Biodegradable composites based on lignocellulosic fibers-An overview. *Progress in Polymer Science.* 2009, Vol. 34, 9, pp. 982-1021.

4. **Sathy C, Satyananarayana KG, Pramada PN, Raghavan P.** Processing, properties and applications of reactive silica from rice husk-An overview. *Master Sci.* 2003, Vol. 38, pp. 3159- 3168.

5. **Ton-That MT., Denault J.** *Development of composites based on natural fibers.* Ottawa : The Institute of Textile Science, 2007.

6. **Michael K, Sven O, Christian G, Cezar P.** *Use of natural fibres in composites for the German automotive production from 1999 t0 2005.* Hurth : Nova-Institut, 2006.

7. **Aart van Vuure.** *Natural Fibers Composites; Recent Development.* Bruges : Innovation for Sustainable Production, 2008.

8. **Torben L.** Insite-biodegradable products. *design insite.* [Online] 2008. [Cited: October 20, 2011.] http://www.designinsite.dk.

9. **Richard A. Gross, Bhanu Kalra**. Biodegradable Polymers for the Environment. Science 02 Aug 2002. Vol. 297.

10. **European Bioplastics.** [Online] [Cited: July 12, 2018.] **https**://www.european-bioplastics.org/bioplastics/

11. **William BH, Thomas P.** Introduction to organic chemistry. 3rd. s.l. : Wiley, 2005. ISBN 0- 471-44451-0.

12. **Chen GQ, Wu Q.** The application of polyhydroxyalkanoates as tissue engineering materials. *Biomaterials.* 2005, Vol. 26, 33, pp. 6565-78.

13. **. Barreira B, Calmom P, Pedacce P, Mirannda LF, Masson TJ, Pereira NC, et al. s.l.** *Effect in the thermal and mechanical properties of PHB in presence of PVA and stearic acid plasticizers*: World polymer congress and 41st international symposium on macromolecules, MACRO- 2006, 2006. 1638.

14. **Garlotta D.** A Literature Review of Poly (Lactic Acid). *Journal of polymers and the environment.* 2002, Vol. 9, 2, pp. 63-84.

15. **Kauffman GB.** Rubber. *Chemistry Explained-Foundations and Applications.* [Online] 2008. [Cited: December 23, 2011.] http://www.chemistryexplained.com/Ru-Sp/Rubber.html#b.

16. **Kulkarni Vishakha S, Butte Kishor D and Rathod Sudha S.** Natural Polymers – A Comprehensive Review. International Journal of Research in Pharmaceutical and Biomedical Sciences. Vol. 3 (4) Oct – Dec 2012

17. **Whistler RL, BeMiller JN, Paschall BF**. Starch: chemistry and technology. New York: Academic Press, 1984.

18. **Rodriguez-Gonzalez FJ., Ramsay BA., Favis BD.** High performance LDPE/thermoplastic starch blends: a sustainable alternative to pure polyethylene. *Polymer.* 2003, Vol. 44, pp. 1517–1526.

19. **Satyanarayana KG, Gregorio GC. Arizaga, Wypych F.** Biodegradable composites based on lignocellulosic fibers-An overview. Progress in Polymer Science. 2009, Vol. 34, 9, pp. 982-1021.

20. **William BH, Thomas P.** *Introduction to organic chemistry.* 3rd. s.l. : Wiley, 2005. ISBN 0- 471-44451-0.

21. **Whistler RL, BeMiller JN, Paschall BF.** *Starch: chemistry and technology.* New York: : Academic Press, 1984.

22. **Liu H, Xie F, Yu L, Chen L, Li L.** Thermal processing of starch-based polymers. *Progress in Polymer Science.* 2009, Vol. 34, pp. 1348–1368.

23. **Yu L, Dean K, Li L.** Polymer blends and composites from renewable resources. *Progr Polym Sci.* 2006, Vol. 31, pp. 576–602.

24. Characteristics of raw starch. *NIPPON Starch Chemical.* [Online] [Cited: november 12, 2011.] http://www.nichidene.com/Eng/kkh/b/b-2.htm.

25. **Averous L.** Biodegradable multiphase systems based on plasticized starch: Review. *J. Macromolecular Science.* 2004, Vol. 44, pp. 231-74.

26. **Belitz HD, Grosch W, Schieberle P.** *Food chemistry.* 3rd. s.l. : Springer, 2004. pp. 318-323. ISBN 3540408185.

27. **Atwell WA, Hood LF, Lineback DR, Varriano-Marston E, Zobel HF.** The terminology and methodology associated with basic starch phenomena. *Cereal FoodWorld.* 1988, Vol. 33, pp. 306–11.

28. **Yu L, Christie G.** Microstructure and mechanical properties of orientated

thermoplastic starches. *J Mater Sci.* 2005, Vol. 40, pp. 111–6.

29. **Lim MH, Wu HB, Reid DS.** The effect of starch gelatinization and solute concentrations on Tg of starch model system. *J Sci Food Agric.* 2000, Vol. 80, pp. 1757–62.

30. **Keetels CJAM, Oostergetel GT, van Vliet T.** Recrystallization of amylopectin in concentrated starch gels. *Carbohydr Polym.* 1996, Vol. 30, pp. 61–4.

31. **Dufresne A, Vignon MR.** Improvement of starch film performances using cellulose microfibrils. *Macromolecules.* 1998, Vol. 31, pp. 2693–6.

32. **Jagannath JH, Jayaraman KS, Arya SS, Somashekar R.** Differential scanning calorimetry and wide-angle X-ray scattering studies of bread staling. *J. Appl. Polym. Sci.* 1998, Vol. 67, pp. 1597-160.

33. **Wollerdorfer M, Bader H.** Influence of natural fibres on the mechanical properties of biodegradable polymers. *Industrial Crops and Products.* 1998, Vol. 8, pp. 105–112.

34. **Van Soest JJG, de Wit D, Tournois H, J.F.G.** The influence of glycerol on structural changes in waxy maize starch as studied by Fourier transform infrared spectroscopy. *Polymer.* 1994, Vol. 35, pp. 4722-472.

35. **Godbole S, Gote S, Latkar M, Chakrabarti T.** Preparation and characterization of biodegradable poly-3-hydroxybutyrate-starch blend films. *Bioresour Technol.* 2003, Vol. 86, pp. 33–7.

36. **Forssell Pirkko M, Mikkila JM, Moates GK, Parker R.** Phase and glass transition behaviour, of concentrated barley starch-glycerol-water mixtures, a model for thermoplastic starch. *Carbohydrate Polymers.* 1997, Vol. 34, pp. 275-282.

37. **Janssen LPBM.** Influence of Process Conditions on the Physical Properties of TPS. [ed.] Leszek Moscicki Leon P. B. M. Janssen. *Thermoplastic Starch: A Green Material for Various Industries.* s.l. : Wiley-VCH Verlag GmbH & Co, 2009.

38. **Lai LS, Kokini JL.** Physicochemical changes and rheological properties of starch during extrusion (a review). *Biotechnol Progr.* 1991, Vol. 7, pp. 251–66.

39. **Hulleman SHD, Janssena FHP, Feila H.** The role of water during plasticization of native starches. *Polymer.* 1998, Vol. 39, 10, pp. 2043-8.

40. **Burros BC, Young LA, Carroad PA.** Kinetics of corn meal gelatinization at high temperature and low moisture. *J Food Sci.* 1987, Vol. 52, pp. 1372–6.

41. **Wen LF, Rodia P, Wasserman BP.** Starch fragmentation and protein insolubilization during twin-screw extrusion of corn meal. *Cereal Chem.* 1990, Vol. 67, pp. 268–75.

42. **Baltá Calleja JF, Rueda DR, Secall T, Bayer RK, Schlimmer M.** Influence of processing

methods on starch properties. *J Macromol Sci Phys B.* 1999, Vol. 38, pp. 461–9.

43. **Kokini JL, Baumann GC, Bresslauer K, Chedid LL, Herh P, Lai LS, et al.** A kinetic model for starch gelatinization and effect of starch/protein interactions on rheological properties of 98% amylopectin and amylose rich starches. [book auth.] Schubert H Spiess WEL. *Engineering and foods.* New York : advanced process, 1990, pp. 109–21.

44. **Donovan JW.** Phase transition of the starch–water system. *Biopolymers.* 1979, Vol. 18, pp. 263–75.

45. **Levine H, Slade L.** Influences of the glassy and rubbery states on the thermal, mechanical and structural properties of doughs and baked products. [book auth.] Faubion JM Faridi H. *Dough rheology and baked product texture.* NewYork : VanNostrandReinhold, 1990, pp. 157– 330.

46. *Processing and properties of poly (lactic acid)/plasticized starch blends.* **Hunealt MA, Li H, Chapleau N, Favis BD.** [ed.] 41st International Symposium on Macromolecules. s.l. : World Polymer congress, 2006. 841.

47. **Pedroso AG, Rosa DS.** Mechanical, thermal and morphological characterization of recycled LDPE/corn starch blends. *Carbohydrate Polymers.* 2005, Vol. 59, pp. 1-9.

48. **Chandra R, Rustgi R.** Biode ation of maleated linear low-density polyethylene and starch blends. *Polymer Degradation and Stability.* 1997, Vol. 56, pp. 185-202.

49. **Thakore IM, Desai S, Sarawade BD, Devi S.** Studies on biodegradability, morphology and thermomechanical properties of LDPE/modified starch blends. *European Polymer Journal.* 2001, Vol. 37, pp. 151-160.

50. *Hydrophobicitybicity of CVDa-C:H coatings produced on cornstarch plasticized films: contact angle and AFM adhesive forces measurements.* **Simão RA,Martins M, Silva ML, ThireMSM, Andrade CT.** [ed.] 41st International Symposium on macromolecules. s.l. : World polymer congress, 2006. 1844.

51. **Azizi Samir, M. A. S., Alloin, F., & Dufresne, A.** (2005). Review of recent research into cellulosic whiskers, their properties and their application in nanocomposite field. Biomacromolecules, 6(2), 612–626.

52. **Bledzki AK, Gassan J.** Composites reinforced with cellulose based fibers. *Prog Polym Sci.* 1999, Vol. 24, pp. 221–74.

53. **Mohanty AK, Misra M, Hinrichsen GB.** biodegradable polymers and biocomposites: an overview. *Macromol Mater Eng.* 2000, Vol. 276, pp. 1–24.

54. **Spear M.** *Natural Composites in Construction.* Cwmbran : Technium Springboard,, 2009.

55. **Ronga MZ, Zhang MQ, Liub Y, Yang GC, Zeng HM.** The effect of fiber treatment on the mechanical properties of unidirectional sisal-reinforced epoxy composites. *Composites Science and Technology.* 2001, Vol. 61, 10, pp. 1437–1447.

56. **Rao KMM, Rao KM.** Extraction and tensile properties of natural fibers: Vakka, date and bamboo. *Composite Structures.* 2007, Vol. 77, 3, pp. 288–295.

57. **Xue Li, Lope G. Tabil, Satyanarayan P.** Chemical Treatments of Natural Fiber for Use in Natural Fiber-Reinforced Composites: A Review. *J Polym Environ.* 2007, Vol. 15, pp. 25–33.

58. **George H.** What is delignification. *Wise Geek.* [Online] Conjecture Corporation, 2003. [Cited: junuary 22, 2018.] http://www.wisegeek.com/what-is-delignification.htm.

59. **Frederick TW, Norman W.** *Natural fibers plastics and composites.* New York : Kluwer Academic Publishers, 2004.

60. **Mallick PK.** *Fiber-reinforced composites materials, manufacturing & Design.* 2nd. s.l. : Marcel Dekker Inc, 1993.

61. **Mohanty AK, Misra M, Drzal LT.** Surface modifications of natural fibers and performance of the resulting biocomposites: An overview. *Comp Interfaces.* 2001, Vol. 8, pp. 313-343.

62. **Kalia S, Kaith BS, Kaur I.** Pretreatments of natural fibers and their application as reinforcing material in polymer composites—A Review. *Polymer Engineering and Science.* 2009, Vol. 49, 7, pp. 1253–1272.

63. **Alawar A, Hamed AM, Al-Kaabi K.** Characterization of treated date palm tree fiber as composite reinforcement. *Composites: Part B.* 2009, Vol. 40, pp. 601–606.

64. **Joseph K, Mattoso LHC, Toledo RD, Thomas S, Carvalho LHD, Pothen L, Kala S, James B.** Natural fiber reinforced thermoplastic composites. [book auth.] A.L. Lea˜o, and L.H.C. Mattoso, Eds., Sa˜n Carlos E. Frollini. *Natural Polymers and Agrofibers Composites.* Brazil : Embrapa, 2000.

65. **Gassan J, Bledzki AK.** Alkali treatment of jute fibers: Relationship between structure and mechanical properties. *Journal of Applied Polymer Science.* 1999, Vol. 71, 4, pp. 623–629.

66. **Vilaseca F, Mendez JA, Pelach A, Llop M, Canigueral N, Girones J, Turon X, Mutje P.** Composite materials derived from biodegradable starch polymer and jute strands. *Process Biochemistry.* 2007, Vol. 42, pp. 329–334.

67. **Cao Y, Shibata S, Fukumoto I.** Mechanical properties of biodegradable composites reinforced with bagasse fibre before and after alkali treatments. *Composites: Part A.* 2006, Vol. 37, pp. 423–429.

68. **Al-Khanbashi A, Al-Kaabi K, Hammami A.** Date palm fibers as polymeric matrix reinforcement: fiber characterization. *Polymer Composites.* 2005, Vol. 26, 4, pp. 486–497.

69. **Sreekala MS, Kumaran MG, Joseph S, Jacob M, Thomas S.** Oil palm fibre reinforced phenol formaldehyde composites: influence of fibre surface modifications on the mechanical performance. *Applied Composite Materials.* 2000, Vol. 7, pp. 295-329.

70. **Bendahou A, Kaddami H, Sautereau H, Raihane M, Erchiqui F, Dufresne A.** Short palm tree fibers polyolefin composites: effect of filler content and coupling agent on physical properties. *Macromol. Mater. Eng.* 2008, Vol. 293, pp. 140–148.

71. **Bismarck A, Askargorta IA, Springer J.** Surface characterization of flax, hemp and cellulose fibers; surface properties and the water uptake behavior. *Polymer Composites.* 2002, Vol. 23.

72. **Harris B.** *Engineering Composite Materials.* London: The Institute of Materials, 1999.

73. **Cañigueral N, Vilaseca F, Méndez JA, López JP, Barberà L, Puig J, Pèlach MA, Mutjé P.** Behavior of biocomposite materials from flax strands and starch-based biopolymer. *Chemical EngineeringScience.* 2009, Vol. 64, pp. 2651--2658.

74. **Guimarães JL, Wypych F, Saul CK, Ramos LP, Satyanarayana KG. .** Studies of the processing and characterization of corn starch and its composites with banana and sugarcane fibers from Brazil. *Carbohydrate Polymers.* 2010, Vol. 80, pp. 130–138.

75. **Ochi S.** Development of high strength biodegradable composites using Manila hemp fiber and starch-based biodegradable resin. *Composites: Part A.* 2006, Vol. 37, pp. 1879–1883.

76. **Takagi H, Asano A.** Effects of processing conditions on flexural properties of cellulose nanofiber reinforced ‘‘green’’ composites. *Composites: Part A.* 2008, Vol. 39, pp. 685–689.

77. **Shibata S, Cao Y, Fukumoto I.** Flexural modulus of the unidirectional and random composites made from biodegradable resin and bamboo and kenaf fibres. *Composites: Part A.* 2008, Vol. 39, pp. 640–646.

78. **Harriëtte Bos.** The Potential of Flax Fibres as Reinforcement for Composite Materials. *Thesis.* Eindhoven : Eindhoven University of Technology, 2004.

79. **Oksman K, Skrifvars M, Selin JF.** Natural fibres as reinforcement in polylactic acid (PLA) composites. *Composites Science and Technology.* 2003, Vol. 63, pp. 1317–1324.

80. **Romhany G, Kocsis JK, Czigany T.** Tensile fracture and failure behavior of thermoplastic starch with unidirectional and cross-ply flax fiber reinforcements. *Macromol. Mater. Eng.* 2003, Vol. 288, pp. 699–707.

81. **Phattaraporn T, Waranyou S, Fazilah A, Thawien W.** Characteristics and properties of rice starch films reinforced with palm pressed fibers. *International Food Research Journal.* 2010, Vol. 17, pp. 535-547.

82. **Bhadeshia HKDH. .** Thermal analysis techniques. s.l. : University of Cambridge, Materials Science & Metallurgy.

83. **Prachayawarakorn J, Sangnitidej P, Boonpasith P.** Properties of thermoplastic rice starch composites reinforced by cotton fiber or low-density polyethylene. *Carbohydrate Polymers.* 2010, Vol. 81, pp. 425–433.

84. **Guduri BR, Khoathane C, Anandjiwala RD, De Vries A, Sadiku ER, Van Wyk L.** Effect of water absorption on mechanical properties of flax fiber reinforced composites. Pretoria: CSIR Material Science and manufacturing South Africa.

85. **Gaspar M, Benko Zs, Dogossy G, Reczey K, Czigany T.** Reducing water absorption in compostable starch-based plastics. *Polymer Degradation and Stability.* 2005, Vol. 90, pp. 563- 569.

86. **Soykeabkaew N, Supaphol P, Rujiravanit R.** Preparation and characterization of jute- and flax-reinforced starch-based composite foams. *Carbohydrate Polymers.* 2004, Vol. 58, pp. 53– 63.

87. **Di Franco CR, Cyras VP, Busalmen JP, Ruseckaitea RA, Vazquez A.** Degradation of polycaprolactone/starch blends and composites with sisal fibre. *Polymer Degradation and Stability.* 2004, Vol. 86, pp. 95-103.

88. **Kaith BS, Jindal R, Jana AK, Maiti M.** Development of corn starch based green composites reinforced with Saccharum spontaneum L fiber and graft copolymers – Evaluation of thermal, physico-chemical and mechanical properties. *Bioresource Technology.* 2010, Vol. 101, pp. 6843–6851.

89. **Pal, P.; Malas, A.; Maitra, A.; Das, C.K.; Nigam, V.; Saxena, A.K**. Dual effect of polyphosphazene and halloysite nanotubes in the blends of poly(phenylene oxide)/liquid crystalline polymer. Polym.-Plast. Tech- nol. Eng. 2015, *54*, 1765–1771.

90. **Berthier, P.**, 1826. Analyse de l'halloysite. Ann. Chim. Phys. 32, 332–335.

91. **Tayser Sumer Gaaz, Abu Bakar Sulong, Abdul Amir H. Kadhum, Ahmed A. Al-Amiery, Mohamed H. Nassir and Ahed Hameed Jaaz**. The Impact of Halloysite on the Thermo-Mechanical Properties of Polymer Composites. Molecules 2017, 22, 838.

92. **Lvov, Y.; Abdullayev, E.** Functional polymer–clay nanotube composites with sustained release of chemical agents. *Prog. Polym. Sci.* **2013**, *38*, 1690–1719.

93. **Barrientos-Ramírez, S.; de Oca-Ramírez, G.M.; Ramos-Fernández, E.V.; Sepúlveda-Escribano, A.; Pastor-Blas, M.M.; González-Montiel, A**. Surface modification of natural halloysite clay nanotubes with aminosilanes. Application as catalyst supports in the atom transfer radical polymerization of methyl methacrylate. *Appl. Catal. A Gen.* **2011**, *406*, 22–33.

94. **Paul F. Kerr.** "Formation and occurrence of clay minerals". *Clays and Clay Minerals*. 1: 19–32.

95. **Wang, B.; Huang, H.X.; Guan, W.S.** Squeeze flow- induced hierarchical morphology in microinjection compression molded thin-walled plates of PP/SAN blend and its nanocomposite with halloysite nanotubes. Polym.-Plast. Technol. Eng. 2015, *54*, 814–821.

96. **Pal, P.; Kundu, M.K.; Maitra, A.; Malas, A.; Das, C.K.** Synergistic effect of halloysite nanotubes and MA-g-PE on thermo-mechanical properties of polycarbonate- cyclic olefin copolymer based nanocomposite. Polym.- Plast. Technol. Eng. 2016, *55*, 1481–1488.

97. **Joussein, E., Petit, S., Churchman, J., Theng, B., Righi, D., Delvaux, B., 2005.** Halloysite clay minerals: a review. Clay Miner. 40 (4), 383–426.

98. **R. Klimkiewicz and B.D. Edwarda //** J.Phys.Chem.Solids 65 (2004) 459.

99. **Imai T, Naitoh Y, Yamamoto T and Ohyanagi M, J Ceram Soc Jpn 114:138 (2006).**

100. **Bergaya F, Theng BKG, Lagaly G.** Hand book of clay science. Elsevier Science, First ed. 2006, Netherlands, pp: 4-7.

101. **Ismail**, H.; Pasbakhsh, P.; Fauzi, M.A.; Bakar, A.A. Morphological, thermal and tensile properties of halloysite nanotubes filled ethylene propylene diene monomer (EPDM) nanocomposites. *Polym. Test.* **2008**, *27*, 841–850.

102. **Albdiry, M.T.; Yousif, B.F.** Role of silanized halloysite nanotubes on structural, mechanical properties and fracture toughness of thermoset nanocomposites. *Mater. Des.* **2014**, *57*, 279–288.

103. **Singh, B., 1996.** Why does halloysite roll? — A new model. Clay Clay Miner. 44 (2), 191–196.

104. **Gaaz, T.S.; Sulong, A.B.; Akhtar, M.N.; Kadhum, A.A.H.; Mohamad, A.B.; Al-Amiery, A.A.** Properties and applications of polyvinyl alcohol, halloysite nanotubes and their nanocomposites. *Molecules* **2015**, *20*, 22833–22847.

105. **Manevitch, O.L., Rutledge, G.C., 2004.** Elastic properties of a single lamella of montmorillonite by molecular dynamics simulation. J. Phys. Chem. B 108 (4), 1428–

1435.

106. Lu, D., Chen, H.B., Wu, J.S., Chan, C.M., 2010. Direct measurements of the Young's modulus of a single halloysite nanotube using a transmission electron microscope with a bending stage. J. Nanosci. Nanotechnol. 11 (9), 7789–7793 (7785).

107. Lvov, Y.M., Shchukin, D.G., Mohwald, H., Price, R.R., 2008. Halloysite clay nanotubes for controlled release of protective agents. ACS Nano 2 (5), 814–820.

108. Lecouvet, B., Horion, J., D'Haese, C., Bailly, C., Nysten, B., 2013a. Elastic modulus of halloysite nanotubes. Nanotechnology 24 (10).

109. Guimaraes, L., Enyashin, A.N., Seifert, G., Duarte, H.A., 2010. Structural, electronic, and mechanical properties of single-walled halloysite nanotube models. J. Phys. Chem. C 114 (26), 11358–11363.

110. Manevitch, O.L., Rutledge, G.C., 2004. Elastic properties of a single lamella of montmorillonite by molecular dynamics simulation. J. Phys. Chem. B 108 (4), 1428–1435.

111. DuML,GuoBC,CaiXJ,JiaZX,LiuMXandJiaDM,*e-Polymers*130:1 (2008).

112. GuoBC,ZouQL,LeiYD,DuML,LiuMXandJiaDM,*NewChemMater* 36:32 (2008). [in Chinese].

113. HuangZF,JiaZX,GuoBCandJiaDM,ChinaPlastInd36:29(2008).[in Chinese].

114. Liu, M., Jia, Z., Jia, D., Zhou, C., 2014. Recent advance in research on halloysite nanotubes– polymer nanocomposite. Prog. Polym. Sci. 39 (8), 1498–1525.

115. Lecouvet, B., Sclavons, M., Bourbigot, S., Bailly, C., 2013c. Thermal and flammability properties of polyethersulfone/halloysite nanocomposites prepared by melt compounding. Polym. Degrad. Stab. 98 (10), 1993–2004.

116. Ye, Y.P., Chen, H.B., Wu, J.S., Ye, L., 2007. High impact strength epoxy nanocomposites with natural nanotubes. Polymer 48 (21), 6426–6433.

117. Rooj, S., Das, A., Thakur, V., Mahaling, R.N., Bhowmick, A.K., Heinrich, G., 2010. Preparation and properties of natural nanocomposites based on natural rubber and naturally occurring halloysite nanotubes. Mater. Des. 31 (4), 2151–2156.

118. M. Du et al. / European Polymer Journal 42 (2006) 1362–1369

119. Mingxian L., Rui H., Jing Y., Zheru L., Biao H., Yongwang L. and Changren Z. Polysaccharide-halloysite nanotube composites for biomedical applications: a review. Clay Minerals, (2016) 51, 457–467

120. Liu M., Dai L., Shi H., Xiong S. & Zhou C. (2015) In vitro evaluation of

alginate/halloysite nanotube composite scaffolds for tissue engineering. Materials Science and Engineering: C, 49, 700–712.

121. Chang P.R., Xie Y., Wu D. & Ma X. (2011) Amylose wrapped halloysite nanotubes. Carbohydrate Polymers, 84, 1426–1429.

122. Brindley G., Robinson K. & MacEwan D. (1946) The clay minerals halloysite and meta-halloysite. Nature, 157, 225–226.

123. H. Schmitta, K. Prashanthaa, J. Soulestina, M.F. Lacrampea, P. Krawczak. Preparation and properties of novel melt-blended halloysite nanotubes/wheat starch nanocomposites. Carbohydrate Polymers 89 (2012) 920–927

124. Liu M., Zhang Y., Wu C., Xiong S. & Zhou C. (2012b) Chitosan/halloysite nanotubes bionanocomposites: Structure, mechanical properties and biocompatibility. International Journal of Biological Macromolecules, 51, 566–575.

125. Soheilmoghaddam M., Wahit M.U., Mahmoudian S. & Hanid N.A. (2013) Regenerated cellulose/halloysite nanotube nanocomposite films prepared with an ionic liquid. Materials Chemistry and Physics, 141, 936–943.

126. Liu M., Wu C., Jiao Y., Xiong S. & Zhou C. (2013a) Chitosan–halloysite nanotubes nanocomposite scaffolds for tissue engineering. Journal of Materials Chemistry B, 1, 2078–2089.

127. DeSilvaR.,PasbakhshP.,GohK.-L.,ChaiS.-P.&IsmailH. (2013) Physico-chemical characterisation of chitosan/ halloysite composite membranes. Polymer Testing, 32, 265–271.

128. Liu M., Shen Y., Ao P., Dai L., Liu Z. & Zhou C. (2014b) The improvement of hemostatic and wound healing property of chitosan by halloysite nanotubes. RSC Advances, 4, 23540–23553.

129. A. Mandal and D. Chakrabarty, "Isolation of nanocellulose from waste sugarcane bagasse (SCB) and its characterization," *Carbohydrate Polymers*, vol. 86, no. 3, pp. 1291–1299, 2011.

130. Ahmad I, Mosadeghzad Z, Daik R, Ramli A (2008) The effect of alkali treatment and filler size on the properties of sawdust/ UPR composites based on recycled PET wastes. J Appl Polym Sci 109:3651–3658

131. Troedec M, Sedan D, Peyratout C, Bonnet J, Smith A, Guinebretiere R, Gloaguen V, Krausz P (2008) Influence of various chemical treatment on the composition and struc- ture of hemp fibres. Compos Part A 39:514–522

132. Zhou J P, Zhang L, Deng Q H, Wu X J. Synthesis and characterization of cellulose derivatives prepared in NaOH/urea aqueous solutions. Journal of Polymer Science Part

A: Polymer Chemistry, 2004, 42(23): 5911–5920

133. A. Bhatnagar and M. Sain, "Processing of cellulose nano ber- reinforced composites," Journal of Reinforced Plastics and Com- posites, vol. 24, no. 12, pp. 1259– 1268, 2005.

134. M. J. John and R. D. Anandjiwala, "Recent developments in chemical modi cation and characterization of natural ber- reinforced composites," Polymer Composites, vol. 29, no. 2, pp. 187–207, 2008.

135. P. Yuan, P.D. Southon, Z. Liu, M.E.R. Green, J.M. Hook, S.J. Antill, C.J. Kepert, Functionalization of halloysite clay nanotubes by grafting with c-aminopropyltriethoxysilane, J. Phys. Chem. C 112 (2008) 15742–15751.

136. S. Barrientos-Ramírez, E.V. Ramos-Fernández, J. Silvestre-Albero, A. Sepúlveda-Escribano, M.M. Pastor-Blas, A. González-Montiel, Use of nanotubes of natural halloysite as catalyst support in the atom transfer radical polymerization of methyl methacrylate, Microporous Mesoporous Mater. 120 (2009) 132–140.

137. Hamdy Ibrahim, Mahmoud Farag, Hassan Megahed, Sherif Mehannya. Characteristics of starch-based biodegradable composites reinforced with date palm and flax fibers. Carbohydrate Polymers 101 (2014) 11–19

138. Gwon, J.G.; Lee, S.Y.; Chun, S.J.; Doh, G.H.; Kim, J.K. Physical and mechanical properties of wood-plastic composites hybridized with inorganic fillers. J Compos. Mater. 2011, 46 (3), 301–309.

139. Whitney JM, Knight M. The relationship between tensile strength and flexure strength in fiber.reinforced composites. Experimental Mechanics. 1980, Vol. 20.

140. Wisnom MR. The relationship between tensile and flexural strength of unidirectional composites. Composite Materials. 1991, Vol. 26.